europhysics
conference
abstracts

12 th European Conference on

Controlled Fusion and Plasma Physics

Budapest, 2 - 6 September 1985

Supplement to the proceedings
Part I

Published by: European Physical Society

Series Editor: Prof. S. Methfessel, Bochum

itor: G. Thomas, Geneva

VOLUME
9 F
PART I

12 th European Conference on

Controlled Fusion and Plasma Physics

Budapest, 2 - 6 September 1985

Supplement to the proceedings
Part I

Kiadja a Központi Fizikai Kutató Intézet
Felelős kiadó: Szegő Károly
Példányszám: 520 Törzsszám: 85-660
Készült a KFKI sokszorosító üzemében
Felelős vezető: Töreki Béláné
Budapest, 1985. november hó

This brochure contains the following items:

1. List of registered participants of the 12th European Conference on Controlled Fusion and Plasma Physics.
2. Papers in their full, four page versions, which were accepted by the Programme Committee, and have not been printed in the Proceedings of the Conference.

A. Montvai
scientific secretary

CONTENTS

List of Registered Participants

The participants are listed in alphabetic order grouped according the country signified in their mailing addresse.

Hamberger, S.M. CANBERRA P.O.B.4 AUSTRALIA 2600
The Australian National University

Jones, I.R. BEDFORD PARK AUSTRALIA SA5042
Flinders University Plasma Physics Group

Kirolous, H. Bedford Park AUSTRALIA SA5042
The Flinders University of South Australia
School of Phys. Sciences Sturt Road

Knight, A. Bedford Park AUSTRALIA SA5042
The Flinders University of South Australia
School of Phys. Sciences Sturt Road

Parry, J.K. SUTHERLAND Private Mail Bag AUSTRALIA 2232
Australian Atomic Energy Comission

Cap, Ferdinand INNSBRUCK Karl Innerebnerstr. 40 AUSTRIA 6020
Universitat Innsbruck Institut fuer Teoretische Physik

Edenstrasser, Johann W. INNSBRUCK AUSTRIA A-6020
Institute for Theoretical physics, Univesity of Innsbruck

Heindler, M. GRAZ Petersgasse 16 AUSTRIA A-8010
Technical University Graz Institute for Theoretical Physics
Alternate Energy Physics Program

Kamelander, G. WIEN Lenaugasse 10 AUSTRIA A-1080
Oesterr. Forschungszentrum Seibersdorf

Nassri, A. GRAZ Petergasse 16 AUSTRIA 8010
Technische Universitat Graz Institut fuer Theoretische Physik

Winter, H. WIEN Karlsplatz 13 AUSTRIA A-1040
Institut fuer Allgemeine Physik Technishe Universitaet Wien

Faulconer, D. W. BRUSSELS 30,Av. de la Renaissance BELGIUM 1040
Ecole Royale Militaire Laboratorie da Physique des Plasmas

Maisonnier, Ch. BRUSSELS Rue de la Loi 200 BELGIUM 1049
Commission of the European Communities

Messiaen, A.M. BRUSSELS 30,Av. de la Renaissance BELGIUM 1040
Ecole Royale Militaire Laboratorie da Physique des Plasmas

Palumbo, Donato BRUXELLES Rue de la Loi 200 BELGIUM 1049
Comission of the European Communities - DG XII

Rager, Jean-Pierre BRUSSELS rue de la Loi 200 BELGIUM 1049
Commission of the European Communities
DG XII/Fusion

Saison, R. BRUSSELS rue de la Loi 200 BELGIUM 1049
Commission of the European Communities
DG XII/Fusion

Vandenplas, P. BRUSSELS 30,Av. de la Renaissance BELGIUM 1040
Ecole Royale Militaire Laboratorie da Physique des Plasmas

Weynants, R. BRUSSELS 30,Av. de la Renaissance BELGIUM 1040
Ecole Royale Militaire Laboratorie da Physique des Plasmas

Meyer, J. VANCOUVER, B.C. Agricultural Rd. CANADA V6T2A6
Department of Physics University of British Columbia

Pacher, Horst VARENNES, QUEBEC C.P. 1200 CANADA
INRS-Energie

Panarella, Emilio OTTAWA,ONTARIO CANADA K1A0R6
National Research Council

Skaregard, H.M. SASKATOON S7N 0W0 CANADA
University of Saskatchewan

Chen, Jia-ju HEFEI P.O.B. 26, Hefei CHINA,PEOPL.REP.
Institute of Plasma Physics Academia Sinica

Huo Yu Ping, Director HEFEI, ANHWEI P.O.Box 26 CHINA,PEOPL.REP.
Institute of Plasma Physics Academia Sinica

Ni, Guan-Dong LESHAN SICHUAN CHINA,PEOPL.REP.

Qiu, Xiao-Ming LESHAN SICHUAN CHINA,PEOPL.REP.

Ren, Zhao-xing HEFEI, ANHWEI P.O.Box 26 CHINA,PEOPL.REP.
Institute of Plasma Physics Academia Sinica

Badalec, J. PRAHA 8 Pod vodarenskou vezi 4 CZECHOSLOVAKIA 182 11
Czechoslovak Academy of Sciences Institute of Plasma Physics

Bohacek, Vladislav PRAGUE CZECHOSLOVAKIA 18211
Institute of Plasma Physics CS Acad. Sciences

Clupek, Martin PRAGUE CZECHOSLOVAKIA 18211
Institute of Plasma Physics CS Acad. Sciences

Jakubka, Karel PRAGUE CZECHOSLOVAKIA 18211
Institute of Plasma Physics CS Acad. Sciences

Jungwirth, Karel PRAGUE CZECHOSLOVAKIA 18211
Institute of Plasma Physics CS Acad. Sciences

Klima, Richard PRAGA Pod Vodarenskou Vezi 4 CZECHOSLOVAKIA 18211
Czechoslovak Academy of Sciences Institute of Plasma Physics

Kolacek, Karel PRAGUE CZECHOSLOVAKIA 18211
Institute of Plasma Physics CS Acad. Sciences

Kopecky, V. PRAHA 8 Pod vodarenskou vezi 4 CZECHOSLOVAKIA 182 11
Czechoslovak Academy of Sciences Institute of Plasma Physics

Kovac, Ivan PRAGUE Pod Vodarenskou vezi 4 CZECHOSLOVAKIA 18211
Institute of plasma Physics Czech. Academy of Sciences

Krejci, Ales PRAGUE CZECHOSLOVAKIA 18211
Institute of Plasma Physics CS Acad. Sciences

Krlin, Ladislav PRAGUE CZECHOSLOVAKIA 18211
Institute of Plasma Physics CS Acad. Sciences

Magula, Peter PRAGUE CZECHOSLOVAKIA 18211
Institute of Plasma Physics CS Acad. Sciences

Piffl, Vojtech PRAGUE CZECHOSLOVAKIA 18211
Institute of Plasma Physics CS Acad. Sciences

Preinhaelter, J. PRAGUE 8 Pod vodarenskou vezi 4 CZECHOSLOVAKIA 182 11
Institute of Plasma Physics Czechoslovak Academy of Sciences

Raus, Jaroslav PRAGUE CZECHOSLOVAKIA 18211
Institute of Plasma Physics CS Acad. Sciences

Stoeckel, Jan PRAGUE CZECHOSLOVAKIA 18211
Institute of Plasma Physics CS Acad. Sciences

Sunka, P. PRAHA 8 Pod vodarenskou vezi 4 CZECHOSLOVAKIA 182 11
Czechoslovak Academy of Sciences Institute of Plasma Physics

Ullschmied, Jiri PRAGUE CZECHOSLOVAKIA 18211
Institute of Plasma Physics CS Acad. Sciences

Valovic, Martin PRAGUE CZECHOSLOVAKIA 18211
Institute of Plasma Physics CS Acad. Sciences

Vrba, Pavel PRAGUE 8 Pod vodarenskou vezi 4 CZECHOSLOVAKIA 180 69
Inst. of Plasma Physics

Zacek, F. PRAGUE 8 Pod vodarenskou vezi 4 CZECHOSLOVAKIA 182 11
Institute of Plasma Physics Czechoslovak Academy of Sciences

Andersen, V. ROSKILDE P.O.B.49 DENMARK 4000
Riso National Laboratory Plasma Physics Section
Physics Division

Chang, C.T. ROSKILDE P.O.B.49 DENMARK 4000
Riso National Laboratory Plasma Physics Section
Physics Division

Lynov, Jens-Peter ROSKILDE P.O.B.49 DENMARK 4000
Riso National Laboratory Plasma Physics Section
Physics Division

Sorensen, H. ROSKILDE P.O.B.49 DENMARK 4000
Riso National Laboratory Plasma Physics Section
Physics Division

Heikkinen, Jukka A. HELSINKI 18 P.O. Box 169 FINLAND 00181
Technical Research Center of Finland
Nuclear Engineering Laboratory

Adam, Jean FONTENAY-AUX-ROSES B.P.No.6 FRANCE 92260
Centre d'Etudes Nucleaires

Briffod, G. GRENOBLE CEDEX Rue des Martyrs FRANCE 38041
Centre d'Etudes Nucleaires de Grenoble
Service Ionique Generale

Cabe, Jean COURTRY BP 7 FRANCE 77181
Comissariat a l'Energie Atomique

Chatelier, M. FONTENAY-AUX-ROSES B.P.No.6 FRANCE 92260
Centre d'Etudes Nucleaires

Dubois, M. FONTENAY-AUX-ROSES B.P.No.6 FRANCE 92260
Centre d'Etudes Nucleaires

Fabre, E. PALAISEAU CEDEX Ecole Polytechnique FRANCE 91128
Centre Nationale de la Recherche Scientifique
Groupment de Recherches Coordonnees

Girard, A. GRENOBLE FRANCE 38041
Association EURATOM-CEA Department de Recherches sur la
Fusion Controllee

Giruzzi, G. FONTENAY-AUX-ROSES B.P. 6 FRANCE 92260
Association EURATOM-CEA sur la Fusion
DRFC/STC

Gregoire, Michel GRENOBLE FRANCE 38041
Association EUR CEA CENG 85 X

Gresillon, Dominique PALAISEAU CEDEX FRANCE 91128
Ecole Polytechnique Laboratoire PMI

Hoang, G. T. GRENOBLE FRANCE 38041
Assiciation EURATOM-C.E.A. Departement de Recherches sur la
Fusion Controllee C.E.N.G.

Hutter, Thierry FONTENAY-AUX-ROSES B.P. No. 6 FRANCE 92260
Comissariat a l'Energie Atomique S.C.P.

Krivenski, Vladimir FONTENAY-AUX-ROSES B.P.No.6 ST61 FRANCE 92260
Centre d'Etudes Nucleaires

Laurent, L FONTENAY-AUX-ROSES FRANCE 92260
Departement de Recherches sur la Fusion Controlee

Lehner, Thierry PALAISEAU CEDEX FRANCE 91128
Ecole Polytechnique Laboratorie de Physique
des Milieux Ionises

Nakach, R. GRENOBLE C.E.N.G. 85X FRANCE 38041
Association Euratom-CEA Departement de Recherches sur la
Fusion Controlee

Parlange, F. GRENOBLE CEDEX Rue des Martyrs FRANCE 38041
Centre d'Etudes Nucleaires de Grenoble
Service Ionique Generale

Pellat, R PALAISEAU CEDEX FRANCE 91.28
Ecole polytechnique

Roubin, J.P. FONTENAY-AUX-ROSES B.P.No.6 FRANCE 92260
Centre d'Etudes Nucleaires

Saoutic, Bernard FONTENAY-AUX-ROSES B.P.No.6 FRANCE 92260
Centre d'Etudes Nucleaires

Terenzio, Consoli La Celle St Cloud 9 C Cote de la Jonchere FRANCE 78170
C.E.C.
Residence Elysee 1

Truc, A. PALAISEAU FRANCE 91120
Ecole Polytechnique laboratoire PMI

Becker, Gerhard GARCHING Boltzmannstr. 2 FRG 8046
Max-Planck-Inst. fuer Plasmaphysik

Bennel, J. BOCHUM 1 FRG D-4630
Institut fur Theoretische Physik Ruhr-Universitat Bochum

Behrisch, Rainer GARCHING Boltzmannstr. 2 FRG 8046
Max-Planck-Inst. fuer Plasmaphysik

Bertschinger, G. JULICH P.O.B. 1913 FRG D-5170
Institut fur Plasmaphysik der Kernfoschungsanlage Julich

Bessenrodt-Weberpals, M. DUESSELDORF Universitatsstrasse 1 FRG 4000
Physikalisches Inst. II der Univ. Duesseldorf

Bogen P. JULICH P.F.1913 FRG 5170
Insitut fur Plasmaphysik Kernforschungsanlage Julich GmbH

Borrass, Kurt GARCHING Boltzmannstr. 2 FRG 8046
Max-Planck-Inst. fuer Plasmaphysik

Bruhns, H. HEIDELBERG Albert Uebele str. 3/5 FRG 6900
Universitat Heidelberg Institut fuer Angewandte Physik II.

Canobbio, Ernesto GARCHING Boltzmannstr. 2 FRG 8046
Max-Planck-Inst. fuer Plasmaphysik

Claassen, H. A. JULICH 1 P.O.B.1913 FRG 5170
IPP der KFA

Dippel, K.H. JULICH 1 P.O.B.1913 FRG 5170
IPP der KFA

Eckhartt, D. GARCHING Boltzmannstr. 2 FRG 8046
Max-Planck-Inst. fuer Plasmaphysik

Eckmann, Volker GARCHING bei MUNCHEN Boltzmannstrasse 2 FRG 8046
Max Planck Inst. fuer Plasmaphysik

Feneberg, W. GARCHING FRG D-8046
Max-Planck-Institute fur Plasmaphysik
EURATOM Association

Freisinger,J. GIESSEN Heinrich-Buff-Ring 16 FRG 6300
Universitat Giessen

Fussmann, Gerd GARCHING Boltzmannstr. 2 FRG 8046
Max-Planck-Inst. fuer Plasmaphysik

Gehre, Otto GARCHING Boltzmannstr. 2 FRG 8046
Max-Planck-Inst. fuer Plasmaphysik

Gerhauser, H. JULICH 1 P.O.B.1913 FRG 5170
IPP der KFA

Gierke, Gerhart GARCHING Boltzmannstr. 2 FRG 8046
Max-Planck-Inst. fuer Plasmaphysik

Grieger, G. GARCHING Boltzmannstr. 2 FRG 8046
Max-Planck-Inst. fuer Plasmaphysik

Gruber, Otto GARCHING Boltzmannstr. 2 FRG 8046
Max-Planck-Inst. fuer Plasmaphysik

Haas, Gunter GARCHING Boltzmannstr. 2 FRG 8046
Max-Planck-Inst. fuer Plasmaphysik

Hacker, Herbert GARCHING Boltzmannstr. 2 FRG 8046
Max-Planck-Inst. fuer Plasmaphysik

Hartwig, D. DARMSTADT 11 Planckstrasse 1 FRG 6100
Gesellschaft f.Schwerionenforschung

Heil, J. BONN 2 Postfach 200706 FRG 5300
Bundesministerium fuer Forschung und Technologie

Herold, Hans STUTTGART 80 Pfaffenwaldring 31 FRG 7000
Universitat Stuttgart Institut fur Plasmaforshung

Herrman, Winfred GARCHING Boltzmannstr. 2 FRG 8046
Max-Planck-Inst. fuer Plasmaphysik

Herrnegger, Franz GARCHING Boltzmannstr. 2 FRG 8046
Max-Planck-Inst. fuer Plasmaphysik

Hintz, E. JULICH 1 P.O.B.1913 FRG 5170
IPP der KFA

Jaeger, Ulrich STUTTGART 80 Pfaffenwaldring 31 FRG 7000
Universitat Stuttgart Institut fur Plasmaforshung

Janeschitz, G. GARCHING FRG D-8046
Max-Planck-Institute fur Plasmaphysik
EURATOM Association

Junker, Josef GARCHING Boltzmannstr. 2 FRG 8046
Max-Planck-Inst. fuer Plasmaphysik

Kaleck, Armin JULICH 1 P.O.B.1913 FRG 5170
IPP der KFA

Keilhacker, Martin GARCHING Boltzmannstr. 2 FRG 8046
Max-Planck-Inst. fuer Plasmaphysik

Klingelhofer, Rolf KARLSRUHE 1 P.O.Box 3640 FRG D-7500
Kernforschungszentrum Karlsruhe

Klueber, O. GARCHING Boltzmannstr. 2 FRG 8046
Max-Planck-Inst. fuer Plasmaphysik

Koenen, L. JULICH 1 P.O.B.1913 FRG 5170
IPP der KFA

Koeppendoerfer, W. GARCHING Boltzmannstr. 2 FRG 8046
Max-Planck-Inst. fuer Plasmaphysik

Kramer, M. BOCHUM 1 Postfach 102148 FRG 4630
Ruhr-Universitat Bochum Exp. Phys. II

Kuhnapfl, Michael ESSEN FRG 4300
Universitat Essen-GHS

Lang, Rudolf GARCHING Boltzmannstr. 2 FRG 8046
Max-Planck-Inst. fuer Plasmaphysik

Lengyel, L. GARCHING Boltzmannstr. 2 FRG 8046
Max-Planck-Inst. fuer Plasmaphysik

Leppelmeyer, Gilbet W KARLSRUHE 1 P.O.Box 3640 FRG 7500
Kernforschungszentrum Karlsruhe

Leuterer, F. GARCHING Boltzmannstr. 2 FRG 8046
Max-Planck-Inst. fuer Plasmaphysik

Maassberg, Henning GARCHING Boltzmannstr. 2 FRG 8046
Max-Planck-Inst. fuer Plasmaphysik

Martinelli, A.P. GARCHING FRG D-8046
Max-Planck-Institut fur Plasmaphysik

McCormick, Kent GARCHING Boltzmannstr. 2 FRG 8046
Max-Planck-Inst. fuer Plasmaphysik

Mulser, P. DARMSTADT Hochschulstr. 2 FRG 6100
Technische Hochschule Darmstadt Institut fuer Theor. Phys.

Murmann, Heindieter GARCHING Boltzmannstr. 2 FRG 8046
Max-Planck-Inst. fuer Plasmaphysik

Neuhauser, J. GARCHING Boltzmannstr. 2 FRG 8046
Max-Planck-Inst. fuer Plasmaphysik

Nicolai, A. JULICH 1 P.O.B.1913 FRG 5170
IPP der KFA

Niedermeyer, Helmut GARCHING Boltzmannstr. 2 FRG 8046
Max-Planck-Inst. fuer Plasmaphysik

Nocentini, Aldo GARCHING Boltzmannstr. 2. FRG 8046
Max-Planck-Institut fuer Plasmaphysik

Noterdaeme, Jean-Marie GARCHING Boltzmannstr. 2 FRG 8046
Max-Planck-Inst. fuer Plasmaphysik

Nuhrenberg, Jurgen GARCHING Boltzmannstr. 2 FRG 8046
Max-Planck-Inst. fuer Plasmaphysik

Penningsfeld,Franz-Peter GARCHING Boltzmannstr. 2 FRG 8046
Max-Planck-Inst. fuer Plasmaphysik

Pfirsch, Dieter GARCHING Boltzmannstr. 2 FRG 8046
Max-Planck-Inst. fuer Plasmaphysik

Poschenrieder, W. P. GARCHING FRG D-8046
Max-Plack-Institut fur plasmaphysik ASDEX team

Pospieszczyk, A. JULICH P.O.B. 1913 FRG 5170
Insitut fur Plasmaphysik Kernforschungsanlage Julich GmbH

Raeder, Jurgen GARCHING Boltzmannstr. 2 FRG 8046
Max-Planck-Inst. fuer Plasmaphysik

Rapp, Harald GARCHING Boltzmannstr. 2 FRG 8046
Max-Planck-Inst. fuer Plasmaphysik

Rau, Fritz GARCHING Boltzmannstr. 2 FRG 8046
Max-Planck-Inst. fuer Plasmaphysik

Renner, Hermann GARCHING Boltzmannstr. 2 FRG 8046
Max-Planck-Inst. fuer Plasmaphysik

Riedler, Johann M. GARCHING bei MUNCHEN FRG 8046
MPI, Projekt Technologie

Ringler, Heinz GARCHING Boltzmannstr. 2 FRG 8046
Max-Planck-Inst. fuer Plasmaphysik

Roth, J. GARCHING FRG D-8046
Max-Planck-Institut fur Plasmaphysi EURATOM Association

Schlueter, Joachim JULICH 1 P.O.B.1913 FRG 5170
IPP der KFA

Schmitter, Karlheinz GARCHING Boltzmannstr. 2 FRG 8046
Max-Planck-Inst. fuer Plasmaphysik

Schmidt, H.	STUTTGART Institut fuer Plasmaforschung	Pfaffenwaldring 31 der Universitat Stuttgart	FRG	7000
Seidel, Ulrich	GARCHING Max-Planck-Inst. fuer Plasmaphysik	Boltzmannstr. 2	FRG	8046
Shukla, P.	BOCHUM 1 Ruhr-Universitat Bochum	Postfach 102148	FRG	4630
Smeulders, P.	GARCHING Max-Planck-Inst. fuer Plasmaphysik	Boltzmannstr. 2	FRG	8046
Soeldner, F.X.	GARCHING Max-Planck-Inst. fuer Plasmaphysik	Boltzmannstr. 2	FRG	8046
Speth, Eckehart	GARCHING Max-Planck-Inst. fuer Plasmaphysik	Boltzmannstr. 2	FRG	8046
Steinmetz, Karl	GARCHING Max-Planck-Inst. fuer Plasmaphysik	Boltzmannstr. 2	FRG	8046
Theenhaus, R.	JULICH 1 IPP der KFA	P.O.B.1913	FRG	5170
Toschi, R.	GARCHING Max-Planck-Inst. fuer Plasmaphysik	Boltzmannstr. 2	FRG	8046
Verbeek, H.	GARCHING Max-Plack-Institut fur plasmaphysik		FRG ASDEX team	D-8046
Vlases, George	GARCHING Max Planck	IPP	FRG	8046
Vollmer, Otto	GARCHING Max-Planck-Inst. fuer Plasmaphysik	Boltzmannstr. 2	FRG	8046
Wagner, F.	GARCHING Max-Planck-Inst. fuer Plasmaphysik	Boltzmannstr. 2	FRG	8046
Waidmann, G.	JULICH 1 IPP der KFA	P.O.B.1913	FRG	5170
Wilhelm, R.	STUTTGART Universitat Stuttgart	Pfaffenwaldring 31 Inst. fuer Plasmaforschung	FRG	7000
Winter, Joerg	JULICH 1 IPP der KFA	P.O.B.1913	FRG	5170
Wobig, Horst	GARCHING Max-Planck-Inst. fuer Plasmaphysik	Boltzmannstr. 2	FRG	8046
Wolf, G.	JULICH 1 Association EURATOM/KFA - Julich	P.O.B.1913	FRG	5170

Yugui, Wang GARCHING Boltzmannstr. 2 FRG 8046
Max-Planck-Inst. fuer Plasmaphysik

Zankl, Gerhard GARCHING Boltzmannstr. 2 FRG 8046
Max-Planck-Inst. fuer Plasmaphysik

Zwicker, H. STUTTGART 80 Pfaffenwaldring 31 FRG 7000
Universitat Stuttgart Institut fuer Plasmaforschung

Alexander,K.F. Prof.Dir. BERLIN Hausvogteiplatz 5-7 GDR 1086
Zentralinst. fuer Elektronenphysik

Guenther, Klaus BERLIN Hausvogteiplatz 5/7 GDR 1086
Zentralinst. fuer Elektronenpsysik

Hantzsche, E. BERLIN PSF 1250 GDR 1086
Zentralinstitut fuer Elektronenphysik

Hildebrandt, D. BERLIN Hausvogteiplatz 5/7 GDR 1086
Zentralinst. fuer Elektronenpsysik

Laux, M. BERLIN Hausvogteiplatz 5-7 GDR 1086
Zentralinstitut fur Elektronenphysik
ADW der DDR

Lingertat, J. BERLIN Hausvogteiplatz 5-7 GDR 1086
Zentralinst. fuer Elektronenphysik

Nicklisch, Peter BERLIN Hausvogteiplatz 5/7 GDR 1086
Zentralinst. fuer Elektronenpsysik

Wolff, H. Dr. BERLIN Hausvogteiplatz 5/7 GDR 1086
Zentralinst. fuer Elektronenpsysik

Alper,B. ABINGDON OX14 3DB GREAT BRITAIN
Culham Laboratory

Behringer, Kurt ABINGDON, OXON OX 14 3 EA GREAT BRITAIN
JET JOINT Undertaking

Bickerton, Roy John ABINGDON, OXON OX 14 3 EA GREAT BRITAIN
JET JOINT Undertaking

Bishop, C. ABINGDON, OXON OX 14 3 DB GREAT BRITAIN
UKAEA Culham Laboratory

Brusati, M. ABINGDON, OXON OX 14 3 EA GREAT BRITAIN
JET JOINT Undertaking

Bures, Miroslav ABINGDON,OXON OX14 3EA GREAT BRITAIN
JET Joint Undertaking

Campbell, D. ABINGDON, OXON OX 14 3 EA GREAT BRITAIN
JET JOINT Undertaking

Carolan, Patrick ABINGDON, OXON OX 14 3 DB GREAT BRITAIN
UKAEA Culham Laboratory

Christiansen, Jes Peter ABINGDON, OXON OX 14 3 EA GREAT BRITAIN
JET JOINT Undertaking

Coad, Joseph Paul ABINGDON OXON OX14 3 EA GREAT BRITAIN
JET

Cordey, J. Geoffrey ABINGDON, OXON OX 14 3 EA GREAT BRITAIN
JET JOINT Undertaking

Corti, Sergio ABINGDON, OXON OX 14 3 EA GREAT BRITAIN
JET JOINT Undertaking

Costley, A. E. ABINGDON, OXON OX14 3DB GREAT BRITAIN
JET Joint Undertaking

Cox, M. ABINGDON, OXON OX 14 3 DB GREAT BRITAIN
UKAEA Culham Laboratory

De Kock, L.C.J.M. ABINGDON, OXON OX 14 3 EA GREAT BRITAIN
JET JOINT Undertaking

Denne, Boel ABINGDON OXON OX14 3EA GREAT BRITAIN
JET

Dietz, K.J. ABINGDON, OXON OX 14 3 EA GREAT BRITAIN
JET JOINT Undertaking

Duesch, Diethelm F. ABINGDON, OXON OX 14 3 EA GREAT BRITAIN
JET JOINT Undertaking

Edlington, Trevor ABINGDON, OXON OX 14 3 DB GREAT BRITAIN
UKAEA Culham Laboratory

Edwards, David N ABINGDON, OXON OX 14 3 DB GREAT BRITAIN
UKAEA Culham Laboratory

Ehrenberg, J. ABINGDON, OXON OX 14 3 EA GREAT BRITAIN
JET JOINT Undertaking

Engelhardt, W. ABINGDON, OXON OX 14 3 EA GREAT BRITAIN
JET Joint Undertaking

Evans, R.G. CHILTON,DIDCOT OX11 OQX GREAT BRITAIN
Rutherford Appleton Laboratory

Fielding, S.J. ABINGDON, OXON OX 14 3 DB GREAT BRITAIN
UKAEA Culham Laboratory

Gambier, D.J. ABINGDON, OXON OX 14 3 EA GREAT BRITAIN
JET JOINT Undertaking

Gee, Steven ABINGDON OX14 3BD GREAT BRITAIN
Culham Laboratory

Gibson, Alan ABINGDON, OXON OX 14 3 EA GREAT BRITAIN
JET JOINT Undertaking

Gill, Richard ABINGDON, OXON OX 14 3 EA GREAT BRITAIN
JET JOINT Undertaking

Gottardi, N. ABINGDON, OXON OX14 3DB GREAT BRITAIN
JET Joint Undertaking

Green, E.J. ABINGDON, OXON OX 14 3 EA GREAT BRITAIN
JET JOINT Undertaking

Haines, Malcolm G LONDON SW7 2BZ GREAT BRITAIN
Imperial College Plasma Physics
(Blackett Laboratory)

Harbour, P.J. ABINGDON, OXON OX14 3DB GREAT BRITAIN
Culham Laboratory

Hawkes, N.C. ABINGDON OX14 3DB GREAT BRITAIN
Culham Laboratory

Hellsten, T. ABINGDON, OXON OX 14 3 EA GREAT BRITAIN
JET JOINT Undertaking

Hemsworth, R.S. ABINGDON, OXON OX 14 3 EA GREAT BRITAIN
JET JOINT Undertaking

Howling, A. ABINGDON OX14 3BD GREAT BRITAIN
Culham Laboratory

Hugill, J. ABINGDON, OXON OX 14 3 DB GREAT BRITAIN
UKAEA Culham Laboratory

Hugon, M. ABINGDON, OXON OX 14 3 EA GREAT BRITAIN
JET JOINT Undertaking

Jacquinot, J. ABINGDON, OXON OX 14 3 EA GREAT BRITAIN
JET JOINT Undertaking

Jarvis, O.N. ABINGDON, OXON OX 14 3 EA GREAT BRITAIN
JET JOINT Undertaking

Johnson, P.Ch. ABINGDON, OXON OX 14 3 DB GREAT BRITAIN
UKAEA Culham Laboratory

Keen, B.E. ABINGDON, OXON OX 14 3 EA GREAT BRITAIN
JET JOINT Undertaking

Magyar, G. ABINGDON, OXON OX 14 3 EA GREAT BRITAIN
JET JOINT Undertaking

Matthews, G. F. ABINGDON, OXON OX14 3DB GREAT BRITAIN
Culham Laboratory

McCracken, G.M. ABINGDON, OXON OX 14 3 DB GREAT BRITAIN
UKAEA Culham Laboratory

Mondino, Pier Luigi ABINGDON, OXON OX 14 3 EA GREAT BRITAIN
JET JOINT Undertaking

Morgan, Philip ABINGDON, OXON OX 14 3 EA GREAT BRITAIN
JET JOINT Undertaking

Morris, A W ABINGDON, OXON OX 14 3 DB GREAT BRITAIN
UKAEA Culham Laboratory

O'Brien, Martin ABINGDON, OXON OX 14 3 DB GREAT BRITAIN
UKAEA Culham Laboratory

O'Rourke, J. ABINGDON, OXON OX 14 3 EA GREAT BRITAIN
JET Joint Undertaking
K1/1/54

Pease, Rendel Sebastian ABINGDON, OXON OX 14 3 DB GREAT BRITAIN
United Kingdom Atomic Energy Authority

Rebut, P.H. ABINGDON, OXON OX 14 3 EA GREAT BRITAIN
JET JOINT Undertaking

Schueller, F. ABINGDON, OXON OX 14 3 EA GREAT BRITAIN
JET JOINT Undertaking

Simonini, R. ABINGDON, OXON OX14 3DB GREAT BRITAIN
JET Joint Undertaking

Stamp, Michael ABINGDON, OXON OX 14 3 EA GREAT BRITAIN
JET JOINT Undertaking

Stangeby, Peter ABINGDON, OXON OX 14 3 EA GREAT BRITAIN
JET JOINT Undertaking

Stott, Peter ABINGDON, OXON OX 14 3 EA GREAT BRITAIN
JET JOINT Undertaking

Stringer, TED ABINGDON, OXON OX 14 3 EA GREAT BRITAIN
JET JOINT Undertaking

Sweetman, Donald ABINGDON, OXON OX 14 3 DB GREAT BRITAIN
UKAEA Culham Laboratory

Tanga, A. ABINGDON, OXON OX 14 3 EA GREAT BRITAIN
JET JOINT Undertaking

Taroni, Adolfo ABINGDON, OXON OX 14 3 EA GREAT BRITAIN
JET JOINT Undertaking

Taylor, J.B.,F.R.S.	ABINGDON, OXON UKAEA	OX 14 3 DB Culham Laboratory	GREAT BRITAIN	
Thomas, Paul	ABINGDON, OXON JET JOINT Undertaking	OX 14 3 EA	GREAT BRITAIN	
Thyagaraja, A.	ABINGDON, OXON Culham Laboratory	OX 14 3DB	GREAT BRITAIN	
Todd, Thomas	ABINGDON, OXON UKAEA	OX 14 3 DB Culham Laboratory	GREAT BRITAIN	
Toner, W	CHILTON,DIDCOT Rutherford Appleton Laboratory	OX11 OQX	GREAT BRITAIN	
Wesson, J.A.	ABINGDON, OXON JET JOINT Undertaking	OX 14 3 EA	GREAT BRITAIN	
Abonyi Ivan	BUDAPEST Eotvos Lorand Tudomanyegyetem Elmeleti Fizika Tanszek	Puskin u. 5-7 Termeszettudomanyi Kar	HUNGARY	1088
Ag Arpad	BUDAPEST KFKI	P.F. 49	HUNGARY	1525
Bakos Jozsef	BUDAPEST KFKI	P.F. 49	HUNGARY	1525
Burger Gabor	BUDAPEST KFKI	P.F. 49	HUNGARY	1525
Czibolya Laszlo	BUDAPEST Orszagos Atomenergia Bizottsag	Tanacs korut 9	HUNGARY	1075
Foldes Istvan	BUDAPEST KFKI	P.F. 49	HUNGARY	1525
Fried Miklos	BUDAPEST KFKI	P.F. 49	HUNGARY	1525
Hajdu, Csaba	BUDAPEST KFKI	P.F. 49	HUNGARY	1525
Hordosy Gabor	BUDAPEST KFKI	P.F. 49	HUNGARY	1525
Hrehuss Gyula	BUDAPEST KFKI	P.F. 49	HUNGARY	1525
Ignacz Peter	BUDAPEST KFKI	P.F. 49	HUNGARY	1525
Jaroli Erika	BUDAPEST KFKI	P.F. 49	HUNGARY	1525

Kardon Bela	BUDAPEST KFKI	P.F. 49 RMKI	HUNGARY	1525
Kiraly Peter	BUDAPEST KFKI	P.F. 49	HUNGARY	1525
Kostka Pal	BUDAPEST KFKI	P.F. 49	HUNGARY	1525
Kotay Endre	BUDAPEST KFKI	P.F. 49	HUNGARY	1525
Kovacs Zsolt	BUDAPEST KFKI	P.F. 49	HUNGARY	1525
Lajtai, Albert	BUDAPEST KFKI	P.F. 49	HUNGARY	1525
Lohner Tivadar	BUDAPEST KFKI	P.F. 49	HUNGARY	1525
Manuaba Asrama	BUDAPEST KFKI	P.F. 49	HUNGARY	1525
Mezey Gabor	BUDAPEST KFKI	P.F. 49 RMKI	HUNGARY	1525
Montvai Attila	BUDAPEST KFKI	P.F. 49	HUNGARY	1525
My, N.T.	BUDAPEST KFKI	P.F. 49	HUNGARY	1525
Nagy Denes Lajos	BUDAPEST KFKI	P.F. 49	HUNGARY	1525
Palla, Gabriella	BUDAPEST KFKI	P.F. 49	HUNGARY	1525
Paris Gyula	BUDAPEST KFKI	P.F. 49	HUNGARY	1525
Paszti Ferenc	BUDAPEST KFKI	P.F. 49	HUNGARY	1525
Petravich Gabor	BUDAPEST KFKI	P.F. 49	HUNGARY	1525
Pocs Lajos	BUDAPEST KFKI	P.F. 49	HUNGARY	1525
Sorlei Zsuzsa	BUDAPEST KFKI	P.F. 49	HUNGARY	1525

Szentpetery Imre	BUDAPEST KFKI	P.F. 49	HUNGARY	1525
Szigeti Janos	BUDAPEST KFKI	P.F. 49	HUNGARY	1525
Varga Laszlo	BUDAPEST KFKI	P.F. 49	HUNGARY	1525
Vizkelethy Gyorgy	BUDAPEST KFKI	P.F. 49	HUNGARY	1525
Zoletnik Sandor	BUDAPEST KFKI	P.F. 49	HUNGARY	1525
Mond, M.	BEER SHEVA Ben Gurion University Mechanical Eng.Dept.	P.O.B. 653	ISRAEL of the Negev	84 105
Antoni, V.	PADOVA Istituto Gas Ionizzati del CNR	Via Gradenigo 6/a	ITALY	35131
Bernatici, Marino	PAVIA University of Pavia	University of Pavia Physics Department "A. Volta"	ITALY	27100
Bracco, G.	FRASCATI (Rome) Ass. EURATOM ENEA Sulla Fusione	C.P. 65	ITALY Centro Ricerche Energia Frascati	00044
Briguglio, S.	FRASCATI,ROME Associazione Euratom-ENEA Centro Richerche Energia Frascati	C.P.65	ITALY sulla Fusione	00044
Cenacchi, G.	BOLOGNA ENEA	Via Mazzini, 2 C.R.E. E. Clementel	ITALY	40138
Cima, Giuseppe	MILANO IFP	Via Bassini 15 CNR	ITALY	20133
Frigione, D.	FRASCATI,ROME Associazione Euratom-ENEA Centro Richerche Energia Frascati	C.P.65	ITALY sulla Fusione	00044
Maddaluno, Giorgio	FRASCATI ENEA		ITALY	00044
Malesani, Gaetano	PADOVA Centro di Studio sui Gas Ionizzati del CNR e dell'Universita di Padova	Via Gradenigo 6/A	ITALY	35131
Mantica, Paola	MILANO IFP	Via Bassini 15 CNR	ITALY	20133
Martini, S.	PADOVA Instituto Gas Ionizzati del CNR	Via Gradenigo 6A	ITALY	35131
Miano, Giovanni	NAPLES Dipartimiento Elettrico University of Naples		ITALY per l'Energia	

Minardi, Ettore MILANO Via Bassini 15 ITALY 20133
CNR-EURATOM

Nalesso, G.F. PADOVA Via gradenigo, 6/a ITALY 35100
Instituto di Elettrotecnica ed Elettronica
Universita di Padova

Ortolani, Sergio PADOVA Via Gradenigo 6/a ITALY 35131
Instituto Gas Ionizzati del CNR

Pegoraro, F. PISA Piazza del Cavalieri 7 ITALY 56100
Scuola Normale Superiore

Pericoli Ridolfini, V. FRASCATI (Rome) C.P. 65 ITALY 00044
Ass. EURATOM ENEA Sulla Fusione Centro Ricerche Energia Frascati

Puiatti, S. PADOVA Via Gradenigo 6A ITALY 35131
Instituto Gas Ionizzati del CNR

Rubinacci, Guglielmo NAPOLI Via Claudio 21 ITALY 80125
Universita di Napoli Istituto di Elettronica

Scarin, Paolo PADOVA Via Gradenigo 6/A ITALY 35100
Ist. Gas Ionizzati(C.N.R.)

Tuccillo, A. A. FRASCATI (Rome) C.P. 65 ITALY 00044
Ass. EURATOM ENEA Sulla Fusione Centro Ricerche Energia Frascati

Abe Mitsushi Ibaraki-ken JAPAN 316
Hitachi, Ltd. Energy Res. Lab.
1168 Moriyama-cho

Asakura, N. TOKYO Hongo 7-3-1,Bunkyo-ku JAPAN
University of Tokyo

Etsuo, Fujiwara SUITA,OSAKA JAPAN
Insitute of Laser Engineering Osaka University

Fujita Junji NAGOYA Furocho, Chikusaku JAPAN 464
Institute of Plasma Physics Nagoya University

Fukuyama, A. OKAYAMA 700 JAPAN
Okayama University Department of Electronics
3-1-1,Tsushima-Naka

Hoshino Katsumichi IBARAKI-KEN Tokai-Mura JAPAN
Japan Atomic Energy Research Institute

Itoh, S.I. HIROSHIMA 730 JAPAN
Hiroshima University Institute for Fusion Theory
1-1-89,Higashi-senda,Naka-ku

Kawata, Shigeo YOKOHAMA 227 Nagatsua, Midori-ku JAPAN
Department of Energy Sciences Tokyo Institute of Technology

Kumazawa, R. NAGOYA 464 JAPAN
Institute of Plasma Physics Nagoya University
Chikusa-ku

Mase Atsushi SAKURA-MURA IBARAKI 1-1-1, Tennodai JAPAN 305
Plasma Research Center University of Tsukuba

Motojima, O. KYOTO 611 JAPAN
Kyoto University Plasma Physics Laboratory
Gokasho,Uji

Nagao, Shigeo KASUGAI-SHI 487 JAPAN
Chubu University

Ninomiya, Hiromasa IBARAKI-KEN Naka-machi,Naka-gun JAPAN 311-02
Naka Fusion Research Establishment
JAERI

Nishikawa, Masana TOKYO JAPAN 105
Mitsubishi Atomic Power Industries, Inc. (MAPI)

Saito Katunori TOKYO Chiyoda-ku TOKYO 101 JAPAN
Nihon University Atomic Energy Research
Institute Kanda-Surugadai

Shimizu Katsuhiro IBARAKI-KEN Naka-Machi, Naka-Gun JAPAN 311-02
Japan Atomic Energy Research Institute
Fusion Research Center Mukouyama

Shoji Teruaki IBARAKI-KEN Tokai-mura,Naka-gun JAPAN
Japan Atomic Energy Research Institute
Tokai-mura,Naka-gun

Shoji, Tatsuo NAGOYA Furocho, Chikusaku JAPAN 464
Institute of Plasma Physics Nagoya University

Toyama Hiroshi TOKYO Bunkyo-ku JAPAN 113
University of Tokyo Department of Physics
Faculty of Science

Tsuji, S IBARAKI JAPAN 311-02
Japan Atomic Energy Research Inst.
Naka-machi, Naka-gun

Tsunematsu, T. IBARAKI JAPAN 319-11
Japan Atomic Energy Research Institute
Tokai, Naka

Uo, Koji KYOTO 611 JAPAN
Kyoto University Plasma Physics Laboratory
Gokasho,Uji

Yokoyama, M. OSAKA 565 JAPAN
Osaka University Institute of Laser Engineering
1-1, Yamada-oka, Suita

Yoshikawa, M. IBARAKI-KEN 311-02 JAPAN 92139
Japan Atomic Energy Research Institute
Mukouma,Naka-Machi,Naka-Gun

Alabyad, A. M. TAJURA, TRIPOLI P.O.B. 397 LIBYA
P.P.D. TNRC

Berge, G. BERGEN Allegb. 53/55 NORWAY 5000
University of Bergen Department of Applied Mathematics

Denus, Slawomir WARSAW P.O.B.49 POLAND 00908
Inst. of Plasma Physics and Laser Microfusion

Fiedorowicz, H. WARSAW P.O.Box 49 POLAND 00 908
Institute of Plasma Physics and Laser Microfusion

Kozlarkiewicz, W. WARSAW P.O.Box 49 POLAND 00 908
Institute of Plasma Physics and Laser Microfusion

Sadowski, Marek OTWOCK-SWIERK POLAND 05400
Institute for Nuclear Studies

Wolowski, J. WARSAW P.O.B.49 POLAND 00908
Institute of Plasma Physics and Laser Microfusion

Wolski, Janusz WARSAW P.O.B.49 POLAND 00908
Inst. of Plasma Physics and Laser Microfusion

Dumitrescu-Zoita, Carmen BUCHAREST ROMANIA 76900
Central Institute of Physics

Novac, Bucur-Mircea BUCHAREST ROMANIA 76900
Central Institute of Physics

Zambreanu, Viorel BUCHAREST ROMANIA 76900
Central Institute of Physics

Zoita, V. BUCHAREST P.O.B.MG-7 ROMANIA 76900
Central Institute of Physics State Committee for Nuclear Energy

Michaelis, Maximilian DURBAN SOUTH AFRICA

Alvarez Rivas, J.L. MADRID Complutense 22 SPAIN 28040
Junta de Energia Nucleaar Div. Fusion Termonuclear

Guasp Perez, J. MADRID 3 Complutense 22 SPAIN 280407
Junta de Energia Nuclear Dis. Fusion Termonuclear

Pardo Sanjurjo, Cecilia MADRID SPAIN 28040
Div. Fusion Junta de Energia Nuclear

Perez-Navarro, Angel MADRID Av. Complutense 22 SPAIN 28040
TJ-1 Group Junta de Energia Nuclear
Division de Fusion

Zurro Hernandez, B. MADRID 3 Complutense 22 SPAIN 28040
Junta de Energia Nuclear Dis. Fusion Termonuclear

Anderson, Dan GOTEBORG Chalmers Univ. of Techn. SWEDEN 41296
Chalmers University of Technology Electrom. Field Theory

Andersson, Per GOTEBORG Chalmers Univ. of Techn. SWEDEN 41296
Chalmers University of Technology Electrom. Field Theory

Bonnevier, Bjoern STOCKHOLM SWEDEN 10044
Royal Institute of Technology

Eriksson, G.	UPPSALA	Box 534	SWEDEN	S-751	
	Uppsala University		Department of technology		
Karlson, Erik T.	UPPSALA	Box 534	SWEDEN	75121	
	Uppsala University		Dept. of Technology		
Lisak, Mietek	GOTEBORG	Chalmers Univ. of Techn.	SWEDEN	41926	
	Chalmers University of Technology		Electrom. Field Theory		
Persson, Hans	STOCKHOLM 70	Drottning Kristinas V.25	SWEDEN	100044	
	KTH Fusionsforskning				
Wahlberg, Christer	UPPSALA	Box 534	SWEDEN	75121	
	Institute of Technology		Uppsala University		
Weiland, Jan	GOTEBORG	Chalmers Univ. of Techn.	SWEDEN	41926	
	Chalmers University of Technology		Electrom. Field Theory		
Wilhelmsson, Hans	GOTEBORG	Chalmers Univ. of Techn.	SWEDEN	41926	
	Chalmers University of Technology		Electrom. Field Theory		
Witalis, E.A.	STOCKHOLM	P.O. Box 27322	SWEDEN	10254	
	National Defence		Research Institute		
Appert, Kurt	LAUSANNE	21, Av. des Bains	SWITZERLAND	1007	
	CRPP - EPFL				
Collins, George A.	LAUSANNE	21, Av. des Bains	SWITZERLAND	1007	
	CRPP - EPFL				
Heym, Alexandre	LAUSANNE	21, Av. des Bains	SWITZERLAND	1007	
	CRPP - EPFL				
Hofmann, Ferdinand	LAUSANNE	21, Av. des Bains	SWITZERLAND	1007	
	CRPP - EPFL				
Joye, Bernard	LAUSANNE	21, Av. des Bains	SWITZERLAND	1007	
	CRPP - EPFL				
Keller, Robert	LAUSANNE	21, Av. des Bains	SWITZERLAND	1007	
	CRPP - EPFL				
Nowak, Stefan	FRIBOURG		SWITZERLAND	1700	
	Dept. of Physics		Univ. of Fribourg		
	Perolles				
Pochelon, A	LAUSANNE	21 av. des Bains	SWITZERLAND	CH-100	
	CRPP-EPFL		Euratom-Switzerland Association		
Thomas, G.	PETIT-LANCY 2	P.O.Box 69	SWITZERLAND	1213	
	EPS Main Secretariat		Executive Secretary		
Troyon, Fancis	LAUSANNE	21, Av. des Bains	SWITZERLAND	CH1007	
	CRPP - EPFL				

Turnbull, A.D. LAUSANNE 21, Av. des Bains SWITZERLAND 1007
CRPP - EPFL

Barbian, E.P. UTRECHT THE NETHERLANDS
FOM-Institute for plasmaphysics

Bobeldijk, C. NIEUWEGEIN Postbus 7 THE NETHERLANDS 3430AA
FOM-Institut voor Plasmafysica

Braams, Bastian J. NIEUWEGEIN postbus 7 THE NETHERLANDS 3430
FOM-INSTITUT voor Plasmafusica

Braams, C.M. NIEUWEGEIN Postbus 7 THE NETHERLANDS 3430
FOM-Institut voor Plasmafysica

Brandt, Berthold NIEUWEGEIN P.O.Box 1207 THE NETHERLANDS 3430BE
FOM-Instituut voor Plasmafysica "Rijnhuizen"

Eggen, J B H M NIEUWEGEIN P.O.Box 1207 THE NETHERLANDS 3430BE
FOM-Instituut voor Plasmafysica "Rijnhuizen"

Engelmann, Folker NIEUWEGEIN(JUTPHAAS) Postbus 1207 THE NETHERLANDS 3430BE
FOM-Institut voor Plasmafysica

Goedbloed, J.P. NIEUWEGEIN Postbus 1207 THE NETHERLANDS 3430BE
FOM-Institut voor Plasmafysica

Goedheer, W. J. NIEUWEGEIN P.O.B. 1207 THE NETHERLANDS 3430BE
FOM Rijnhuizen Institut v. Plasmafysica

Kistemaker, J. AMSTERDAM P.O.B.41883 THE NETHERLANDS 1009
FOM Institute for Atomic and Molecular Physics

Lok, Jaap NIEUWEGEIN P.O.Box 1207 THE NETHERLANDS 3430BE
FOM-Instituut voor Plasmafysica "Rijnhuizen"

Lopes Cardozo, N.J. NIEUWEGEIN(JUTPHAAS) Postbus 7 THE NETHERLANDS 3430
FOM-Institut voor Plasmafysica

Niestadt, Rob NIEUWEGEIN P.O.Box 1207 THE NETHERLANDS 3430AA
FOM-Instituut voor Plasmafysica "Rijnhuizen"

Oomens,A.A.M. NIEUWEGEIN Postbus 1207 THE NETHERLANDS 3430
FOM-Institut voor Plasmafysica

Piekaar, H. W. NIEUWEGEIN OX14 3EA THE NETHERLANDS 3430AA
FOM Institute for Plasma Physics

Polman, R.W. NIEUWEGEIN Postbus 1207 THE NETHERLANDS 3430
FOM-Institut voor Plasmafysica

Schep, T.J. NIEUWEGEIN Postbus 1207 THE NETHERLANDS 3430
FOM-Institut voor Plasmafysica

Schram, D.C. EINDHOVEN P.O.B.513 THE NETHERLANDS 5600
Eindhoven University of Technology

Tubbing, Ben NIEUWEGEIN P.O.Box 1207 THE NETHERLANDS 3430AA
FOM-Instituut voor Plasmafysica "Rijnhuizen"

Van Toledo, Wiebe NIEUWEGEIN P.O.Box 1207 THE NETHERLANDS 3430BE
FOM-Instituut voor Plasmafysica "Rijnhuizen"

Weening, M.P.H. EINDHOVEN THE NETHERLANDS 5612AZ
University of Techn. Eindhoven

van der Meer, Alexander NIEUWEGEIN P.O.Box 1207 THE NETHERLANDS 3430BE
FOM-Instituut voor Plasmafysica "Rijnhuizen"

Sinman, Sadrettin ANKARA TURKEY
Turkish Physical Society

Berk, H.L. AUSTIN,TEXAS USA 78712
University of Texas at Austin Fusion Research Center

Blanken, Ronald A WASHINGTON DC USA 20545
U.S.Department of Energy

Boozer, Allen H. PRINCETON, NJ P.O.B.451 USA 08544
Princeton Plasma Physics Lab.

Bostick, W PRINCETON, NJ P.O.B. 451 USA 08544
Plasma Physics Laboratory Princeton University

Callen, J.D. MADISON,WISCONSIN 425 Eng. Res. Bldg. USA 53706
University of Wisconsin Nuclear Engineering Department

Conrad, H USA

Demeter, Laszlo SAN LEANDRO, CALIF. USA 94577
Physics International, Co.

Drummond, W.E. AUSTIN,TEXAS USA 78712
University of Texas at Austin Fusion Research Center

Fried, B.D. LOS ANGELES,CA 1-130 Knudsen Hall USA 90024
University of California, Los Angeles

Furth, H.P. PRINCETON,NEW JERSEY P.O.B.451 USA 08544
Princeton University Princeton Plasma Physics Laboratory

Gross, R.A. NEW YORK,NY USA 10027
Columbia University Scholl of Engineering and Applied Science

Hickok, R.L. TROY,NEW YORK USA 12181
Rensselaer Polytechnic Institute Plasma Dynamics Laboratory

Hoida, Hiroshi W. LOS ALAMOS,NM USA 87545
Los Alamos National Lab. CTR-5

Hosea, J.C. PRINCETON,NEW JERSEY P.O.B.451 USA 08544
Princeton University

Isler, Ralph OAK RIDGE, TENNESSEE P.O.Box Y USA 37831
Martin Marietta Energy Systems Oak Ridge National Laboratory
Bldg. 9201-2, MS 2

Kammash, Terry ANN ARBOR,MICHIGAN USA 48109
University of Michigan Department of Nuclear Engineering
Cooley Building North Campus

Knowlton, S CAMBRIDGE,MASS USA
Plasma Fusion Center MIT

Kritz, Arnold NEW YORK NY 695 Park Avenue USA 10021
Hunter College (CUNY) Department of Physics

Litwin, C. MADISON, WISCONSIN USA 53706
Nuclear Engineering Department University of Wisconsin-Madison

Lohr, J. SAN DIEGO Ca. Box 85608 USA 92138
GA Technologies

McGuire, K.M. PRINCETON,NEW JERSEY P.O.B.451 USA 08544
Princeton University Plasma Physics Laboratory

McKenna, Kenneth LOS ALAMOS NM Box 1663 CTR-3 , F639 USA 81545
Los Alamos National Laboratory

Medley, S.S. PRINCETON,NJ USA 08544
Princeton Plasma Physics Lab. Princeton Univ.

Murakami, M. PRINCETON, NJ P.O.Box 451 USA 08544
Princeton Plasma Physics Laboratory

O'Connor, G WASHINGTON USA 20850
Iterscience

Ohkawa, T. SAN DIEGO,CALIFORNIA P.O. Box 85608 USA 92138
GA Technologies Inc.

Oktay, Erol WASHINGTON,D.C. USA 20545
U.S. Dept. of Energy Office of Fusion Energy
Div.of Toroidal Confinement Systems

Peng, Y.K.M. OAK RIDGE,TENNESSEE 104 Union Valley Road USA 37831
Oak Ridge National Lab.

Phillips, M. W. PRINCETON, N.J. 105 College Road East USA 08540
Grumman Aerospace Corporation

Rej, Donald J. LOS ALAMOS, N.M. P.O.B. 1663 USA 87545
Los Alamos National Lab.

Riedel, Kurt	NEW YORK NY New York University	251 Mercer Str	USA	10012
Scharer, J.	MADISON,WISCONSIN University of Wisconsin		USA	53706
Schmidt, G. Prof.	PRINCETON, NJ Plasma Physics Laboratory	P.O.B. 451 Princeton University	USA	08544
Shanny, R.A.	LA JOLLA,CALIFORNIA INESCO Inc.	7033 Via Estrada	USA	92037
Shohet,J. Leon	MADISON,WISCONSIN University of Wisconsin	1415 Johnson Drive Torsatron/Stellarator Laboratory	USA	53706
Sigmar, D.J.	CAMBRIDGE, Mass. Massachusetts Inst. Techn. Plasma Fusion Center	Room NW16-243	USA	02139
Stevens, J.E.	PRINCETON, NJ Princeton Plasma Phys. Lab.		USA	08544
Takahashi, H.	PRINCETON, NJ Plasma Physics Laboratory	P.O.B. 451 Princeton University	USA	08544
Taylor, Robert J	LOS ANGELES,CA University of California,	2567 Boelter Hall Los Angeles	USA	90024
Weber, P.	LOS ALAMOS, NM Los Alamos National Laboratory	MS F 639 Group CTR-8	USA	87545
Andryukhina, E.D.	MOSCOW General Physics Institute	USSR Academy of Sci.	USSR	
Bogdanov, V A			USSR	
Bulanin, V.V.	LENINGRAD M.I. Kalinin Polytechnical	Institute,Leningrad	USSR	
Burtsev, V.A.	LENINGRAD D.V. Efremov Scientific Research	Inst.of Electrophysical Equipment	USSR	188631
Cindadze, N L			USSR	
Degtyarev, L.M.	MOSCOW Keldysh Institute of USSR Academy of Sciences	Applied Mathematics	USSR	
Dnestrovskij, Yu.N.	MOSCOW Kurchatov Inst. of Atomic Energy of Atomic Energy	P.O.B.3402 USSR State Commitee for Utilization	USSR	123182
Elfimov, A.G.	SUKHUMI Sukhumi Physical Technical Institut		USSR	

Esipchuk, Yu.V. MOSCOW P.O.B.3402 USSR 123182
Kurchatov Inst. of Atomic Energy USSR State Commitee for Utilization of Atomic Energy

Fedianin, O I MOSCOW USSR
General Physics Institute USSR Academy of Sciences

Grekov, D.L. KHARKOV USSR 310108
Kharkov Institute of Physics and Technology

IgitKhanov, Yu.L. MOSCOW P.O.B.3402 USSR 123182
Kurchatov Inst. of Atomic Energy USSR State Commitee for Utilization of Atomic Energy

Iurchenko, E I USSR

Ivanov, R.S. MOSCOW USSR 127412
Institute of High Temperatures Academy of Sciences of the USSR

Kadomtsev, B.B. MOSCOW P.O.Box 3402 USSR 123182
Kurchatov Inst. of Atomic Energy USSR State Commitee for Utilization of Atomic Energy

Kalinin, Iu G USSR

Karjavin, Iu Iu USSR

Knyazev, B. NOVOSIBIRSK 90 USSR 630090
Institute of Nuclear Physics, Siberian Div. USSR Acad. of Sci.

Kojevin, V M USSR

Kolesnichenko, Ia I KIEV USSR
Institute for Nuclear Research
Ukrainian SSR Academy of Sciences

Kudriashov, A S USSR

Kuteev, B V LENINGRAD Politekhnicheskaja 29 USSR 19525
Plasma Physics Department M.I. Kalinin Polytechnic School

Kuznecov, E I USSR

Litvak,A.G. GORKY USSR
Institute of Applied Physics USSR Acad. of Sciences

Moiseeva, M P USSR

Parail,V.V. MOSCOW USSR 123182
I.V.Kurchatov Institute of Atomic Energy

Piatak, A I			USSR	
Putvinski, S V	MOSCOW Kurchatov Institute of		USSR Atomic Energy	
Ruchko, L F			USSR	
Rudakov, L.I.	MOSCOW Kurchatov Inst. of Atomic Energy of Atomic Energy	P.O.Box 3402	USSR USSR State Commitee for Utilization	123182
Ryjov, Iu V	MOSCOW Kurchatov Inst. of Atomic Energy of Atomic Energy	P.O.Box 3402	USSR USSR State Commitee for Utilization	123182
Ryutov, D D	NOVOSIBIRSK Nuclear Physics Institute Siberian Branch	Prospect Nauki 11	USSR Academy of Sciences of USSR	630090
Scerbinin, O N			USSR	
Sigov, Iu S			USSR	
Smirnov, Iu S			USSR	
Stepanenko, M M	MOSCOW I.V. Kurchatov Institute	P.O.B 3402	USSR of Atomic Energy	123182
Strelkov, V.S.	MOSCOW Kurchatov Inst. of Atomic Energy of Atomic Energy	P.O.Box 3402	USSR USSR State Commitee for Utilization	123182
Kormendi, Ferenc	BEOGRAD		YUGOSLAVIA	11000
Miskovic, Zoran			YUGOSLAVIA	
Pesic, Slavoljub	BELGRAD Institute "B.Kidric" - Vinca	P.O.Box 522	YUGOSLAVIA Laboratory of Physics - 010	11001

PAPERS

FEATURES OF SPHERICAL TORUS PLASMAS OF ULTRA-LOW ASPECT RATIO AND LARGE ELONGATION*

Y-K. M. Peng

Oak Ridge National Laboratory
Oak Ridge, Tennessee 37831, U.S.A.

Introduction: High beta, good confinement and steady-state operation in compact configuration and at modest field have long been major goals of magnetic fusion energy research. Accomplishing these in a single device will permit cost-effective and attractive embodiments of future fusion reactors. The introduction of the spherical torus concept [1] was so motivated to a large degree. An equally important motivation is its prospect of reducing cost and time of fusion research and development. In comparison with alternate confinement concepts of RFP and spheromak, a spherical torus experiment is expected to be similar in compactness, low field, and high beta; but with better, tokamak-like confinement times by more than an order of magnitude.

The idea of very small aspect ratio (A) tokamaks per se has been discussed recently [2,3], based primarily on conventional tokamak assumptions such as high poloidal beta (β_p), modest elongation (κ), and inductive startup of the plasma current. This leads to beta values much higher than permitted by the more recent understanding of the first stability regime [4]. In contrast, the spherical torus projects high beta through naturally large κ and plasma current at a modest β_p, and stays within the first stability regime projections. The spherical torus concept is made plausible by recent progress in advanced current drive schemes, such as initiation and rampup by lower hybrid waves [5] and maintenance by oscillating fields [6] (helicity injection [7]). It permits compact long-pulse spherical tori with little or no solenoid and $A < 2$. Assuming these advanced current drive schemes, ignition spherical tori are estimated to be compact (R = 1.0 to 1.6 m) and at low fields (B_{t0} = 3 T to 2 T) [8]. In the case of small-size, low-field, and short-pulse experiments using pulsed high current density coils, full inductive current startup should remain feasible.

Natural Elongation: Free-boundary MHD equilibrium calculations show that $\kappa = 2$ occurs naturally in a spherical torus when only a dipole vertical field is applied. When a quadrupole shaping field is applied, $\kappa = 3$ can be obtained (Fig. 1). The dependence of poloidal and toroidal field coil currents on A is shown in Fig. 2 for a constant safety factor at edge (q) of 2.4. Is is seen that the total coil ampere-turns, relative to the plasma current, are reduced by more than an order of magnitude when A

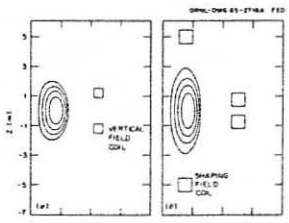

Fig. 1. Naturally elongated and strongly elongated plasma cross sections at A = 1.5.

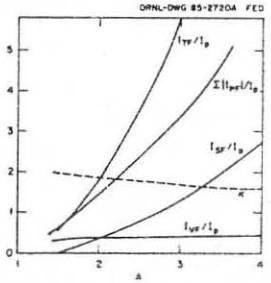

Fig. 2. Dependence of vertical field (VF), shaping field (SF), poloidal field (PF), and toroidal field (TF) coil ampere-turns, relative to the plasma current on A and κ.

*Research sponsored by the Office of Fusion Energy, U.S. Department of Energy, under Contract No. DE-AC05-84OR21400 with Martin Marietta Energy Systems, Inc.

is reduced from 4 to 1.5. The toroidal and poloidal coil currents become comparable in a spherical torus, giving comparable fields. Large elongation is a natural feature of the spherical torus.

Plasma Current and Beta: The plasma current for these equilibria can be approximated by:

$$I_p(\mathrm{MA}) = [5a(m)B_{t0}(\mathrm{T})/q][C_t\epsilon/(1-\epsilon^2)^2][(1+\kappa^2)/2] \ , \tag{1}$$

where B_{t0} is the vacuum toroidal field at the major radius R, $\epsilon = 1/A$ and $C_t = 1.22 - 0.68\ \epsilon$. Thus for a spherical torus with $A = 1.67$, $\kappa = 2$, and $q = 2.2$, we find that $I_p(\mathrm{MA})/[a(\mathrm{m})B_{t0}(\mathrm{T})] = 7$, which leads to a high potential of plasma beta in the first stability regime [4]. Recent experimental results [9] suggest that the beta limit can be approximated by:

$$\beta_c = 2\mu_0\langle P\rangle/B_{t0}^2 = 0.033 I_p(\mathrm{MA})/a(\mathrm{m})B_{t0}(\mathrm{T}) \ , \tag{2}$$

indicating β_c values above 20% for the spherical torus. That such high plasma current is permitted in a spherical torus can be seen in Fig. 3. The moderately pitched field lines in the inboard region of the spherical torus introduce a large toroidal rotation because of the relatively small toroidal circumference there, more than compensating for the small toroidal rotation due to the highly pitched field lines in the outboard region. That such a magnetic field configuration should give high beta for MHD stability can be seen also in Fig. 3. In comparison with a conventional tokamak, the spherical torus has a short field line length in the bad-curvature region relative to that in the good-curvature region.

Plasma Paramagnetism: Relative to the line-averaged poloidal field along the plasma poloidal circumference, β_p can be approximated by:

$$(\beta_p/\beta) = [5a(\mathrm{m})B_{t0}(\mathrm{T})/I_p(\mathrm{MA})]^2[(1+\kappa^2)/2] \ . \tag{3}$$

It is seen that β_p is comparable to the toroidal beta and much less than 1, leading to essentially force-free, paramagnetic equilibrium configurations. The highly pitched magnetic field lines then produce a large poloidal current that strongly enhances the toroidal field (B_t) at R. The dependence of B_t/B_{t0} on A and κ is plotted in Fig. 4, showing that it can become greater than 1.5 when A is reduced to below 2. The enhanced B_t contributes to increasing I_p for a given q. The presence of a large B_t/B_{t0} thus serves as an indicator of the spherical torus characteristics. Strong paramagnetism also introduces an important uncertainty in the application of Eq. (2) with respect to B_t and B_{t0}. The uncertainty in the limiting pressure is proportional to $(B_t/B_{t0})^3$, dependent on the definition of B on either side of Eq. (2), as long as $\beta_p < 1$.

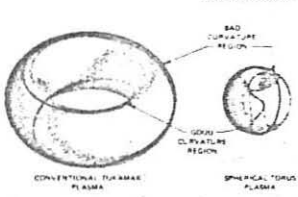

Fig. 3. The contours of mangetic field lines on the $q = 2$ surfaces of a conventional tokamak and spherical torus. The portion of the field lines in the good-curvature region is dashed.

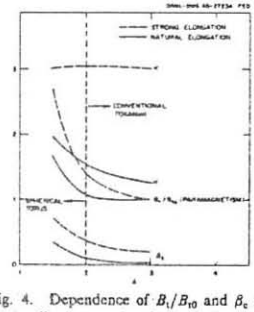

Fig. 4. Dependence of B_t/B_{t0} and β_ϵ on A for naturally elongated and $\kappa = 3$ plasmas.

Near-Omnigeneity: As shown in Fig. 5, the strongly enhanced B_t at the plasma core and the large poloidal field near the plasma edge create a strong curvature of the surfaces of $|B|$, making them largely parallel to the flux surfaces at the outboard region of the plasma. In this region, the particle drift orbits coincide with the flux surfaces since the curvature and gradient drifts are now parallel to the flux surfaces. This nearly omingeneous [10] region largely coincides with the region of bad curvature of MHD instability. This region is nearly free of locally trapped particles and hence has improved kinetic stability, although trapped particles still exist between the top and bottom regions of the plasma. These trapped particles have reduced "banana" width, leading to a reduced neoclassical transport. Since the size of the region depends on κ, β and B_t/B_{t0}, it is subject to external controls of the shaping field, plasma heating and q.

Plasma Helicity: Toroidal plasma helicity can be expressed by the helicity parameter [11], θ $(=\langle B_p\rangle_S/\langle B_t\rangle_V)$, where the subscripts S and V indicate surface and volume averages. For the spherical torus configuration ($A = 1.6$ and $\kappa = 2$), the dependence of θ on q can be plotted in the F-θ space, where the pinch parameter, F $(=\langle B_t\rangle_S/\langle B_t\rangle_V)$, depicts averaged inverse plasma paramagnetism (Fig. 6). It is seen that, as the helicity increases, the spherical torus evolves from weakly paramagnetic spherical tokamak ($q = 10$), to strongly paramagnetic spherical tokamak ($q > 1$), to spherical pinch ($1 > q > 0$), to spheromak ($q = 0$), and eventually to spherical RFP ($q < 0$). In the case of spherical tokamak, $F = 0.8$ to 0.5 and $\theta = 0.8$ to 1.5, and current maintenance via oscillating fields [7,8] is suggested. The efficacy of this approach is enhanced by its relatively modest stored magnetic flux.

Discussion: Based on a limited number of MHD equilibrium calculations, the features of the spherical torus plasma discussed here appear qualitatively different from the conventional tokamak plasmas. These features include naturally large elongation, large plasma current, high beta in the first stability regime, low poloidal beta, comparable toroidal and poloidal fields, strong paramagentism, near-omnigeneity, and strong helicity. In discussing the implications of these plasma features, much of the conventional wisdom of toroidal plasma physics is applied. Since there is no concrete data base for spherical tori, our discussions serve primarily to indicate possible important directions of theoretical analysis and experimental testing. Examples include the effects of strong paramagnetism on achievable plasma beta, the effects of near-omnigeneity on plasma kinetic properties, plasma energy confinement in these configurations of ultra-low A and high current, the efficacy of lower hybrid wave and oscillating

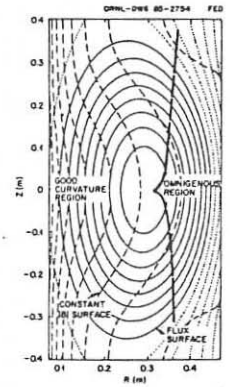

Fig. 5. Configurations of spherical torus plasma flux surfaces (solid and dotted lines) and $|B|$ -surfaces (dashed lines). The near-omnigeneous region is to the right of the bold dashed line.

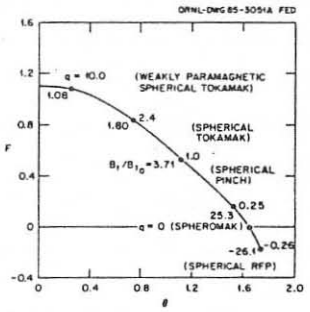

Fig. 6. The dependence of F and θ on q in a spherical torus configuration with $A = 1.6$ and $\kappa = 2$.

field current drive, and the viability of the spherical pinch and spherical RFP configurations. The attractiveness of the spherical torus as a compact magnetic fusion concept depends on the resolution of such questions as these.

The author wishes to thank T. E. Shannon, E. A. Lazarus, and J. Sheffield for stimulating discussions, and D. J. Strickler and J. B. Miller for equilibrium computations.

References:

[1] Y-K. M. Peng, ORNL/FEDC-84/7 (1985).
[2] D. L. Jassby, Comm. Plasma Phys. and Contr. Fusion, 3, 151 (1978).
[3] Y-K. M. Peng and R. A. Dory, ORNL/TM-6535 (1978).
[4] F. Tryon et al., in *Proc. 11th Europ. Conf. on Plasma Phys. Contr. Nucl. Fusion Res., Aachen, 1983*, (European Phys. Soc., 1984), Vol 26, No. 1A, p. 209.
[5] N. J. Fisch and C. F. F. Karney, PPPL-2132 (1984).
[6] K. F. Schoenberg et al., J. Appl. Phys. 56, 2519 (1984).
[7] P. M. Bellan, Phys. Fluids 27, 2191 (1984).
[8] Y-K. M. Peng et al., paper presented at the 6th Topical Meeting on the Technology of Fusion Energy, March 3–7, 1985, San Francisco.
[9] R. D. Stambaugh et al., in *Plasma Phys. Contr. Nucl. Fusion Res., 1984*, (IAEA, Vienna 1985) Vol. 1, p. 217.
[10] D. Palumbo, Nuovo Cimento, 53, Part B, 507 (1968).
[11] J. B. Taylor, Phys. Rev. Lett. 33, 1139 (1974).

THE EFFECT OF MAGNETIC FIELD RIPPLING ON MERCIER MODE STABILITY OF FINITE-PRESSURE PLASMA IN TOROIDAL MAGNETIC TRAPS

V.V.Demchenko, A.Ya.Omel'chenko

Institute of Physics and Technology, the Ukrainian Academy of Sciences, Kharkov 310108, USSR

It has recently been shown [1] that the longitudinal rippling of the magnetic field in a low-pressure tokamak plasma produces an additional destabilizing effect on small-scale MHD modes. The aim of this paper is to investigate the finite-pressure plasma stability in rippled magnetic traps with a complicated form of a magnetic axis. The analysis of the stability is based on the methods taking into account the complicated magnetic -field geometry [2] and the rippling of a longitudinal magnetic field [1].

We assume the magnetic axis of a closed toroidal magnetic trap to be a spatial curve characterized by a curvature $k(\zeta)$ and a torsion $\varkappa(\zeta)$, where ζ is the toroidal angle. In case of an arbitrary dependence of the curvature and torsion on ζ and a strong magnetic field rippling the criterion of stability relative to the small-scale mode build-up is very cumbersome. For this reason, we restrict ourselves here to the analysis of the stability criteria for simple magnetic configurations such as tokamaks and Spitzer "figures-of-eight" filled with a finite-pressure plasma.

Let us assume that the rippling of the longitudinal magnet-

ic field is given by

$$B_0=\frac{\bar{B}}{(1+\delta)^2}\,,\quad \delta=\sum_n \delta_n e^{in\zeta}\,,\quad |\delta_n|\ll 1\,,\quad \delta_c=0\,. \tag{1}$$

In this case the MHD criterion in relation to the Mercier mode build-up has the form

$$\frac{s^2}{4}-4\beta_\theta\frac{r^2}{\bar{R}^2}\Big\{\mu_1^2+R^2\big(K^2\big)^{(\theta,\zeta)}-2\mu_1\sum_n\frac{|K_n|^2}{\mu+n}R^2+3\Big[\frac{1}{2}\mu_1^2\big(\delta^2\big)^{(\theta,\zeta)}+\Big(\frac{\partial\delta}{\partial\zeta}\Big)^{(\theta,\zeta)^2}\Big]+$$
$$+2R^2\Big[\big(K^2\delta\big)^{(\theta,\zeta)}-2\mu_1\sum_{nn_1}\Big(\frac{K_nK_{n_1}^*\delta_{n-n_1}}{\mu+n}+\text{k.c.}\Big)+\frac{1}{4}\sum_{nn_1}\frac{K_n^*K_{n_1}(n-n_1)^2}{(\mu+n)(\mu+n_1)}\delta_{n-n_1}\Big\}+$$
$$+4\beta_\theta^4\Big(\frac{r^2}{\bar{R}^2}\Big)^2\Big\{3\Big[\sum_n|X_n|^2\Big(\frac{N}{\mu+n}\Big)^3\Big]^2-\frac{\mu^4}{4}\Big[\sum_{nn_1n_2}\frac{X_n^*X_{n_1}^*X_{n_2}X_{n+n_1-n_2}}{(\mu+n_1)(\mu+n_2)(\mu+n+n_1-n_2)^2}\Big(\frac{5}{2}\frac{1}{(\mu+n)(\mu+n_2)}- \tag{2}$$
$$-\frac{3}{2}\frac{1}{(\mu+n_1)(\mu+n_2)}+\frac{1}{(\mu+n)(\mu+n_1)}+\frac{4(\mu+n+n_1-n_2)}{(\mu+n)(2\mu+n+n_1)^2}+\frac{(n-n_1)^2}{2(\mu+n)^2(\mu+n_1)(\mu+n_2)}+\text{k.c.}\Big]\Big\}>0\,.$$

where $X\equiv KR\bar{B}^{3/2}/B_0^{3/2}$, $\beta_\theta=P_cR^2/r^2\bar{B}^2\mu^2$, , the rest notation being standard (see refs. [1-2]).

It follows from eq.(2) that in traps with a spatial magnetic axis the Fourier components of the rippled magnetic field, δ_n, and of the magnetic axis curvature, K_n , get coupled. This leads to additional terms appearing in the stability criterion which are proportional to the first power of δ_n (in the tokamak case, the stability criterion involves the terms quadratic in δ_n).

Now we consider the effect of the finite plasma pressure on the Mercier mode stability in a tokamak. It is known [1] that the rippling of the longitudinal magnetic field in a tokamak plays a destabilizing role. On the other hand, as the plasma pressure grows, the effect of plasma self-stabilization takes place [3]. We shall demonstrate that this effect is also observed in a rippled tokamak. For this case criterion (2) reduces to

$$\frac{s^2}{4}-4\beta_\theta\frac{r^2}{R^2}\Big[-3+35|\delta_2|^2\Big]+6\beta_\theta^4\frac{r^4}{R^4}\Big[1+\frac{3}{64}\big(22|\delta_1|^2+24\,\mathrm{Re}\,\delta_2^2\big)\Big]>0\,, \tag{3}$$

where we took into account that in eq.(1) only $\delta_{\pm 2}$ are non-zero.

It follows from inequality (3) that the field rippling has a destabilizing effect in a low-pressure tokamak ($\beta_\theta \ll (R/a)^{2/3}$) and an inverse effect in a high-pressure tokamak ($\beta_\theta \gtrsim (R/a)^{2/3}$).

The analysis of the stability criterion (2) for traps with spatial magnetic axes has shown that the rippling of the longitudinal magnetic field in such systems exerts either a stabilizing or destabilizing effect depending on a specific geometry of the confining magnetic field and the type of the machine. In particular, for traps of the Spitzer "figure-of-eight" type $[K(\zeta) = K_0 + K_2 e^{2i\zeta}$ and a rippled longitudinal magnetic field of the form $B_0 = \bar{B}/(1 + \delta_2 e^{2i\zeta})^2$ criterion (2) implies that the effect of rippling on the Mercier mode stability is determined here by the sign and the modulus of $\mathrm{Re}\,\delta_2$.

References

1. A.B. Mikhajlovskij, Fiz. Plazmy 10 (1984) 83.

2. A.B. Mikhajlovskij, Kh.D. Aburdzhaniya, Pl. Phys. 21 (1977) 109.

3. A.B. Mikhajlovskij, V.D. Shafranov, Zh. Ehksp. Teor. Fiz. 66 (1974) 90.

THERMONUCLEAR TRAP "DRACON"

L.I.Artemenkov, T.F.Volkov, V.M.Glagolev, A.V.Dobryakov, A.E.Leneva, P.A.Mukhin, B.A.Trubnikov

I.V.Kurchatov Institute of Atomic Energy, Moscow, USSR

A closed magnetic trap "DRACON", consisting of two rectilinear equilibrium elements and of two curvilinear ones (CRELs), was suggested in the USSR, in 1981 /1,2/. The parameters of CRELs are specially chosen so that the Pfirsch-Schlüter currents are closed within CRELs themselves. For a plasma with low β and with circular magnetic surfaces, the condition mentioned has a form: $\int_{-\ell_K/2}^{\ell_K/2} K \cos\alpha \, dS = 0$ (1)

where, ℓ_K is the length of CREL, k (s) is the curvature of the magnetic axis, $\alpha(S)$ is the angle of rotational transform, S is the length of the magnetic axis arc counted off from the CREL-centre. The equilibrium value of β in CRELs and in the rectilinear equilibrium elements are practically independent under the condition (1), that allows to raise β in the rectilinear elements up to 0.4-0.5 characteristic for the mirrors. The equilibrium value of β in the rectilinear elements is independent of their length under the condition (1).

If the magnetic field in the rectilinear elements is less than the field in CRELs, at the sufficient length at rectilinear elements, when the plasma volume in them considerably exceeds the plasma volume in CRELs, the main fusion energy release will occur within the technologically simple rectilinear sections. At the same time, these sections make a small contribution into heat conduction in plasma due to the absence of the radial drift motion of particles. Thus, DRACON is a closed trap with high equilibrium β and with comparatively small energy losses due to heat conduction in plasma. The estimates for the

DRACON-reactor parameters have been done in /2/.

§ 1. Hydrodynamical plasma equilibrium

The problem of plasma equilibrium in DRACON has been solved in /2/. We have proceeded from the assumption that the plasma column with a radius a, inside the ideally-conducting case with a radius b , is in equilibrium. The calculations show that the equilibrium β in CRELs, made of toroidal and helical elements, is equal to 6-8% at k.b=1/3 and slightly dependent on the CREL-configuration. The angle of rotational transform in CREL is 190-200°.

§ 2. Plasma stabilization

According to /3/, the systems with spatial magnetic axis, at the uniform field along the axis and at circular magnetic surfaces, always have a magnetic hill, and hence they are unstable respective to perturbations of the convective type. Different methods of producing a magnetic well (D-shaped deformation of magnetic surfaces, stabilization with a quadrupole anchor or with a relativistic electron beam) have been considered in /2/.

We considered a new method of producing a magnetic well /4,5/, based on a displacement of the magnetic axis within the toroidal and helical sections of CRELs outwards from the curvature centre of the magnetic axis. A region of enhanced magnetic field extends over the magnetic surfaces at such a displacement, that results in the production of a magnetic well in the system. Such a displacement is made in the section with a curvilinear magnetic axis and with a non-uniform magnetic field along the axis (stabilizing S-mirror).

As the well is obtained at circular magnetic surfaces in the stabilization with the S-mirror, such a stabilization technique provides the following advantages:

1) low aspect ratio along the separatrix,
2) small azimuthal asymmetry of the field,
3) simplicity in the design and technology of the system as a whole,
4) possibility of designing a divertor of the toroidal type.

A general theory of the magnetic well production technique with the S-mirrors in the DRACON-trap is given in /4,5/ and different CREL-modifications are considered there.

§ 3. Plasma heat conduction

The theory of plasma heat transfer coefficients for stellarators /6/ and for helical tori /7/ is spread to the DRACON trap in /2/. In the regime of rare collisions (fusion reactor regime) under the condition

$$\omega_0 < \nu/\varepsilon_h < \varepsilon_t/\varepsilon_h t_n \qquad (2)$$

the main contribution into heat conduction is made by electrons trapped by the helical field non-uniformity in CREL, ε_h. In (2) $\varepsilon_t = a\pi/\ell_K$ is the toroidal non-uniformity of CREL, ω_0 is the azimuthal drift frequency. In this case, the plasma energy confinement time (without regard for the S-mirrors) is determined as:

$$\tau_E^{(e)} = \frac{1{,}1\cdot 10^{-23}(a^2 B_0)^2 n}{\varepsilon_h^{3/2}\,\varepsilon_t^2\,T_e^{3,5}}\left(1+\frac{\mathcal{R}\,l_0}{J_1\sqrt{2}}\right)^2 \qquad (3)$$

Here, $\mathcal{R}$ is the mean torsion of the CREL-magnetic axis, T_e is the electron temperature (keV), n is the plasma density in cm^{-3}, a is the plasma radius in cm, $\tau_E^{(e)}$ in sec* In the presence of the S-mirrors and at their high mirror ratio, the energy confinement time can drop due to a radial drift of electrons trapped within the S-mirrors in the oppositely-located CRELs. This effect can be taken into account qualitatively, when ε_h in (3) is replaced by the non-uniformity of the field in the S-mirror. Thus, it is desirable to use a stabilizer with a great number of mirrors and with low non-uniformity of the field in the S-mirrors ($\frac{n_s-1}{n_s+1} \sim \varepsilon_h$, n_s - mirror ratio).

§ 4. Principles of an experimental program

An initial stage of experiments has the following goals:

1. to find out the plasma equilibrium conditions for DRACON,
2. to study the hydrodynamical plasma stability,
3. to find out the plasma transfer coefficients.

*B_0 - the magnetic field (in T).

The solution of these problems is possible, using a plasma with hot electrons obtained by ECRH. The maximum magnetic field in the trap is 4-5 kOe, plasma density $n \simeq 5 \times 10^{11} cm^{-3}$, T_e is up to 5÷10 keV. The plasma transier coefficients in this regime are determined by the electron component of plasma; therefore, the ion temperature cannot be high: $\sim$ 100-200 eV. It is sufficient to have the plasma diameter of 10-20 cm.

The authors express their gratitude to V.D.Shafranov for his interest to this work and for useful discussions.

References

1. V.M.Glagolev, B.B.Kadomtsev, V.D.Shafranov, B.A.Trubnikov. Proc. X Europ.Conf. on Contr. Fusion and Plasma Phys. Moscow v.1, Rep. E-8, 1981.
2. V.V.Arsenin, V.M.Glagolev, B.B.Kadomtsev, V.P.Pastukhov, B.A.Trubnikov, B.D.Shafranov, Plasma Phys. and Contr. Nucl. Fusion Res. IAEA, Vienna, 1983, v.III, p.159.
3. L.S.Soloviev, V.D.Shafranov. In Voprosy teorii plasmy, issue 5, Moscow, Gosatomizdat, p.47, 1967.
4. B.A.Trubnikov, V.M.Glagolev. Fizika plasmy, v.10, issue 2, p.288, 1984.
5. B.A.Trubnikov, V.M.Glagolev, S.L.Lazarev, A.V.Dobryakov. Fizika plasmy, v.II, issue 2, p.155, 1985.
6. A.A.Galeev, R.Z.Sagdeev. Voprosy teorii plasmy, issue 7, Moscow, Gosatomizdat, p.243, 1973.
7. V.V.Nemov, Nucl. Fusion, 17, 1977, p.101.

Inertial Confinement Fusion by Short Wavelength GEKKO Series Lasers at ILE, OSAKA

E.Fujiwara, H.Azechi, H.Nishimura, N.Miyanaga, H.Niki, S.Sakabe, T.Norimatsu, T.Jitsuno, S.Ido, Y.Kitagawa, M.Nakatsuka, T.Sasaki, K.Yoshida, T.Yabe, M.Yamanaka, Y.Izawa, Y.Kato, K.Mima, T.Mochizuki, S.Nakai, K.Nishihara, T.Yamanaka and C.Yamanaka

Institute of Laser Engineering
Osaka University
Suita, Osaka, Japan

1. Introduction

In laser fusion research the wavelength scalings of laser plasma interaction and implosion dynamics are very important in order to decide the implosion scheme for the future ICF reactor. According to the recent experiments the shorter wavelength lasers have benefit of higher absorption rate, less hot electrons and higher soft X-ray generation efficiency for high Z target. In order to investigate the laser wavelength scaling of imploded plasma we are pursuing the laser-plasma interaction experiments as well as the implosion experiments by using the four wavelength lasers, 1.05, 0.53, 0.35 and 0.26 μm.

In this proceeding we describe the glass laser systems and the recent results of implosion experiments.

II. Laser systems

Three glass laser systems named GEKKO are used for the implosion experiments. The GEKKO XII, a large glass laser system of twelve beams, can deliver 30 kJ (1 nsec), 55 TW (100 psec) in 1.053 μm wavelength, and the output diameter of which is 35 cm. The second harmonic system has been completed in the GEKKO XII which uses large single KDP crystals of 38 cm in diameter. The KDP crystals are cut to type II with the thickness of 20mm. The targets are usually aligned by the fundamental wavelength laser (1.05 μm). The difference of pointing and focusing for the each wavelength (red and

green) are automatically corrected by a minicomputer. All beams are uniformly irradiated to the target through the F/3 aspheric lenses of 108 cm in focul length. The focused spot diameter of the beam is about 50 μm in red and green, respectively. The pointing accuracy is less than 20 μm for the green beams. The temperature of the target room is adjusted to the accuracy of 0.2 degree because the KDP matching angle is sensitive to the temperature. The conversion efficiency attains 80 percent in maximum and 70 to 80 percent for twelve beams. The KDP crystals have been adjusted to the mismatching angle of less than 50 μrad.

GEKKO MII glass laser is the two beam blue system which is mainly dedicated for the basic research. It can deliver 1 kJ (1 nsec) for blue. The maximum conversion efficiency of 60 percent has been attained. GEKKO IV glass laser is a four beam system in green and uv with the diameter of 10cm. This is mainly used for the fundamental experiments of laser-plasma interaction.

III. Implosion Experiments

Success in laser fusion depends on achievement of high hydrodynamic efficiency, uniform and stable implosion and suppression of fuel preheating. We have been investigating these physics for both direct and indirect irradiation scheme such as Cannonball targets. Items of our recent investigation are flux-limiting, Rayleigh-Taylor instability, hot electron generation and X-ray conversion for fundamental interaction, and comparison of final fuel density-compressed core radius product ρR and fuel temperature (neutron yield) between direct and indirect implosion. In this proceeding the flux-limiting factor measurement and X-ray conversion measurement are introduced.

(1) Energy Transport

In the strong temperature gradient the free streaming of electron $q_f = n_e T_e v_{th}$ is limited by a factor f. Large pellets are irradiated by 1.05 and 0.53 μm (500 psec), which are coated by multilayers including thin high Z tracers (CHCl or Mg, Al, Si). The X-ray streak photographs and the spectral measurements of the tracers yield the mass ablation rate and the spatial profiles of the temperature and the density of ablating plasma.

The temperature profile in Fig.1 is determined by the line ratio of Cl lines (H-α and He-α, and/or Li-like satellite He-α) and the density is obtained by the line intensity ratio of He-α and its intercombination lines. The experimental profiles are compared with the simulation results for various flux limiting factors in Fig.2. Since the measured profiles are in

the critical region, they are sensitive to the cold electron flux limiter f_c, but not to the hot electron limiter f_h. The comparisons between the experiments and simulations in Fig. 1 yield f_c = 0.06, where f_h = 0.03 in the simulation.

According to our theoretical study using Fokker-Planck simulation, the heat transfer factor f is suppressed less than the Spitzer-Harm classical heat conduction in the heated region where the temperature scale length L_T $(T_e/\nabla T_e)$ is very large and the factor f is increased in heat front where the temperature scale length is small. The experimental data are compared with the Spitzer-Harm in Fig.2.

(2) X-ray Conversion

The soft X-ray spectrum and its generation efficiency have been measured by using a transmission grating spectrometer coupled with a X-ray streak camera and the filtered fast response diodes. A gold planar target and various types of Cannonball targets are mainly used. A specially designed target has been used to study the emission dynamics in the cavity plasma.

Figure 3 shows the wavelength dependence of soft X-ray emission from Au planar target at the laser intensity of 7×10^{13} W/cm^2. The emissivity of lower energy X-ray increased with decrease of laser wavelength. For the 0.26 μm laser the emission of $h\nu$ > 1.3 keV was strongly suppressed and most of the energy was in $h\nu$ < 1 keV.

Figure 4 shows the wavelength dependence of soft X-ray generation efficiency for gold planar target. The generation efficiency decreased monotonically with increase of laser wavelength. The generation efficiency of 63 % was obtained at the 4ω laser intensity of 7×10^{13} W/cm^2. The high generation efficiency of 4ω laser is very useful for the radiation Cannonball target.

IV. Summary

The GEKKO XII glass laser (1.05 and 0.53 μm) has been operated for the implosion experiments using various targets. Excellent experiments for flux-limiting factor has been done using pellets with high Z tracers. The factor of 0.06 for 1.05 and 0.53 μm was obtained.

The shorter wavelength laser showed the higher X-ray generation efficiency. The generation efficiency of 63 % was obtained at the 4ω laser intensity of 7×10^{13} W/cm^2.

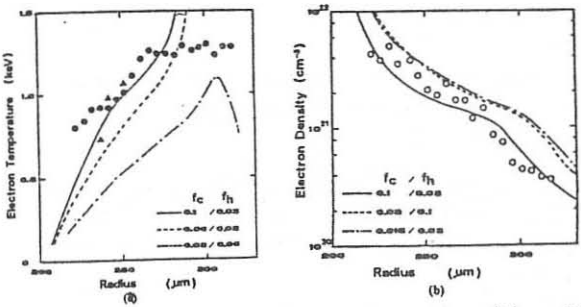

Fig.1 Electron density (a) and electron temperature (b) profile along a tracer trajectory. The symbols are experimental results and the lines are the computer simulation results.

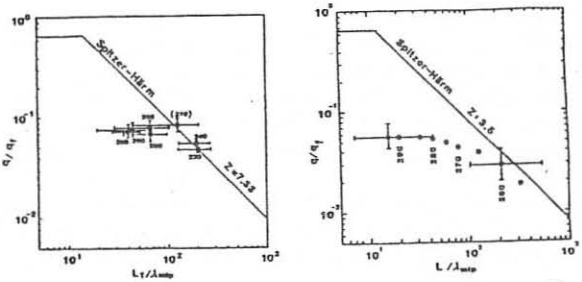

Fig.2 Normalized thermal flux q/q_f as a function of normalized temperature gradient length L_T/λ_{mfp} for 1.05 (left) and 0.53 μm (right). Number at data point indicate measurement position in micron from the target center.

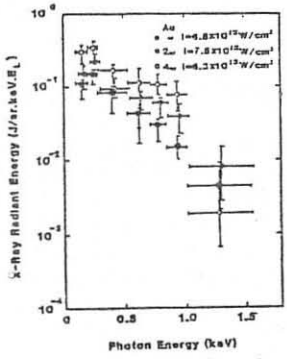

Fig.3 Laser wavelength dependence of soft X-ray spectrum obtained using gold planar targets.

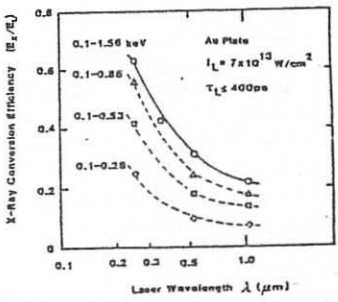

Fig.4 Laser wavelength dependence of soft X-ray generation efficiency obtained using gold planar targets.

TOROIDAL EFFECTS ON CURRENT DRIVEN FREE BOUNDARY MODES AND β OPTIMIZATION IN TOKAMAKS

A.D. Turnbull and F. Troyon
Centre de Recherches en Physique des Plasmas
Association Euratom - Confédération Suisse
Ecole Polytechnique Fédérale de Lausanne
21, Av. des Bains, CH-1007 Lausanne, Switzerland

Abstract. Recent Tokamak β optimization studies have indicated the existence of a β limit proportional to the plasma current. A new two step β optimization procedure is described that attempts to decouple kink and ballooning stability so that the two can be optimized independently. Results for the zero β case are given as a basis for clarifying the results of the optimization. Stability in a circular cross-section tokamak at zero β requires $q_{axis} > 1$, $q_{surface} > 2$ and zero current density gradient at the surface. If $q_{axis} < 1$, modes appear that are higher order in aspect ratio than the kink ordering. These have the form of internal modes inside q = 1, but are stabilized by a conducting shell. For one value of the plasma current, a β optimization is performed and this predicts an optimized, stable, circular cross-section equilibrium with a β that is 40% above the limit.

I. Motivation. The existence of a limiting β in tokamak discharges has been indicated by numerical stability optimization studies[1] and corroborated from experimental data[2,3], but the reasons for it are poorly understood. The optimization studies reported to date have been restricted to a few narrow ranges of equilibrium profiles in which the pressure gradient $p'(\psi)$ and either the toroidal field profile[1,4] $TT'(\psi)$ or the safety factor profile[5] $q(\psi)$ are specified independently, usually as expansions or exponentials in ψ. In these studies, there is limited direct control over the toroidal current density which largely determines the kink stability.

We have developed an alternative optimization procedure consisting of two "orthogonal" steps in the sense that kink and ballooning modes are stabilized independently. This is acheived by: (i) specifying $p'(\psi)$ and either $I'(\psi)$, the derivative of the current within a flux surface ψ, or equivalently $J(\psi)$, the average current density, and (ii) constructing these profiles from simple piecewise polynomials, matched to keep them differentiably continuous. The first feature provides us with the desired direct control over the toroidal current density. The second provides independent control over the centre and edge regions.

A third feature of our approach is to begin with the zero β case. We find the stability criteria at zero β and use those criteria to define an operating regime for the optimization at finite β.

II. Equilibrium and Stability. The equilibria used in the present study are computed by solving the Grad Shafranov equation with $I'(\psi) \equiv \iint j_\phi dS/r|\nabla\psi|$ (or equivalently $J(\psi) = I'(\psi)/\iint dS/r|\nabla\psi|$) specified. $p'(\psi)$ and $I'(\psi)$ are constructed from piecewise polynomials in three independent sections. For simplicity, we restrict ourselves to the forms given in figure 1 and also to circular cross-section plasmas. Stability is determined using the ERATO code[6].

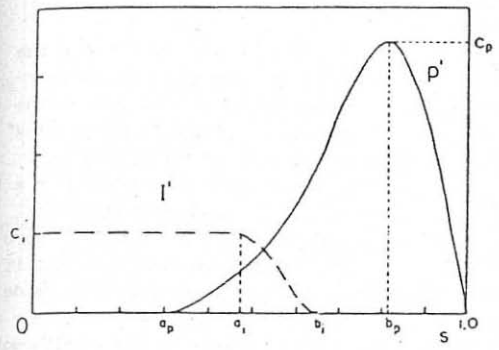

Fig. 1: Current (I') and pressure gradient (p') profiles as a function of $s = 1-\psi/\psi_o$.

If $b_I - a_I$ (Fig. 1) is held fixed, then $I'(\psi)$ has two independent parameters b_I and c_I that determine q_o and q_s, the safety factor at the axis and surface respectively, giving a two-dimensional operating space to optimize kink stability at any total current. c_p is determined by the required β_p. The two remaining parameters a_p and b_p are determined by the requirements for ballooning stability. For given total current, the optimization proceeds in two distinct steps. The β is maximized with regard to kink stability by varying the current channel width b_I, keeping the pressure gradient maintained entirely outside the current channel, thereby de-coupling the kink and ballooning driving forces. The second step stabilizes the ballooning by spreading the pressure gradient inside at constant β_p. This has a relatively small effect on the kink stability since the average current density is maintained constant. Only small adjustments are then required to obtain the optimum.

III. Current driven Modes: $\beta = 0$. The results of a parameter survey over zero β equilibria are summarized in Fig. 2. At zero β, the parameters c_I and b_I directly control q_s and q_s/q_o respectively. The third parameter a_i controls the shape of the q profile. $q_o > 1$ and $q_s > 2$ are necessary for stability. The limit shown near $q_s/q_o = 1$ is a soft limit in the sense that it is profile dependent, and, for a given class of profiles, the limit is made up of the envelope over limits for all $n > 1$.

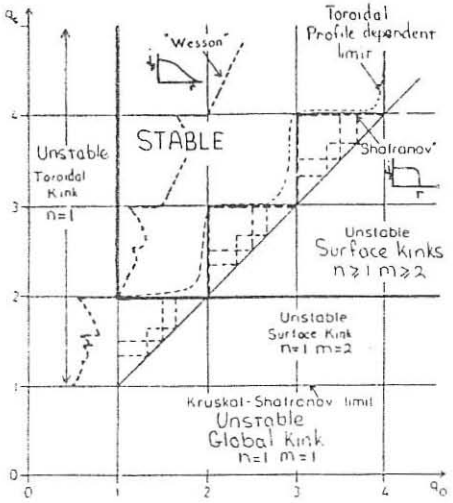

Fig. 2: Stability Diagram for Force-Free equilibria. Stability requires $q_o > 1$ and $q_s > 2$ and that q_s/q_o be larger than some value that dependes on the profiles. The lines labelled "Wesson" and "Shafranov" are the known limits for a straight tokamak for two classes of current density profile[7].

The results differ from the "straight tokamak" results reviewed by Wesson[7] notably in the appearance of the "toroidal kink" for $q_o < 1$. In the straight tokamak, this is an internal n = 1 kink that has been shown to be stabilized by toroidicity at zero β[8]. However, we find here that it reappears as a free boundary mode. The mode resembles an internal kink inside q = 1 with a large m = 1 motion near q = 1, coupled by toroidicity to an m = q component restricted almost entirely to the other integer q surfaces. Although there is very little motion of the surface, the freedom to move the surface is necessary for the mode to appear. The growth rates are higher order than $(a/R)^2$ and are therefore not seen in the standard kink ordering.

IV. Optimization. Figure 3 shows the result of increasing β_p for four different current channel widths. The current is kept constant at $I_N = \mu_o I/R_o B_o = 0.1$ and the aspect ratio is $a/R_o = 0.20$. The pressure gradient is kept outside the current channel in each case. The unstable equilibria with $q_o > 1$, $q_s > 2$ are pressure driven "ballooning-kinks" (cf. ref. 9).

To optimize β, we choose the highest β_p equilibrium that is stable according to a σ^2 criterion[10] of 10^{-4} and stable according to the zero β criteria discussed in Section III. That equilibrium (indicated as an "x" in Fig. 3) is strongly ballooning unstable. Spreading $p'(\psi)$ inside (i.e. $a_p \to 0$) at constant β_p stabilizes most of this but slightly destabilizes the kink. Decreasing β_p would stabilize both this and the residual ballooning, but does not result in the optimum β. Instead, moving b_I outwards slightly at constant β_p, raises q_o to re-stabilize the kink and the residual ballooning is then stabilized by only a small drop in β_p. The final β is only slightly lower (a few percent of the original β) than the

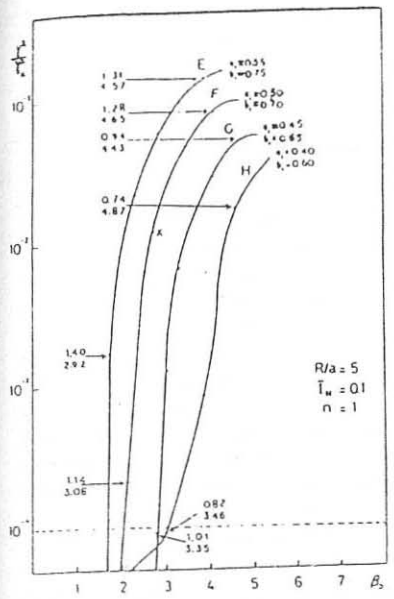

Fig. 3: β_p vs. n = 1 kink growth rate at four values of the current channel width. q_o and q_s are indicated for the endpoints of each curve.

original ballooning unstable equilibrium. A convergence study indicated no instability for $\sigma^2 > 10^{-7}$ and subsequent checks found no instability for $n > 2$.

The final stable, optimum β has $a_I = 0.47$, $b_I = 0.67$, $a_p = 0.0$, $b_p = 0.80$, $\beta_p = 2.47$ and $\beta = 1.58\%$. This is to be compared with the limiting value[1] of $\beta_T = 2.2\ I_N A = 1.1\%$. The optimum β is closer to the ballooning limit of Wesson and Sykes[11] $\beta_W = 3.6\ I_N A = 1.8\%$.

Acknowledgements. The authors have benefitted greatly from numerous discussions with colleagues A. Roy, O. Sauter and M.A. Secrétan. This work was partly supported by the Swiss National Science Foundation.

References:

[1] F. Troyon, R. Gruber, H. Saurenmann, S. Semenzato and S. Succi, Plasma Physics and Controlled Fusion, 26 (1984) 209.
[2] F. Troyon and R. Gruber, Physics Letters 110A, (1985) 29.
[3] G.H. Neilson et al., Nucl. Fusion 25 (1985) 825.
[4] F. Troyon, R. Gruber and H. Saurenmann, NET Report, EUR XII-324/14, Brussels.
L.C. Bernard et al., Nucl. Fusion 20 (1980) 1199.
W. Kerner et al., Nucl. Fusion 21 (1981) 1383.
[5] A.M.M. Todd et al., Nucl. Fusion 19 (1979) 743.
[6] R. Gruber et al., Comput. Phys. Commun. 21 (1981) 323.
[7] J.A. Wesson, Nucl. Fusion 18 (1978) 87.
[8] M.N. Bussac et al., Phys. Rev. Lett. 35 (1975) 1638.
[9] J. Manickam, Nucl. Fusion 24 (1984) 595.
[10] J.P. Goedbloed and P.H. Sanaka, Phys. Fluids 17 (1974) 908.
[11] J.A. Wesson and A. Sykes, Nucl. Fusion 25 (1984) 85.

POLOIDAL ASYMMETRY OF THE DENSITY PROFILE ASSOCIATED WITH A FLOW IN A TOKAMAK

S. Semenzato, R. Gruber, R. Iacono, F. Troyon and H.P. Zehrfeld*
Centre de Recherches en Physique des Plasmas
Association Euratom - Confédération Suisse
Ecole Polytechnique Fédérale de Lausanne
21, Av. des Bains, CH-1007 Lausanne, Switzerland

* Max-Planck-Institut für Plasmaphysik, Garching (RFA)

Abstract. In stationary Tokamak equilibria with poloidal and toroidal flows the density is no longer constant on a flux surface. The relationship between the size of the density variation and the direction and magnitude of the flow is examined. The case of a poloidal flow with no net toroidal velocity leads to a large density variation at moderate values of the Mach number. We show as an example that the reported anomalies in the density profiles measured in the PDX Tokamak in presence of strong neutral beam heating could be explained with a poloidal flow of 0.06 c_{so} and a counterstreaming toroidal flow of $< 0.20\ c_{so}$.

I. Introduction. Measurements performed on the PDX experiment with a neutral beam heating have shown strong asymmetries in the mass density profile[1]. This anomaly cannot be explained by an effect of the centrifugal force coming from a toroidal rotation, since very high and therefore easily measurable velocities of the order of the sound speed, i.e. $v_\phi \sim c_{so} = \sqrt{\gamma p_o / \rho_o}$, at the axis would be necessary. The influence of a poloidal rotation on the mass density profile was regarded to be negligible. We suggest that this may not be correct.

II. Analytic results. The magnetic flux ψ in a stationary tokamak equilibrium with poloidal and toroidal non-vanishing flow is given by the set of equations 1.

$$\nabla \cdot \left[D \frac{\nabla \psi}{r^2} \right] = - \frac{J}{r^2} \frac{dJ_M}{d\psi} - \rho \frac{dH}{d\psi} + \frac{\rho^\gamma}{\gamma - 1} \frac{dC}{d\psi} - \frac{1}{\rho} \frac{d^2 \psi_M}{d\psi^2} \left(B^2 \frac{d\psi_M}{d\psi} - \rho J \frac{d\Phi_E}{d\psi} \right)$$

$$+ \frac{d^2 \Phi_E}{d\psi^2} \left(J \frac{d\psi_M}{d\psi} - \rho r^2 \frac{d\Phi_E}{d\psi} \right)$$

$$B_p = \frac{|\nabla \psi|}{r}, \quad r B_\phi \equiv J(r,z) = \left(J_M - r^2 \frac{d\psi_M}{d\psi} \frac{d\Phi_E}{d\psi} \right) / D,$$

$$\rho v_p = B_p \frac{d\psi_M}{d\psi} ,$$

$$\rho v_\phi = B_\phi \frac{d\psi_M}{d\psi} - \rho r \frac{d\Phi_E}{d\psi} \qquad (1)$$

$$p = C\rho^\gamma$$

$$H = \frac{1}{2} B^2 \left(\frac{d\psi_M}{d\psi}\right)^2/\rho^2 - \frac{1}{2} r^2 \left(\frac{d\Phi_E}{d\psi}\right)^2 + \frac{\gamma C}{\gamma-1} \rho^{\gamma-1}$$

where J_M, ψ_M, Φ_E, C and H are five arbitrary functions of ψ and $B^2 \equiv B_\phi^2 + B_p^2$, $D \equiv 1-(d\psi_M/d\psi)^2/\rho$. For $\gamma = 1$, the last term in H must be replaced by $C\,\ell n\rho$.

With a flow, the density is no longer constant on a magnetic surface. This density variation can be characterized by the quantity

$$A = \left(\frac{d\rho}{dr}\right)_\psi \frac{R}{\rho} , \qquad (2)$$

where R is the major radius of this surface. By expanding eq. 1 around R we find that the density asymmetry can be explained by the combination of a poloidal flow v_p and a pure m = 1 toroidal flow with not net toroidal momentum[3].

$$v_\phi = \sqrt{A(A+2)}\, \frac{r-R}{R}\, c_{so}$$

$$v_p = \sqrt{\frac{A}{A+2}}\, \frac{B_p}{B}\, c_{so} \qquad (3)$$

For a circular cross-section tokamak, the toroidal flow velocity reduces to

$$v_\phi = \sqrt{A(A+2)}\, \frac{\rho_s}{R}\, c_{so} \cos\theta$$

$$v_p = \sqrt{\frac{A}{A+2}}\, \frac{\rho_s}{Rq}\, c_{so} \qquad (4)$$

where $\rho_s(\psi)$ is the radius of the ψ surface considered and θ is the poloidal angle. Note that v_ϕ vanishes on the magnetic axis.

III. Numerical results. We have developed a code CLIO[2] which solves eq. 1. For convenience, the five arbitrary functions J_M, Φ_M, Φ_E, C and H are defined by the profiles of five related equivalent quantities J, p, ρ, v_ϕ and $v_p^* \equiv \frac{v_p}{rB_p}$ on the equatorial ring between the inner surface and the magnetic axis. We apply it to fit a particular PDX equilibrium which exhibits a strong density asymmetry[1].

The following choice of the profiles

$$
\begin{aligned}
J &= J_o \ (1 + 0.0152s - 0.0148s^2 + 0.0036s^4) \\
p &= p_o \ (1 - 0.375s - 1.162s^2 + 0.263s^4 + 0.274s^6) \\
\rho &= \rho_o \ (1 - 0.371s + 0.171s^2 - 0.7s^4) \qquad (5) \\
v_\phi &= c_{so} \ (0.566s - 0.566s^2) \\
v_p^* &\equiv \frac{v_p}{rB_p} = \frac{c_{so}}{J_o} \ (0.653 + 0.399s - 1.052s^2),
\end{aligned}
$$

where the constants J_o, p_o, ρ_o and c_{so} are adjusted to reproduce the values of the current, β, density on axis and central temperature given in ref. 1, provides a good fit of the experimental profiles of the density and temperature (Fig. 1). In equation (4) $s \equiv \sqrt{(\psi-\psi_{axis})/\psi_{axis}}$. The fit has been made with $\gamma = 1.01$.

The essential features of this fit are:

- The magnetic surfaces are indistinguishable from those obtained with a static fit having the same global parameters.
- The toroidal flow is almost pure m = 1 and the maximum velocity is off-axis with $|v_p/c_{so}| < 0.2$, a value five times smaller than that required to fit the profile with a purely toroidal flow.
- The poloidal flow velocity is very small $|v_p/c_{so}| < 0.06$.

This fit is not unique but it is the one which has the lowest maximum toroidal flow velocity[3]. This example shows that an appreciable density asymmetry can reult from a small poloidal flow associated with an m = 1 toroidal flow (no net toroidal flow).

References

[1] B. Johnson et al., Plasma Physics and Controlled Nuclear Research, IAEA, Vienna (1982), Vol. 1, p. 9.

[2] S. Semenzato et al., Comp. Physics Reports, 1, 389 (1984).

[3] S. Semenzato et al., submitted for publication in Phys. of Fluids.

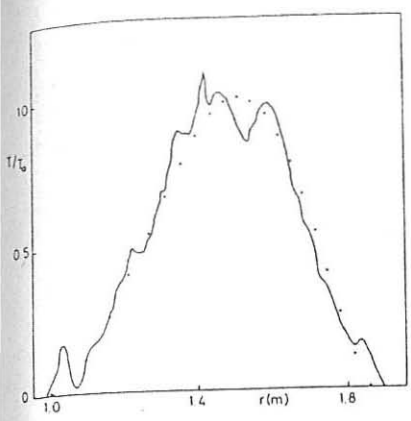

a)

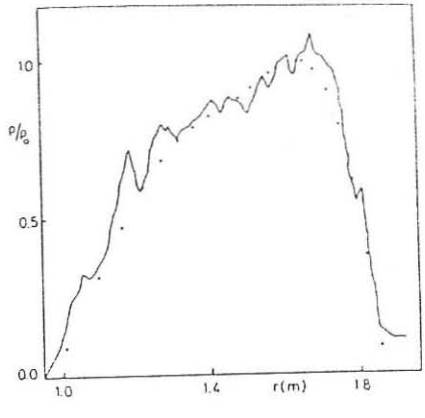

b)

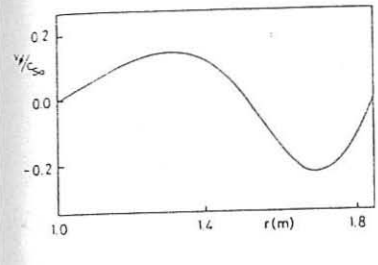

c)

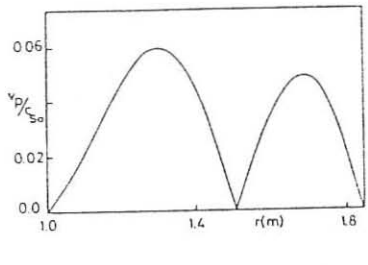

d)

Fig. 1: Profiles of temperature, density and flow velocities across the equatorial plane.

a) Electron temperature profile T/T_0. The calculated values are shown as dots. The continuous curve is a fit through the measured electron temperature profile[1]. It has been assumed that the average temperature of the fluid has the same profile as the electron temperature.

b) Mass density profile ρ/ρ_0. The calculated values are shown as dots. The continuous curve is a fit through the measured electron density profile[1].

c) and d)
Calculated toroidal v_ϕ and poloidal v_p flow velocities normalized to the sound speed on axis c_{s0}.

BALLOONING REGIME AND STIMULATED VISCOSITY IN A COMPACT TORUS

Bogdanov B.B., Golenev E.M., Kurtmullaev R.Kh., Laukhin Ya.N., Malutin A.I., Martushov Yu.S., Semenov V.N.

I.V.Kurchatov Institute of Atomic Energy, Moscow

1. This paper is devoted to the question why the ballooning regime of CT formation [1] gives drastic advantages in plasma heating and suppression of losses. Experiments were performed on the TOR device (r_c=16 cm, B_{max}=10-18 kGs without crowbar). Two characteristic types of CT formation named "soft" and "hard" are extracted from whole experimental massive. The optimal soft formation mode (SM) is characterized by the following attributes obtained with the help of diamagnetic loops, optic, neutron and other diagnostics:

1.1. Just after beginning of axial compression a nonstationary shock waves develop from the both ends of the system. Leading edge of the shock with jump of electron temperature propagates with velocity $V_{||}=(0.3-0.8)10^8$ cm/s (at B_m=18 kGs) corresponding to $V_{||}=2V_p$ (V_p is the piston velocity)(Fig.1,3).

1.2. Axial shock transition length rapidely increases up to $l_s/2$. This process is accompanied by simultaneous radial expansion of the heating zone ($\Delta r \sim r_s$) which helps in establishing minimal gradients of inhomogenieties (Fig.2,4).

1.3. Ballooning configuration of the piston leads to early initiation of viscous thermalization mechanism: appearance of plasma diamagnetism in end regions and simultaneous beginning of neutron emission (Fig.1,3).

1.4. The general view of compression dynamics looks as follows: initial axial push-off gives way to rapid drop of piston velocity (by 3-10 times, Fig.3) and then all plasma parameters approach comparatively slowly their ultimate values: $T_i \approx$ 2.8 keV, $T_e \approx$ 200-350 eV, $n \sim (3-8)10^{15} cm^{-3}$ (Fig.2a). Due to spreading the relaxation process onto whole plasma the characteristic

overshoot in the middle section is practically fully suppressed and the process smoothly transformes into adiabatic compression by rising external field, plasma having minimal level of the post-shock oscillations ($W_{osc}/W_{\Sigma} < 10^{-4}$-$10^{-3}$, see Fig.2a,3).

1.5. The soft mode with ballooning start structure is observed to have minimal rate of energy and magnetic flux losses. It is important that the characteristic fall time of these parameters increases with T_i; so $\tau_{\phi}=\phi_{cl}/\dot{\phi}_{cl}$ for closed magnetic flux achives 200 mks on equilibrium phase at $T_i > 2$ keV.

1.6. Fig.5 demonstrates plasma temperature in the shock wave vs delay of compression on ballooning phase. The effect of balloon control [1] is clearly seen.

2. The following experimental facts are of importance for choice of appropiate physical model:

2.1. In the soft mode of compression diamagnetic probes register quick separatrix oscillations with amplitude getting maximum in piston zones (up to $\Delta r_s/r_s \sim 10^{-2}$, Fig.1). These oscillations are accompanied by the rise of plasma diamagnetizm (that is of $P_{\perp}$) and neutron emission which indicates an effective plasma thermalization in the accelerated flow. Taking this fact into account one can suggest a specific relaxation mechanizm based on particle scattering on vibrating internal magnetic surfases of the balloon. As far as at the ends $B_{\perp} \sim B_{\parallel}$ one can expect here much more effective relaxation then that governed by a firehose instability in a pure axial field [2].

2.2. The character of relaxation changes in the middle part of the CT. Multichord measurements of the $C\bar{V}$ and D_{β} spectral line emission and bremstrahlung radiation at λ=224 nm indicate that the leading part of the perturbation has a complicated structure of a hollow cone. This imparts the process of the flows interaction a character a quasispheric collapse which is followed by a rapid rise of plasma pressure $P_{\perp}$. As far as the interaction is localized primarily in the zero field region one can expect here another dissipative and heating mechanism for example a two-stream ion-sound instability taking into account that necessary conditions of sub- and supersound flows [3] are fulfilled in the experiment. This gives a natural explanation of observed effective plasma decceleration and thermaliza-

tion and high ion temperature. As to the condition $T_e \gg T_i$ it can be fulfilled locally in the wave front and in the zone of counterstreaming flows collision.

3.1. The hard mode of CT formation posesses the following characteristic features: delayed parting of the shock transition from the piston, sharp overshoot in the middle plane, strong postshock plasma oscillations (Fig.2b,6). But the most distinguishing is a powerful channel of energy and particle losses. It is natural to link it with the specific shape of plasma ends which are radially overcompressed ($r_{min} \ll r_s^{max}$) and highly extended in axial direction ($\Delta z \sim B/(dB/dz) \sim l_s/2$) [1]. Rough estimates show that ion-sound current instability can arise in the neutral layer of CT [4] giving $\nu_{eff} \gg \nu_{ei}$. In the mensioned magnetic tails where $B_\perp/B_\parallel \sim r_s/l_s \ll 1$ magnetizing parameter for electrons $\omega_{Bl}\nu_{eff} \sim \omega_{B\parallel}\nu_{eff}\cdot(r_s/l_s)$ can approach unity. Waste of heat and particles through that axial channel supports in its turn enhanced plasma resistivity in the neutral layer region. Note that this model agrees with antiparallel field diffusion velocity $V_{dif} \sim c^2/4\pi\sigma > 10^6$cm/s observed in tearing phenomena in these experiments.

3.2. In the soft mode absence of long magnetic tail and "leak-proof" piston contribute to an opposite, stabilizing, role of end regions relative to dissipative mechanisms. This can be explained by heat flow from hot ends to the center along neutral layer for example in the fasion of heat wave which was observed in similar conditions in [5].

4. Results on stimulated viscosity described and refueling problem cause a particular interest in experiments on torii merging. In soft mode it takes time l_s/V_{12} (V_{12}-counter velocity) and torii energies add. In other conditions interaction occures as a hard impact with subsequent axial expansion and loss of the most part of closed flux and energy.

R E F E R E N S I E S

1. B.B.Belikov et al. 9 Int. Conf. on Plasma Phys. and Cont. Nucl.Fus.Res. Baltimore, 1982. Paper IAEA-CN-41/M-6
2. V.M.Alipchenkov et al. Preprint IAE-3793/6, Moscow, 1983
3. M.A.Beresovsky et al. DAN SSSR, v.268,6,1983
4. A.G.Es'kov et al. Nucl.Fus. Suppl.,1976,p.155
5. O.A.Zolotovsky et al. DAN SSSR, v.197,3,1971

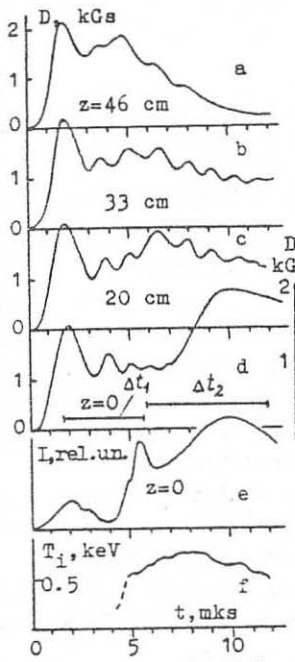

Fig.1. Soft mode: a-d - relaxation oscillations of D in shock wave; e - bremstrahlung radiation; f - T_i from neutron measurements. B_{max}=10 kGs. Δt_1-development of a shock and viscous termalization; Δt_2-CT relaxation and maximum of compression

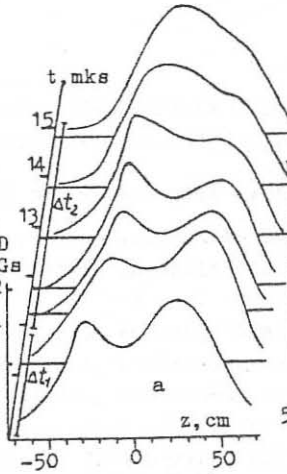

Fig.2. CT evolution in soft(a) and hard (b) regimes

Fig.3. Viscous relaxation characteristics (SM) and adiabatic phase at B_m=18 kGs. 1-T_i, 2-adiabatic law $(V^{-2/3})$

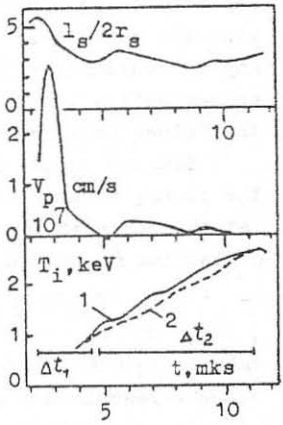

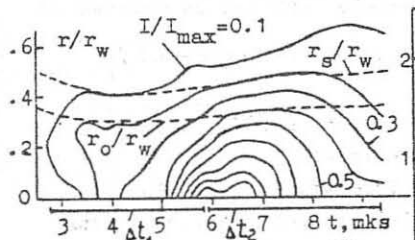

Fig.4. Lines of constant CV intensity in shock flows collision in the middle plane of CT (SM). $r_0 = r/\sqrt{2}$

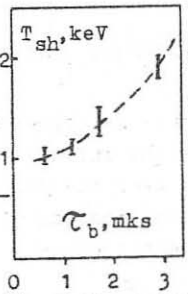

Fig.5. Shock heating temperature vs balloon delay time τ_B

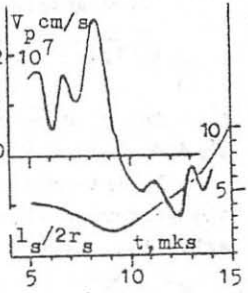

Fig.6. Characteristics of the hard mode (B_m=10 kGs)

EFFECT OF RIPPLED MAGNETIC FIELD ON DAMPING OF FAST MAGNETOSONIC WAVES UNDER MULTIPLE ION CYCLOTRON RESONANCE

S.V. Kasilov, A.I. Pyatak and K.N. Stepanov

Kharkov Institute of Physics and Technology, Ukrainian SSR Academy of Sciences, 310108 Kharkov, USSR

The magnetic field inhomogeneity in tokamaks results in peculiarities of the interaction of fast magnetosonic waves (FMSW) with resonance ions under multiple cyclotron resonances, viz. the nonlinear dependence of the wave phase on the poloidal angle occurring in the equations of resonance ion motion, and consequently, the local damping coefficients differing from the values obtained for a homogeneous plasma [1,2].

Similar peculiarities are found for FMSW propagating in the plasma in straight traps with a rippled magnetic field. Let the magnetic field in this trap be generated by coils spaced a distance L apart along the z-axis, then we have

$$B_z = B_0[1+\varepsilon_M g(r,z)] \ , \ B_\varphi = 0 \ , \ B_r \sim \varepsilon_M B_z \ , \qquad (1)$$

where $g(r,z+L)=g(r,z)$, $\langle g\rangle_z = L^{-1}\int_0^L g\,dz = 0$ and the parameter $\varepsilon_M \ll 1$ describes the degree of magnetic field modulation.

The electric field of small-scale FMSW can be defined as

$$\vec{E}(\vec{r},t) = \vec{\mathcal{E}}(\vec{r})\exp\left\{i\left[\int_{r_0}^{r} dr'\,k_r(r',z) + m\varphi + k_z z - \omega t\right]\right\}. \qquad (2)$$

The z-dependence as represented by eq.(2) is valid if $\mathrm{Im}\,N \ll \mathrm{Re}\,N$ (N is the refractive index).

By integrating over the particle trajectories to find the perturbed electron and ion distribution function we can write the current densities as

$$j_\alpha^{\pm} = \sum_{\alpha=e,i} j_\alpha^{\pm} + j_{res}^{\pm} \ , \quad \text{where } j^{\pm} = j_r \pm j_\varphi$$

and the contribution of resonance and nonresonance particles is described by the expressions

$$j_\alpha^{\pm} = i\,\frac{\omega_{p\alpha}^2\,\mathcal{E}^{\pm}}{4\pi[\omega \mp \omega_{c\alpha}(\vec{r})]}\,, \qquad j_{res}^{-} = 0, \tag{3}$$

$$j_{res}^{+} = \frac{\omega_{pi}^2}{(2\pi)^{3/2}\,v_{Ti}}\,\frac{n^2}{2^n n!}\left(\frac{\kappa_\perp v_{Ti}}{\omega_{ci}}\right)^{2n-2}\cdot\int_{-\infty}^{\infty} dv_\parallel \exp\left(-\frac{v_\parallel^2}{2v_{Ti}^2}\right)\cdot\int_{-\infty}^{0} d\tau\; \mathcal{E}^{+}(\tau)\times$$

$$\exp\left[i\kappa_z v_\parallel \tau + i\,\frac{\kappa_z}{B_0}\int_0^{v_\parallel\tau} dz'\,B_z(r, z'+z) + in\int_0^{\tau} d\tau'\,\omega_{ci}(r, z+v_\parallel\tau') - i\omega\tau\right]. \tag{4}$$

Through substitution of the expressions(3) and (4) for the current densities into the Maxwell equation and on the assumption that $\kappa_z \ll \kappa_\perp$ and $m \ll \kappa_\perp \tau$ we obtain $\kappa_\parallel = \kappa_A + \Delta\kappa_\parallel(z)$ ($|\Delta\kappa_\parallel| \ll \kappa_A$). As a first approximation $\kappa_A = \omega/v_A$, with v_A being the Alfven velocity. As a next approximation

$$\Delta\kappa_\parallel(z) = i\,\frac{\omega^2 n(n-1)^2}{v_A^2\,2^n n!}\left(\frac{\kappa_A v_{Ti}}{\omega_{ci}}\right)^{2n-3} \cdot I,$$

$$I = \int_{-\infty}^{\infty} dv_\parallel \exp\left(-\frac{v_\parallel^2}{2v_{Ti}^2}\right)\cdot\int_{-\infty}^{0} d\tau \exp\left\{i\kappa_z v_\parallel\tau + i\,\frac{\kappa_z}{B_0}\int_0^{v_\parallel\tau} dz'\,B_z(r, z+z') + \right.$$

$$\left. + in\int_0^{\tau} d\tau'\,\omega_{ci}(r, z+v_\parallel\tau') - i\omega\tau\right\},$$

$$\omega_{ci} = \bar{\omega}_{ci}(1+\varepsilon_M g)\,, \qquad \bar{\omega}_{ci} = eB_0/m_i c\,. \tag{5}$$

The damping coefficient $\varkappa = \mathrm{Im}\,\Delta\kappa_\parallel$ was found to depend on the ripple pitch L and depth ε_M, frequency difference $(\omega - \bar{\omega}_{ci})$, longitudinal wave number $\kappa_\parallel = \vec{\kappa}\vec{B}/B$, and ion Larmor radius ρ_i.

If the local resonance points $z_{res} = z_\pm$ determined from the equation $\omega = \omega_{ci}(r, z)$ are located far from the extremum points z_m of the $g(r, z)$ function, the behavior of the damping coefficient $\varkappa$ as a function of z is dependent on $\kappa_\parallel$. In the short-wave range $\kappa_\parallel L \gg \sqrt{L|g'|\zeta_\parallel}$ (with $g' = dg/dz$, $\zeta_\parallel = \varepsilon_M \bar{\omega}_{ci} L/2\sqrt{2}\,v_{Ti}$)

$$\mathrm{Re}\,I = \frac{\pi}{|\kappa_\parallel|}\exp(-z_i^2)\left\{1 + 2\theta(-dz_i/dz)\cos\left[2\kappa_\parallel(z - z_{res})\right]\right\}, \tag{6}$$

where $z_i = [\omega - n\omega_{ci}(z)]/\sqrt{2}\,|\kappa_\parallel| v_{Ti}$, $\theta(x) = 1\ (x>0)$, $\theta(x) < 0\ (x<0)$.

In the long-wave range $\kappa_\parallel L \ll \sqrt{L|g'|\zeta_\parallel}$,

$ReI = 1/4\,\Gamma(1/4)(4\pi L/\zeta_{\parallel}|g'|)^{1/2}$ in the vicinity of the resonance point z_{res}, $|z - z_{res}| \ll L/\sqrt{\zeta_{\nu}}$. Far from the resonance point z_{res}

$$ReI = \sqrt{\frac{2\pi^2 L^2}{3\zeta_{\parallel}|g'||x_0|}}\exp\left[-\frac{3}{2}\left(\frac{x_0}{4}\right)^{4/3}\right]\cos\left[\frac{3\sqrt{3}}{2}\left(\frac{x_0}{4}\right)^{4/3} - \frac{\pi}{6}\operatorname{sgn} x_0\right]\left(\frac{4}{x_0}\right)^{1/3}\sqrt{\frac{x_0}{4}} \quad (7)$$

where $x_0 = 2\operatorname{sgn} g'\sqrt{|g'|\varepsilon_M n\bar{\omega}_{ci}/\sqrt{2}\,v_{Ti}}\,(z - z_{res})$.

By contrast, the averaged value $\langle \varkappa \rangle_z$ describing the power absorbed in the plasma within a pitch L does not depend on and coincides with the averaged over z value of $\varkappa$ obtained from the homogeneous plasma theory.

$$\langle \varkappa \rangle_z = \kappa_A \frac{\pi(n-1)^2}{2^{n+2}n!}\frac{(\kappa_A \rho_i)^{2n-2}}{\varepsilon_M L}\left(\frac{1}{g'_+} + \frac{1}{g'_-}\right), \quad \left(g'_{\pm} = \frac{dg}{dz}\Big/_{z=z_{\pm}}\right). \quad (8)$$

If the resonance points are located close to each other, i.e. in the vicinity of the extreme z_m of the function $g(z)$, then we get

$$\langle ReI \rangle_z = \frac{4\pi}{L}\left(\frac{v_{Ti}}{\varepsilon_M n\bar{\omega}_{ci} g''(z_m)}\right)^{2/3}\int_{-\infty}^{\infty} du\, e^{-u^2}|u|^{-1/3}\Phi^2\left(\frac{\lambda_3 u^2 + \lambda_2 u - \lambda_1}{u^{2/3}}\right) \quad (9)$$

with

$$\lambda_1 = \frac{\omega - n\bar{\omega}_{ci} - \varepsilon_M n\bar{\omega}_{ci} g(z_m)}{\sqrt[3]{\varepsilon_M n\bar{\omega}_{ci} v_{Ti}^2 g''(z_m)}},$$

$$\lambda_2 = \kappa_{\parallel} L\left[\pi\zeta_{\parallel} L^2 g''(z_m)\right]^{-1/3},$$

$$\lambda_3 = 2\zeta_{\parallel}^{2/3}\frac{v_{Ti}^2}{v_A^2}\left[\frac{\pi^2}{L^2 g''(z_m)}\right]^{1/3}\frac{\left[B_z'(z_m)\right]^2}{B_0^2 g''(z_m)}, \quad (10)$$

Φ is the Airy function.

When $\lambda_{1,2,3} \ll 1$ (which corresponds to the small difference $|\omega - n\omega_{ci}(z_m)|$, long-wave range and negligible effect of the B_z component), we can write

$$\langle ReI \rangle_z = \left[\Gamma^3(1/3)/\sqrt{3}\,L\right]\left[v_{Ti}/\varepsilon_M n\bar{\omega}_{ci} g''(z_m)\right]^{2/3}. \quad (11)$$

In the short-wave range ($\lambda_2 \gg 1$) for $\lambda_3 \ll 1$ we have

$$\langle Re\, I\rangle_z = (4\pi/L)\left[\upsilon_{Ti}/\sqrt{2}\,|k_{\parallel}|\,g''(z_m)/\varepsilon_M n\bar{\omega}_{ci}\right]^{1/2} K(\xi), \qquad (12)$$

where

$$K(\xi) = \int_0^{\infty} dt \exp\left[-(t^2+\xi)^2\right], \quad \xi = |\omega - n\bar{\omega}_{ci}|/\varepsilon_M n\bar{\omega}_{ci}|g|/\sqrt{2}\,|k_{\parallel}|\,\upsilon_{Ti}. \qquad (13)$$

For $\xi \to -\infty$, as was expected, eq.(12) is transformed into eq.(8).

Finally consider the case when the component has a pronounced effect on the wave damping. E.g., when $|\lambda_3| > |\lambda_2|$ and $\lambda_1 \gg 1$ we obtain

$$\langle Re\, I\rangle_z = \frac{4\pi}{L}\left(\frac{\upsilon_{Ti}}{\sqrt{2}|k_{\parallel}|\,g''/\varepsilon_M n\bar{\omega}_{ci}}\right)^{1/2} K(\xi,\eta), \qquad (14)$$

where

$$K(\xi,\eta) = \sqrt{\eta/2}\int_{-\pi/2}^{\pi/2} dt \exp\left\{-\eta^2\left(1+\sqrt{1-2\xi/\eta}\,\sin t\right)^2\right\}, \qquad (15)$$

$$\eta = \frac{|\lambda_2|}{2\lambda_3} = \frac{|k_{\parallel}|L}{4\pi\varsigma_{\parallel}}\,\frac{\upsilon_A^2}{\upsilon_{Ti}^2}\,\frac{g''(z_m)B_0^2}{[B_z'(z_m)]^2}. \qquad (16)$$

For $|\lambda_1| \ll 1$, $|\lambda_2| \ll 1$ and $\lambda_3 \gg 1$, corresponding to the small difference $(\omega - \bar{\omega}_{ci})$ and long-wave range of oscillations, we have

$$\langle Re\, I\rangle_z = \pi^2 \upsilon_A B_0 / L\varepsilon_M n\bar{\omega}_{ci}|B_z'(z_m)|. \qquad (17)$$

Thus the damping coefficient of FMSW acquires the highest value at $\omega \to n\,\omega_{ci}(z_m)$. In the short-wave case it exceeds the value(8) by a factor of $(\upsilon_A/\upsilon_{Ti})^{1/2}$. A still larger damping might occur in the long-wave range. Note if the effect of the B_z component is appreciable, the damping increases by a factor of υ_A/υ_{Ti} as compared with the value (8), otherwise the damping increases by a factor of $(\varepsilon_M L/\rho_i)^{1/3}$.

REFERENCES

1. T.D. Kaladze, A.I. Pyatak, K.N. Stepanov, Ukr.Fiz.Zh. 28 (1983) 995.
2. S. Itoh, A. Fukujama, K. Itoh, Preprint HIFT-91, Hiroshima, Japan, July 1984.

SELF-FOCUSING OF RELATIVISTIC INTENSE ELECTROMAGNETIC BEAMS IN AN INHOMODENEOUS PLASMA

D.P.Garuchava, Z.I.Rostomashvili, N.L.Tsintsadze

Institute of Physics, Academy of Sciences of the Georgian SSR, Tbilisi, USSR

The paper presents an investigation of the nonlinear stationary refraction of relativistic intense ($I = \frac{e^2|E|^2}{m_e^2\omega_0^2c^2} \sim 1$) circularly polarized electromagnetic Gaussian beams in an inhomogeneous plasma. The dynamics of the wave propagation is strongly affected by the relativistic effect of electron mass oscillation in the HF pumping wave field and the electron striction, due to this effect, as well. The characteristic time of the self-focusing is small and the ions can be considered stationary. The electron density is determined from the equation

$$n_e = n_0 W(z)\left(1 + \frac{c^2}{\omega_{pe}^2 W(z)}\Delta\sqrt{1+I(z,r_\perp)}\right) \qquad (1)$$

where Langmuir electron frequency is $\omega_{pe}^2 \ll \omega_0^2$, $W(z)$ is the plasma inhomogeneity profile. Then the equation describing the nonlinear wave propagation in plasma is as follows

$$\Delta\vec{E} + \frac{\omega_0^2}{c^2}\vec{E} = \frac{\omega_{pe}^2 W}{c^2}\frac{\vec{E}}{\sqrt{1+I}} + \frac{\Delta\sqrt{1+I}}{\sqrt{1+I}}\vec{E} \qquad (2)$$

where

$$\vec{E} = E_0(z,r_\perp)\{\hat{x}\cos\varphi + \hat{y}\sin\varphi\} \qquad (3)$$

$$\varphi(z,r_\perp) = \int_0^z K_\parallel(z')dz' + \frac{r_\perp^2}{2}\beta(z) + \ldots \qquad (4)$$

$$I = I_0(z)\exp\left[-\frac{r_\perp^2}{a^2 f^2}\right] \qquad (5)$$

$I_0(z)$ is the field intensity on the beam akis, $\beta(z)$ - is the front curvature, $f(z)$ - is the dimensionless width of the beam, $r_\perp^2 = x^2 + y^2$.

In the aberrationless parraxial ray approximation

$(r_\perp^2 \ll a^2 f^2)$ we obtain the set of equations:

$$\left.\begin{aligned} k_\parallel^2 &= \frac{\omega_0^2}{c^2} - \frac{\ell}{a^2 f^2}\frac{1}{1+I_0} - \frac{\omega_{pe}^2 W}{c^2}\frac{1}{\sqrt{1+I_0}} \\ -2\frac{\beta}{k_\parallel} &= \frac{d}{dz}\ln(k_\parallel I_0) \\ k_\parallel \beta' + \beta^2 + \frac{\omega_{pe}^2 W}{2c^2}\frac{1}{a^2 f^2}\frac{I_0}{(1+I_0)^{3/2}} + \frac{1}{a^4 f^4}\frac{I_0(4+I_0)}{(1+I_0)^2} - \frac{1}{a^4 f^4} &= 0 \\ \beta'' + \beta'(\ln I_0)' - \frac{4}{a^4 f^4}\left[\beta - k_\parallel (\ln f)'\right] &= 0 \end{aligned}\right\} \quad (6)$$

The boundary conditions are

$$I_0(z=0) = I_{00}, \quad f(z=0) = 1, \quad \beta(z=0) = \beta_0 \qquad (7)$$

In the third equation of the set (6), the term $\frac{\omega_{pe}^2 W}{2c^2}\frac{1}{a^2 f^2}\frac{I_0}{(1+I_0)^{3/2}}$ is caused by the relativistic effect, whereas the term $\frac{1}{a^4 f^4}\frac{I_0(4+I_0)}{(1+I_0)^2}$ is due to nonlinear striction of electrons. Both of them determine the force of the nonlinear refraction and promote the self-focusing of the beam. For narrow ($a \sim 10 \div 100\lambda$) beams (that occurs in the most of experiments with ultra-high power lasers) those are terms of the same order of the magnitude and both of them, like the differential term, affect the dynamics of beam propagation and the self-focusing length. In the area of the focus the strictional term becomes a dominating one. For wide beams ($a \gg 100\lambda$) the self-socusing length is mainly determined by the relativistic effect, but in this case, as well as in the case of narrow beams, for determation of the minimum transverse sizes of the formed channels one must take into the consideration the effect of striction. In the case of the self-focusing to the sizes $r_{min} = \left\{\frac{2c^2}{\omega_{pe}^2 W} \times \frac{I_0}{\sqrt{1+I_0}}\right\}^{1/2}$ a self-trapping channel is produced and the beam, propagating in it can penetrated the ultradense plasma. We consider the case when $\omega_{pe}^2 \ll \omega_0^2$. Self-focusing and channel formation occur before the critical density. A diffracting ring with the intensity lower then critical is formed from the peripheral part of the

beam and it does not penetrate the ultradense plasma. The intensity produced in the channel in the paraxial part of the beam due to self-focusing is almost homogeneous. The dielectric constant of the medium in this range is positive and the density jump and effects associated with it are negligable.

Fig.1 shows the plot of the dimensionless width of the beam ξ vs z/a for various characteristic lengths of the plasma inhomogeneity. We have considered a linearly increasing inhomogeneity profile $W = 1 + z/L$ (where L is characteristic length of the inhomogeneity). For such set of plasma and beam parameters, when $I_0 > I_{cr}$, with decreasing inhomogeneity length the self-focusing length first decreases and then starts to increase. ξ first increases and then decreases. For definite L the beam is focused to certain sizes, and then broadens fast. It occurs because the terms corresponding to nonlinear refraction, decrease with the increase of $I_0(z)$ and become less than the diffraction term. With the further increase of the inhomogeneity the beam begins to defocus. With the increase of the density and the beam width one observes fast broadening at longer lengths of the plasma inhomogeneity. The sizes of the focus decrease with the increase of the inhomogeneity and then grow as the length of the self-focusing. Dependence of the self-focusing length and the focus sizes upon the length of the inhomogeneity is more essential for small too, than for large ones. It is noteworthy that the plot of critical intensity VS plasma density and beam width for strongly relativistic beams ($I_{cr} \sim \omega_{pe}^2 a^4$) defers from weakly relativistic ones ($I_{cr} \sim 1/\omega_{pe}^2 a^2$).

As it is seen from Fig.2, the normalized self-focusing length z_f/a (where z_f is the self-focusing length) decreases with the decrease of the initial beam width. With the increase of the initial density the self-focusing length decreases and then grows. The self-focusing length depends strongly upon the initial curvature of the beam, the beam intensity and the inhomogeneity profile.

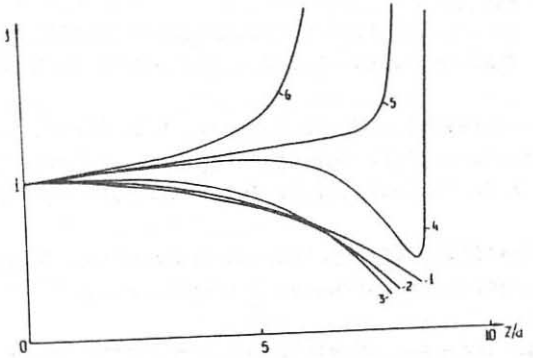

Fig.1 Plot of dimensionless beam width f vs z/a for various characteristic inhomogeneity lengths L at $\frac{\omega_{pe}^2}{\omega_0^2} = 0.1$, $\frac{\omega_0^2 a^2}{c^2} = 400$, $\beta_0 = 0$, $I_{00} = 0.5$; 1) $L = 100$, 2) $L = 10$, 3) $L = 5$, 4) $L = 2.9$, 5) $L = 2.75$, 6) $L = 2.5$.

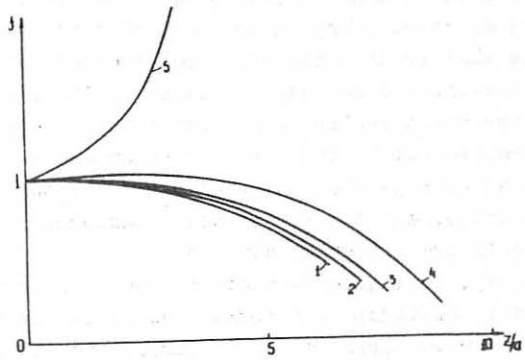

Fig.2 Plot of dimensionless beam width f vs z/a for various a at $\frac{\omega_{pe}^2}{\omega_0^2} = 0.1$, $\beta_0 = 0$ $L = 10$, $I_{00} = 0.75$; 1) $\frac{\omega_0^2 a^2}{c^2} = 10^2$, 2) $\frac{\omega_0^2 a^2}{c^2} = 2 \cdot 10^2$, 3) $\frac{\omega_0^2 a^2}{c^2} = 4 \cdot 10^2$, 4) $\frac{\omega_0^2 a^2}{c^2} = 10^3$, 5) $\frac{\omega_0^2 a^2}{c^2} = 4 \cdot 10^3$

STUDIES OF STELLARATOR MAGNETIC CONFIGURATIONS USING A STATIONARY ELECTRON SOURCE

A.V. Georgievskij, Yu.V. Gutarev, A.G. Dikij, V.M. Zalkind, V.I. Kurnosov, O.S. Pavlichenko, V.K. Pashnev, D.P. Pogozhev, E.I. Skibenko, V.T. Tolok and V.M. Tonkopryad

Kharkov Institute of Physics and Technology, Ukrainian SSR Academy of Sciences, 310108 Kharkov, USSR

1. In the case of stellarator magnetic traps with the vacuum magnetic configuration created by external conductors it is important to know the parameters of the magnetic configuration, viz. the outermost magnetic surface radius and rotational transform. The experimental technique most widely used to derive this information is to study the trajectories of electrons injected into the trap [1]. To this end, electrons with $v_{\parallel} > v_{\perp}$ (transit electrons) are injected into the trap, their energy and pulse duration being chosen such that the electron bunch length is smaller than the stellarator axial length. By measuring the location of successive passes of the electron bunch through the cross section under study we can obtain the particle surface mapped out by the electron bunch and associated magnetic surfaces as well as the number of times the bunch circuited the stellarator and the rotational transform. However, these measurements are rather complicated.

Clearly, a stationary electron source driven across the magnetic configuration would respond to the varying electron confinement with varied emission current due to the distributed space charge potential of the electron cloud accumulated in the trap. This idea was verified in experiments on the URAGAN 2 stellarator with the magnetic configuration already known [2] and used to study the magnetic surfaces in the URAGAN 3 torsatron [3].

2. The experiments were performed with a miniature spiral

tungsten cathode (area $\simeq 1$ mm^2) mounted on an isolated support of 3 mm diameter. The cathode could be moved horizontally within the straight section of the vacuum chamber in the URAGAN 2 stellarator, while in the URAGAN 3 torsatron it could be placed at any point in the space enclosed with the helical winding. Between the cathode and the vacuum chamber a d.c. voltage or a d.c. current source was switched on. The values to be measured (emission current J_{em} or "cathode-wall" voltage U_w) were registered together with a signal proportional to the radial cathode shift by means of an X-Y recorder.

During the experiments the pressure in the vacuum chambers was in the range 3×10^{-7} to 1×10^{-6} Torr and the confining magnetic field was 600÷4500 Oe.

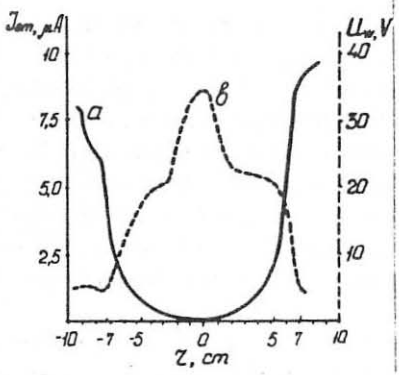

Fig. 1

3. The most notable effect, i.e. strong suppression of emission from the cathode driven to the region of closed magnetic surfaces is illustrated in fig.1, a) for the constant "cathode-wall" voltage in the URAGAN 2 stellarator. The difference in the emission currents outside the confinement region and near the magnetic axis amounted to three orders of magnitude. With the constant emission current the current source responds to the cathode being moved to the confinement region with the increased "cathode-wall" voltage (fig.1, curve b)). A step in the curve (arrowed) corresponds to the cathode crossing the outermost undestroyed magnetic surface and can be used to determine its position and size.

A qualitative explanation of the data obtained (fig.1, a) and b)) can be the following. When the electron source is placed on the closed magnetic surface in the stellarator, the electrons with $v_{\parallel} > v_{\perp}$ occupy the drift surface rapidly if $2\pi R \ll \lambda_{en} \ll L$ (R is the major radius of the torus, λ_{en} is the mean free path of electrons, and L is the length of filed lines until they reach the wall). Further electron motion across and along the magnetic

field lines is similar to the diffusion due to collisions with residual gas molecules. For the steady state spatial distributions of the electron density and space potential the emission current J_{em} compensates for the electron losses across ($J_\perp$) and along ($J_\parallel$) the magnetic field.

$$J_{em} = J_\perp + J_\parallel , \qquad (1)$$

The quantitative theory of electron emission in closed magnetic traps is still under development, nevertheless from the dimensional analysis we can estimate $J_\perp$ and $J_\parallel$:

$$J_\perp \sim \frac{E_\perp \cdot \nu_{en}}{m \cdot \omega_{He}^2} n \cdot R , \qquad (2a)$$

$$J_\parallel \sim \frac{E_\parallel}{m \cdot \nu_{en}} \cdot \frac{n}{L} \cdot a^2 , \qquad (2b)$$

where $E_\perp$ and $E_\parallel$ are, respectively, the perpendicular and parallel component of the electron energy, n and ν_{en} are the electron density and electron-neutral collision frequency, respectively, and a is the radius of the electron confinement region. It is seen from the above expressions that on driving the source to the region where the field lines have a shorter length L , the emission current would increase, and for the emission current to be kept constant while driving the source to the region with a longer L one has to increase , viz. the voltage applied to the source.

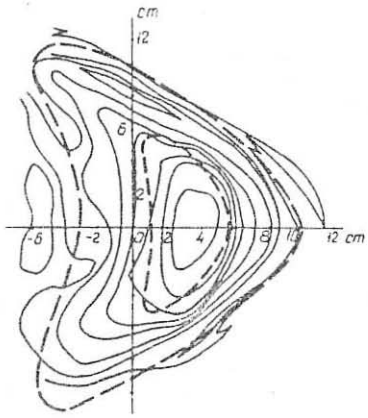

Fig. 2

4. It can be shown for $2\pi R \ll \lambda_{en} \ll L$ that the surfaces of the constant emission current from the electron source coincide with the magnetic surfaces (more specifically, with the drift surfaces). In fact when $\lambda_{en} \gg 2\pi R$, the electrons emitted from the source placed on the irrational surface occupy this surface uniformly whatever the emitter position thereon. Thus the constant distribution of the electron density and space potential is realized, and hence, that of the emission current.

In fig.2 the emission current isolines measured in the URAGAN 3 torsatron are shown for the magnetic field of 0.15 T and residual gas pressure of 3×10^{-7} Torr. Dashed lines correspond to the computed magnetic surfaces of which the outermost one has an average diameter of 8.5 cm and rotational transform $\dot{t} = 0.25$.

One can see that the isolines $J_{em} = \text{const}$ resemble in shape the magnetic surfaces in the center where the condition $\lambda_{en} \ll L$ is satisfied, and observe considerable disturbance of the peripheral region.

The studies of the magnetic configuration in the URAGAN 3 torsatron will be described elsewhere. The object of this paper is to present a rather simple and fast technique for examining the stellarator magnetic surfaces which permits complete automation of the experiment.

REFERENCES

1. M.S. Berezhetskij, S.E. Grebenshchikov, A.P. Popryadukhin, I.S. Shpigel', Zh. Tekhn. Fiz. (1965) 35, 2167.
2. V.F. Aleksin, O.V. Biryukov et al. Preprint KFTI 69-39 (1969) Kharkov.
3. V.V. Bakaev, V.V. Bronnikov, V.S. Vojtsenya et al. X Int. Conf. Plasma Phys. Contr. Nucl. Fus. Res. (1984) London, D-1-3.

TIME AND SPACE RESOLVED X-RAY MEASUREMENTS ON A GAS-PUFF Z-PINCH

C.D.Challis, P.Choi, A.E.Dangor and M.G.Haines
The Blackett Laboratory
Imperial College, Prince Consort Road, London SW7 2BZ

ABSTRACT

Time and space resolved X-ray images of the plasma in a gas-puff Z-pinch in argon show the presence of short lived (5-10ns) localized hot spots on the axis. The hot spots appear to be related to a source of energetic (~10keV) electrons which lead to X-ray emission from the anode. At the time of pinch formation a harder X-ray burst (Cu K lines) appears at the copper anode. The spatially resolved X-ray spectrum from a curved crystal spectrometer indicates that the main constituent of the hot spot is helium like argon (Ar XVII) but the helium satellite line ratios indicate an electron density of 10^{22}-10^{23} cm^{-3}, and the ratio of the hydrogen-like to helium-like resonance lines indicates an electron temperature of 500 eV. Inner shell transitions are observed at the same location of the hot spots consistent with the presence of energetic electron beams rather than a thermal process.

INTRODUCTION

Previous measurements on gas-puff Z-pinches (1,2) showed that the x-rays emitted originated from several hot spots, i.e. localised regions of high density and high temperature plasma with a typical dimension of 200μm or less. Energetic electron beams were also measured through direct Faraday cup measurements (3), inference from observation of inner shell ionisation of the plasma (4,5) and from observation of hard X-rays originating from the anode (1). Here we present an experiment on time and space resolved measurements of X-ray emissions from a gas-puff Z-pinch using double image, filtered X-ray streak photography.

EXPERIMENTAL DESCRIPTION

In a gas-puff Z-pinch a cylindrical hollow shell of gas is imploded electromagnetically by an axial current. The collapsing shell acquires a high radial velocity (~10^7 $cm.s^{-1}$) and the stagnation of the radial kinetic energy on axis results in a plasma with high energy density.

In this experiment the initial hollow gas shell of 15mm radius, 5mm thickness, is produced between two electrodes 20mm apart.The gas is injected by a fast acting valve via an annular supersonic nozzle through a copper plate electrode. The other electrode is a high aspect ratio steel honeycomb. The discharge is energised by a 9μf capacitor bank, charged to 28kV (3kJ). To observe the effect of the electron beams, the device is normally operated with the solid copper electrode as an anode.

The circuit inductance with a shorted load is 60nH, the peak discharge current is 300kA, and the quarter-period of the circuit is 1.15μs. The mass of the gas-shell (~100μg) can be adjusted by altering the plenum pressure (typically 6atms.) or the discharge time relative to gas injection. The mass of the gas-shell is optimised such that the

stagnation on axis occurs at peak current.

Time-resolved X-rays observations are made by a filtered, dual pin-hole camera with a scintillating detector viewing the pinch radially to resolve the axial structure. The recording is made by a Hadland 675 high speed, optical streak camera. A schematic of the set up is shown in fig.1. Time correlation is achieved by pulsing a fast LED in the field of view of the streak camera, and simultaneously displaying the electrical pulses on oscilliscope traces of current and X-ray emission. Both pin-holes are 100μm diameter in copper and are separated by 9.5mm in the axial direction. Aluminium, Beryllium, Kimfoil, Cobalt and Nickel filters are paired and mounted behind the pin-holes with 90nm of Aluminium deposited on the scintillator for light tightness. The Nickel and Cobalt pair is chosen such that their transmission is similar except in the region of the Copper K-line emission. This gives an energy diagnostic for the anode emission. During each shot time integrated measurements are made with a bare aluminium cathode X-ray diode (XRD) and a separate double pinhole X-ray camera using calibrated X-ray film. These measurements allow us to obtain a calibration on the X-ray streak record.

Time integrated spectra is recorded on Kodak DEF X-ray film using a convex curved PET crystal spectrometer. The spectral region observed is between 3.5-4.5Å. A 1mm slit located between the plasma and the spectrometer provides a limited axial resolution while permitting spectra to be recorded in a single shot.

OBSERVATIONS

From time-integrated X-ray pin-hole photography it is known that the gas-puff Z-pinch produces a plasma column between the electrodes within which exist small, intense X-ray emitting regions.(2) Copious X-ray emission is also observed from the anode and this has been attributed to suprathermal electrons.(1)

Time-resolved X-ray diode measurements show that the hard X-rays are emitted in very short (10ns) duration pulses, (fig.2) repeated several times over a period of 400ns. Softer X-rays are produced throughout this period.

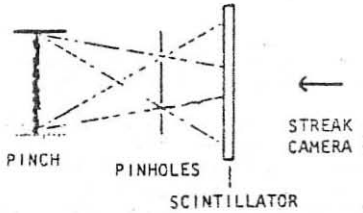

FIG.1

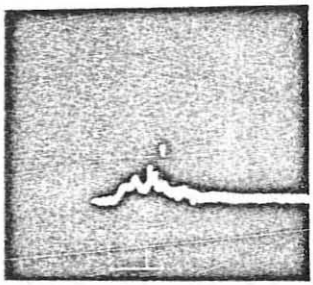

FIG.2

Recordings made with the X-ray pin-hole streak camera show that the pinch is characterised by 2 or 3 bursts of electron beams, each lasting for 30-100ns and causing the anode to light up (fig.3). The time between each burst ranges from 20ns to 150ns. At the time of the stagnation of the plasma shell on axis, the presence of a high energy electron beam (~20keV) is inferred from the hard X-ray K lines emission from the anode which typically lasts for 30ns. Subsequent burst of electrons are inferred to be less energetic and more intense.

Associated with the anode emission is intense localised plasma emission. These localised hot-spots do not occur during the first high energy beam, but are common during the subsequent lower energy bursts. Hot spots are always observed to be accompanied by anode emission. The radial extent of these regions are measured from time-integrated X-ray pin-hole photographs to be <200μm.

Using Kimfoil filters which let through softer X-rays the streak recording (fig.4) shows the existence of a cool emitting plasma in the region between the electrodes, present at all times between bursts of electron beams. Plasma emission is first observed from near the electrode opposite to the nozzle. The emission then sweeps up towards the nozzle, indicating the occurence of a 'zipper' effect. When the polarity of the discharge is reversed, the zipper effect and the hot spot emission is unaffected. Emission from the solid copper electrode, which is now the cathode, is no longer observed.(fig.5) It can also be seen that hot spots appearing at different time and originating from similar axial positions are related to the same colder, longer lasting plasma.

Fig. 6 is a microdensitometer trace of an X-ray spectrum taken with the spectrometer. The dominant lines are He-like and H-like resonance lines and satellites. There are also inner shell transition lines from partially stripped ions. A steady state model for K-Shell spectroscopy(6) is used to compare with the spectra. From the He-like to H-like resonance line ratio, an electron temperature of ~500eV is obtained. From the ratio of Lithium like satellites of the He-like resonance line, an electron density of 10^{22}-10^{23} cm^{-3} is inferred. This model assumes a maxwellian electron velocity distribution. Within the limited spatial resolution of the spectrometer, inner shell transitions are observed to originate from the same axial position as the hot, dense plasma exhibiting the helium like complex. It is inferred that the hot spot is a result of the interaction between a highly energetic electron beam and a relatively cold plasma rather than a thermal process.

REFERENCES

1. C.D. Challis, A.E. Dangor, E.S. Wyndham, D. Mosher, W.G. Bessel and D.J. Bond. 11th Europ. Conf. on Controlled Fusion And Plasma Phys., 1983, Aachen, paper E07.
2. J. Shiloh, A. Fisher and N. Rostoker, Phys. Rev. Lett. 40,515 (1978)
3. D.R. Kania and L.A. Jones, Phys.Rev. Lett. 53,166 (1984)
4. J.D. Hares, R.E. Marrs and R.J. Fortner, J. Phys. D 18,627 (1985)
5. B.A. Hammel and L.A. Jones, Appl. Phys. Lett. 44,667 (1984)
6. R.W. Lee, B.L. Whitten and R.E. Stout,II, J. Quant. Spect. Rad. Transfer, 32,91 (1984).

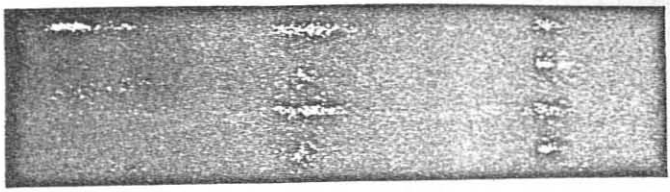

FIG.3

TIME ⟶

TOP FILTER- 7.5μm Aluminium ; BOTTOM FILTER- 2μm Cobalt.

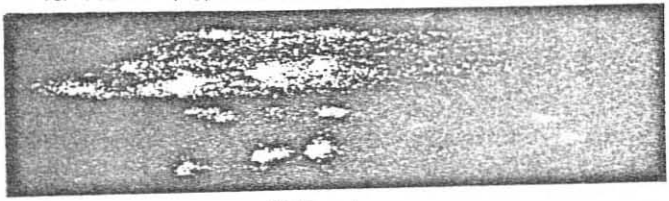

FIG.4

TIME ⟶

TOP FILTER- 7.5μm Kimfoil ; BOTTOM FILTER- 1μm Cobalt.

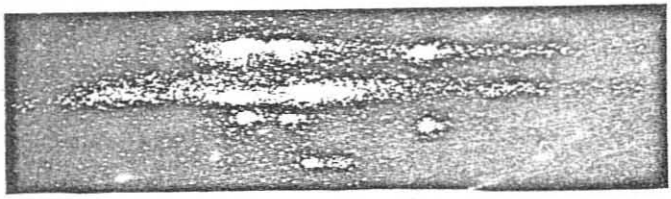

FIG.5

TIME ⟶

TOP FILTER- 7.5μm Kimfoil ; BOTTOM FILTER- 1μm Berylium.

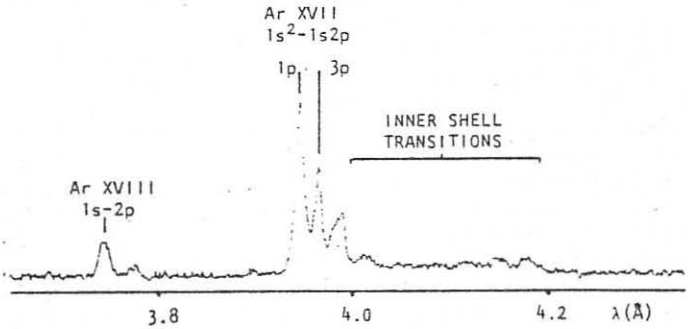

FIG.6 X-ray spectrum.

MODIFICATION OF THE DISRUPTIVE DENSITY LIMIT BY ECRH AND ℓ=3 HELICAL WINDINGS

T N Todd, D C Robinson, B Lloyd, T Edlington, B J Parham, P R Collins
J Riley, D Atkinson, S Hall, F Ma M O'Brien and J Ellis
Culham Laboratory, Abingdon OX14 3DB, UK
(Euratom/UKAEA Fusion Association)

INTRODUCTION

The ubiquitous density limit disruption of tokamak discharges (at $I/N \lesssim 1.5 \times 10^{-14}$Am, where $N=\pi ab\bar{n}_e$) is widely believed to be primarily a consequence of peripheral losses eroding the current density profile to the point where a steep current-density gradient appears just inside the q=2 surface. The disruption follows the ensuing destabilisation of the 2,1 mode, either directly as an ideal kink or via the overlap of islands of this and higher order tearing modes subsequently evolved.

Thus the density limit should be raised by any technique which permits higher peripheral losses while maintaining the stability of the 2,1 surface, eg (i) increasing the power arriving there (core or local heating), (ii) directly affecting the current gradient (local current drive, externally induced islands [1]) or (iii) adding vacuum rotational transform, $\bar{\iota}_{vac}$. Methods (i) and (iii) are addressed by this paper. It should be noted that the close thick shell and powerful feedback systems of CLEO make it very rare for hard disruptions to fully quench the plasma current.

RESULTS WITH ECRH

This study was performed with 60 GHz second harmonic ($2\omega_{ce}$) heating using a TE_{01} mode launched inwards along a midplane major radius. X-mode absorption dominates, and has a cut-off density of $2.2 \times 10^{19}/m^3$, corresponding to critical $\bar{n}_e$ of $\lesssim 1.6 \times 10^{19}/m^3$ for core heating with moderately peaked profiles. Thus for interestingly low values of I/N in CLEO (a=0.13m, circular) the plasma current has to be $\lesssim$ 11 kA. At the resonant field of 1.07T this corresponds to a high q (10 at 10 kA for example), and hence a tendency towards rather narrow temperature profiles. For strong absorption XM $2\omega_{ce}$ ECRH requires an initial electron temperature $\gtrsim$ 150 eV which is unlikely to be achieved in CLEO in the vicinity of the q=2 surface close to the high density limit. Accordingly, the best I/N limits were found with the resonance placed at or near the hot core of the plasma ($\sim$ 350 eV under OH only) although ray tracing calculations show that refractive effects displace the heating zone as $\bar{n}_e$ is increased. Such an ECRH assisted shot is compared with its OH equivalent in Fig 1. Since the initial effect of the ECRH is to cause a drop in $\bar{n}_e$ (probably mostly due to profile flattening), a downward step in plasma current was programmed to facilitate the fall in I/N while the density was forced back up.

When the plasma current was programmed to fall below ~ 7 kA (ie $q \gtrsim 14$) then both OH and ECRH discharges would evolve without major disruptions to cool, quiescent plasmas which were of very low I/N but were not considered relevant to conventional tokamak operation. One interpretation is that there is some critical poloidal Lundquist number (~ 10^3 here) below which MHD activity is suppressed (as is evidenced by decreasing Mirnov signals). Some ECRH assisted shots testing the density limit transferred to this regime at a plasma current ~ 9 kA (at which the OH cases would only disrupt) consistent with suppression of the m=2 mode during the critical part of the density rise.

RESULTS WITH HELICAL WINDINGS

Another technique which should affect the density limit is to modify the profile of $\bar{\iota}_{tot}$, making it difficult for the q=2 ($\bar{\iota} = 0.5$) surface to be close to any significant current density gradient. This approach has been demonstrated on essentially shearless ℓ=2 stellarators already [2] and is found to be capable of a pronounced effect in our strongly sheared ℓ=3 machine. However unlike those earlier results, on CLEO the disruption is not eliminated in this manner, only shifted to a different I/N ratio. In addition there generally exists an upper limit to the amount of strongly sheared $\bar{\iota}_{vac}$ that can be added before the profile of $\bar{\iota}_{tot}$ is unstable at any density [3].

To compare easily with the ECRH assisted cases above the $\bar{\iota}_{vac}$ was added to a servo-controlled 9 kA discharge at various toroidal fields. During this period the normal tokamak density limit was ~ $4.8 \times 10^{18}/m^3$ for this current (wall conditions were not as good as during the ECRH assisted sequence described above). The usual CLEO behaviour is a rapid sequence of disruptions progressively cooling the plasma and thus raising the OH input power. As indicated in the introduction any technique which raises the net power input should raise the density limit. Figure 2 shows the result of programming a slow density rise in a simple CLEO tokamak. The plasma current servo increases the mean loop voltage as the sequence of disruptions occurs, thus progressively raising the OH input power. This sequence starts disrupting at ~ $4.8 \times 10^{18}/m^3$ at ~ 20 kW OH and eventually reaches ~ $7.5 \times 10^{18}/m^3$ at ~ 54 kW.

At low toroidal field values (and hence low q) adding significant helical field was found to make the plasma MHD unstable even at very low density. However at toroidal fields of around 9.5 kG the density limit was raised substantially by increasing the helical winding current, I_ℓ, to ~ 6 kA, above which no further improvement was seen. Discharge waveforms for an optimum case with I_ℓ are shown in Fig 3, which can be directly compared with Fig 2. A few small disruptions can be seen in the SXR activity but the loop voltage stays low until a large disruption occurs (which is considered to define the density limit). The variation of critical density with I_ℓ for various values of B_ϕ is shown in Fig 4.

CONCLUSIONS

Raising the total power input to a conventional tokamak discharge (here by ECRH or by achieving a low conductivity temperature) allows the density limit to be substantially increased, while the nature of the disruption is unchanged. The operational I/N limit was lowered from 1.7×10^{-14} to 1.0×10^{-14} Am. Adding highly sheared vacuum rotational transform to a low q tokamak plasma only adversely affects its stability, but when added to a high q tokamak allows a much higher, but still disruptive, density limit to be achieved. In this (slightly dirty) case the operational limit was lowered from 3.8×10^{-14} to $\sim 2.0 \times 10^{-14}$ Am.

We note that very high q ($\gtrsim$ 14) tokamaks in CLEO do not exhibit density limit disruptions but merely cool smoothly to quiescence. The critical density for rf accessibility combined with the aim of producing interesting I/N values provides a lower limit to q. The resulting window in q would be widened by increasing the critical density for accessibility, for example by raising the ECRH frequency or changing to X-mode fundamental heating.

ACKNOWLEDGEMENTS

This work could not have been accomplished without the support of the CLEO technical team and for the ECRH work the loan of one of GA Technologies' 60 GHz gyrotrons and the help and advice of Ron Prater with its installation and commissioning.

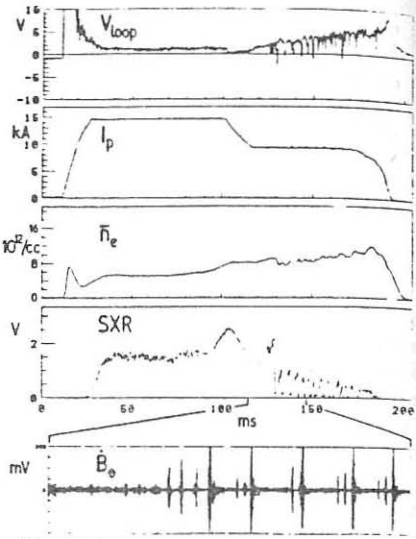

Fig 1(a) OH tokamak at B_ϕ = 1.07T

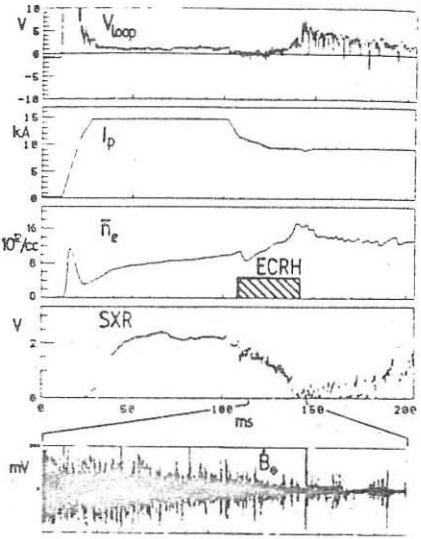

Fig 1(b) 120 kW ECRH tokamak at B_ϕ = 1.07T

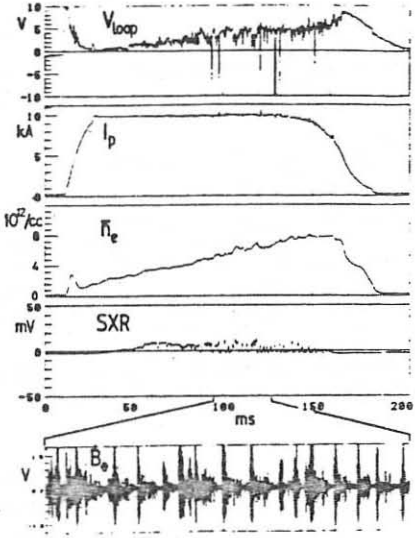

Fig.2 OH tokamak at B_ϕ = 0.90T

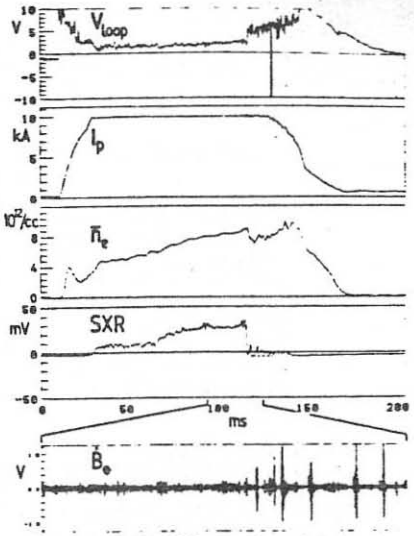

Fig.3 Helically assisted tokamak at B_ϕ = 0.90T, I_ℓ = 7 kA (ie 21 kAt/bundle)

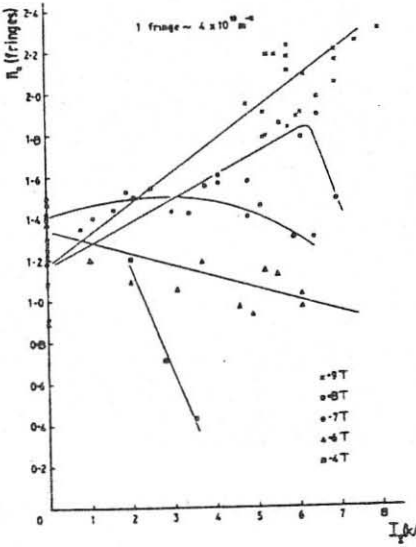

Fig.4 Variation of density limit with I_ℓ and B_ϕ at I_p=9kA.

REFERENCES

[1] A Rowling et al, Wkshp on Magnetic Reconnection and Turbulence, Corsica, 1985

[2] J Fujita et al, (10th EPS), Pl Phys & Cont Fus Vol I, Moscow, 1981, E5

[3] D Atkinson et al, (8th EPS), Pl Phys & Cont Fus Vol II, Prague, 1977, 93

A CATASTROPHIC STUDY OF THE ENERGY BALANCE OF PLASMA IN TOKAMAK

YU,GUO-YANG
THE INSTITUTE OF PLASMA PHYSICS, ACADEMIA SINICA
P.O.BOX 26, HEFEI,CHINA

ABSTRACT. THE ENERGY BALANCE OF PLASMA IN TOKAMAK IS STUDIED.SCALINGS ABOUT THE PARAMETRIC EFFECTS OF THE DENSITY LIMIT OF THERMAL EQUILIBRIUM, FOR BOTH DELAY AND MAXWELL CONVENTION IN CATASTROPHE THEORY, ARE DEDUCED. IT IS SHOWN THAT THE RADIATION DUE TO HEAVY IMPURITY AFFECTS THE DENSITY THRESHOLD SIGNIFICANTLY. MAXWELL CONVENTION OFFERS A MORE SEVERE LIMITATION ON THE ATTAINABLE DENSITY. AN AMPLITUDE OF THE FLUCTUATION IN PLASMA ENERGY AND ITS RATE OF VARIATION, WHICH IS NECESSARY TO CAUSE MAXWELL CONVENTION, IS ALSO GIVEN.

I. INTRODUCTION

MAJOR DISRUPTION IS BELIEVED TO BE OF IMPORTANCE IN TOKAMAK RESEARCH AND MUCH EFFORTS BOTH THEORITICALLY AND EXPERIMENTALLY HAVE BEEN DONE ON THE TOPIC. /1,2/

THEORITICALLY, BESIDES THE MHD APPROACH, THE ABSENCE OF THE ENERGY BALANCE IN PLASMA IS PROPOSED TO BE ANOTHER APPROACH CAUSING DISRUPTION. IT IS REVEALED /1/ THAT THERE EXISTS A DENSITY LIMIT IN PLASMA BEYONG WHICH NO THERMAL EQUILIBRIUM EXISTS. THUS THE DENSITY LIMIT OF DISRUPTION IS ADDRESSED. LATER AN 1-D NUMERICAL STUDY OF THE THERMAL EQUILIBRIUM IN PLASMA SHOWED:/2/ (1) THERE ARE THREE TYPES OF THERMAL EQUILIBRIA DIFFERING IN BOUNDARY TEMPERATURE AND PERFORMIMG DIFFERENT TE(DENSITY) BEHAVIOR, NAMELY, MONOTINIC, CATASTROPHIC AND INTERCHANGABLE; (2)THE CUSP CATASTROPHIC STRUCTURE OF TE UPON CONTROL PARAMETERS (SUCH AS THE APPLIED TOROIDAL FIELD, THE LOOP VOLTAGE, THE GEOMETRY OF PLASMA AND THE BOUNDARY TEMPERATURE) INDICATES THAT DISRUPTION, IN THE STUDY, IS PARAMETRICALLY CONTROLLABLE AND REMOVABLE.

ALL THE RESULTS MENSIONED ABOVE ARE OBTAINED BY USING A MODEL: (A) THE ENERGY PROCESSES CONSIDFRED ARE THERMAL CONDUCTION, OHMIC HEATING AND E-I EQUILIBRATION; (B)DELAY CONVENTION IN ELEMENTARY CATASTROPHE THEORY IS APPLIED ONLY.

HOWEVER MORE ENERGY PROCESSES. SUCH AS RADIATION LOSSES AND AUXILIARY HEATING, SHOULD BE INCLUDED. FROM A VIEW OF CATASTROPHE THEORY, IN ADDITION TO DELAY CONVENTION, MAXWELL ONE IS ALSO INTERESTING TO STUDY. THESE ARE THE PURPOSE OF THIS PAPER.

THE BASICS ARE IN SECTION II. RESULTS IN A FORM OF SCALING OF THE PARAMETRIC EFFECTS OF THE CRITICAL DENSITY AND THE CONDITION CAUSING MAXWELL CONVENTION ARE GIVEN IN SECTION III.

II. THE BASICS

THE ELECTRON'S ENERGY BALANCE IS CONSIDERED ONLY AND THE EQUATION NORMALIZED AS IN /2/ IS:

$$\frac{\partial}{\partial t} nT = P_{COND.} + P_{OHM.} + P_{EI} + P_{LOSS} + P_{NBI} \qquad (1)$$

ON THE RIGHT HAND SIDE ARE THE CONTRIBUTIONS DUE TO THERMAL CONDUCTION, OHMIC HEATING, E-I EQUILIBRATION, LOSS TERM INCLUDING BREMSSTRAHLUNG, CYCLOTRON EMISSION, LIGHT AND HEAVY IMPURITIES RADIATION, AS WELL AS NBI HEATING. LIKE IN /1-3/, THE ELECTRON'S THERMAL CONDUCTIVITY IS TAKEN TO BE ANORMALOUS DUE TO MAGNETIC FLUCTUATION/4/

$$P_{COND.} = \frac{1}{r}\frac{\partial}{\partial r} C_2 r \frac{nR}{B^2} T_e^{3/2} \frac{\partial T_e}{\partial r} \qquad (2)$$

THE REST ARE AS FOLLOWS: /1-3, 5-9/

$$P_{OHM.} = C_3 V_L^2 T_e^{3/2}/R^2 \qquad (3)$$

$$P_{EI} = C_4 n^2 (T_e - T_i)/T_e^{3/2} \qquad (4)$$

$$P_{LOSS} = P_{BRM.} + P_{CYC.} + P_{IMPL.} + P_{IMPH} \qquad (5)$$

$$P_{BRM.} = C_5 n^2 T_e^{1/2}$$

$$P_{CYC.} = C_5 B^2 T_e (1 + T_e/204)$$

$$P_{IMPL} = C_6 n\, n_{EL} f_L (Z_L, T_e)$$

$$P_{IMPH} = C_7 n\, n_{EH} f_H (Z_H, T_e)$$

$$P_{NBI} = P(NB) \cdot H \cdot G \qquad (6)$$

WHERE TE AND TI ARE ELECTRON`AND ION'TEMPERATURE RESPECTIVELY; Z,ZL AND ZH THE CHARGE NUMBERS OF THE BULK IONS, THE LIGHT IMPURITY IONS AND THE HEAVY IMPURITY IONS WHILE N, NL AND NH THE CORRESPOUNDING DENSITIES; P(NB),H AND G ARE THE INJECTED POWER, THE SPATIAL DISTRIBUTION OF FAST IONS AND THE SPECIES DISTRIBUTION OF THE POWER ABSORBED. ALL C'S IN EQUATIONS ARE CONSTANTS.

FOR SIMPLICITY, A ZERO-D MODEL IS USED SINCE WE ARE INTERESTED IN THE QUALITATIVE BEHAVIOR.

ACCORDING TO THE ELEMENTARY CATASTROPHE THEORY, DELAY CONVENTION OCCURS AT THE BIFURCATION SETS, I.E. WHEN THE LOCAL POTENTIAL MINIMUM WHERE THE SYSTEM STAYS DISAPPEARS. BY MAXWELL CONVENTION ONE MEANS A TRANSITION OCCURING WITHIN THE BIFURCATION SPACE WHEN THE SYSTEM TENDS TO STAY IN THE GLOBAL MINIMUM OF THE POTENTIAL. ITS OCCURENCE DEPENDS ON A FINITE-AMPLITUDE FLUCTUATION OF THE GENERIZED POTENTIAL IN PLASMA WHEN THE CHARACTERISTIC TIME OF THE FLUCTUATION IS SHORTER THAN THAT OF EITHER THE THERMAL EQUILIBRIUM OF THE SYSTEM OR THE VARIATION OF THE CONTROL PARAMETER (PLASMA DENSITY IN OUR CASE).

III. RESULTS: SCALINGS AND CONDITION FOR MAXWELL CONVENTION

IN OUR STUDY, TWO OPERATING CONDITIONS ARE CONSIDERED: (1) THE LOOP VOLTAGE IS FIXXED AS DENSITY VARIES; (2)THE PLASMA CURRENT IS KEPT CONSTANT.

(1) VL=CT.

SHOWING IN FIG. 1-7, A SCALING IS DEDUCED

$$n_{cr} \propto B_T a\, V_L^{3/4}/R^2 \qquad (7)$$

(2) QA=CT. I.E. IP=CT. (FIG. 8-14)

$$n_{cr.} \propto B_T/(R q_a)^{.8} \sim B_T (I_p/B_T a^2)^{.8} \qquad (8)$$

WHICH IS CLOSE TO MURAKAMI SCALING /10/.

SCALINGS LISTED ABOVE ARE FOR DELAY CONVENTION. UNDER CERTAIN CONDITIONS ABOVE-STATED IT IS INTERSTING TO CONSIDER MAXWELL CONVENTION AS ANOTHER POSSIBLE TRANSITION FOR THE STATE OF SYSTEM.

IF A GRADIENT SYSTEM IS ASSUMED, WE CAN FIND THE POTENTIAL BY INTEGRATING EQUATION (1) W.R.T. TE AND BY APPLYING CLAUSIUS-CLAPEYRON EQUATION/11/ TO FIND THE TRANSIT POINTS FOR MAXWELL CONVENTION. THE PARAMETRIC EFFECTS ARE DRAWN IN ABOVE FIGURES WITH AN INDEX "M". IT IS SEEN THAT MAXWELL CONVENTION OFFERS A MORE SEVERE LIMITATION ON PLASMA PARAMETERS. FURTHERMORE THE POTENTIAL BARRIER WHEN MAXWELL CONVENTION OCCURS, WHICH EQUALS THE MINIMUM AMPLITUDE OF THE FLUCTUATION IN PLASMA ENERGY AND ITS RATE OF VARIATION, CAN BE CALCULTED. A SAMPLE VALUE IS

$$\Delta(T\frac{\partial T}{\partial t}) = 2\ (kev)^2/ms \qquad (9)$$

SOME PARAMETRIC EFFECT OF THE CRITICAL POTENTIAL BARRIER IS GIVEN IN THE FIGURES.

ACKNOWLEDGEMENT

HELPFUL DISCUSSTION WITH PROFS. Y.P.HUO AND Y.C.LEE IS GRATEFULLY ACKNOWLEDGED.

REFERENCES

/1/ GUZDAR,P.N. PHYS. FLUIDS 27(1984)449.
/2/ YU,G.Y., GUZDAR,P.N. AND LEE, Y.C. NUCL. FUSION 25(1985)403 AND THE REFERENCES LISTED.
/3/ GUZDAR,P.N. UNIV. OF MD. TECH. REPORT UMLPF 85-019.
/4/ RECHESTER,A.B. AND ROSENBLUTH,M.N. PHYS. REV. LETT. 40(1978) 38.
/5/ ZHANG,C. INST. OF PLASMA PHYS. ACADEMIA SINICA TECH. REPORT ASIPP-09-006-0401; STACEY, W.M. //FUSION PLASMA ANALYSIS//.
/6/ ROME,J.A.,CALLEN,J.D. AND CLARKE,J.F. NUCL. FUSION 14(1979) 141.
/7/ HU,X.W. ASIPP-09-006-0101(1981); CHEN,Z.X. IBID.
/8/ DORY,R.A. AND WIDNER, M.M. NULL. AM.PHYS. SOC. 11(1970)1418.
/9/ MCLESS ET AL. NUCL. FUSION 14(1974)419.
/10/ MURAKAMI,M., CALLEN,J.D. AND BERRY,L.A. NUCL. FUSION 16 (1976) 347.
/11/ GILMORE,R. //CATASTROPHE THEORY FOR SCIENTISTS AND ENGINEERS// JOHN WILEY & SONS 1981.

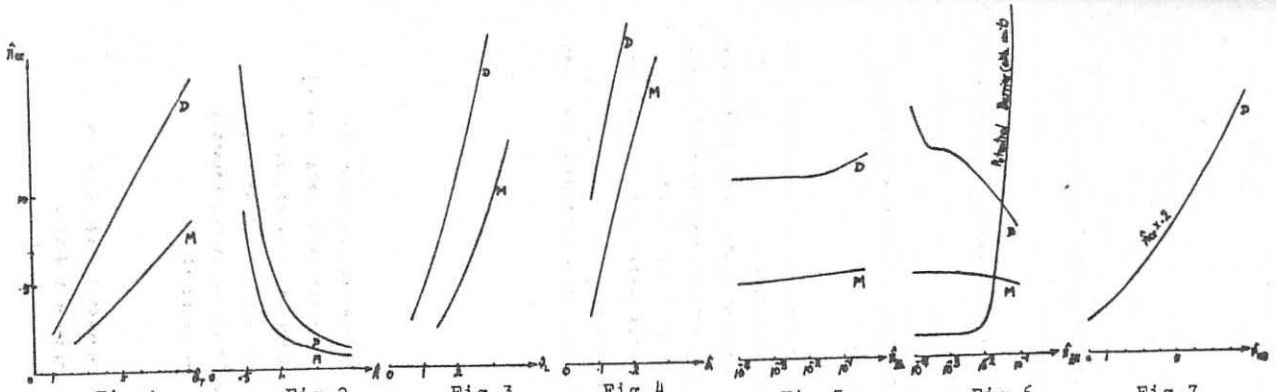

Fig.1 Fig.2 Fig.3 Fig.4 Fig.5 Fig.6 Fig.7

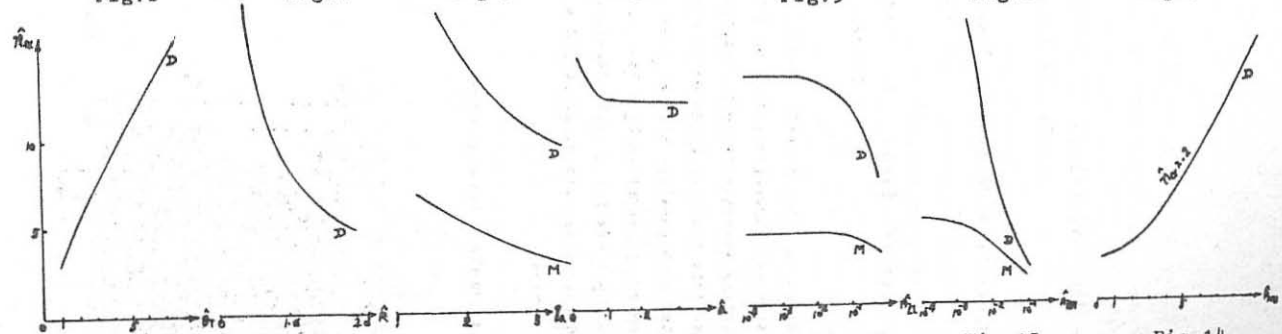

Fig.8 Fig.9 Fig.10 Fig.11 Fig.12 Fig.13 Fig.14

FIGS.1-7 PARAMETRIC EFFECTS OF N_{cr} WITH V_L=CT.

FIGS.8-14 PARAMETRIC EFFECTS OF N_{cr} EITH I_p=CT.

D: DELAY CONVENTION M: MAXWELL CONVENTION

The Generation of Reversed Field Configuration by RF Driven Currents

M. Frank, A. Hardtke, M. Jogwich, M. Kühnapfel, K. Plennis
H. Tuczek

Universität Essen - GHS, FB7/Physik, Universitätsstr. 5
D-4300 Essen 1

According to the "Rotamak" concept /1,2/ toroidal d.c. currents are generated in a hydrogen plasma of spherical shape.
A rotating magnetic field is applied to the preheated and magnetized plasma. This field is produced by r.f. currents through two coil pairs, oriented orthogonally, with a phase shift of 90 degrees /3/.
The power is supplied by a two-channel transmitter of 5 MW at a frequency of 1 MHz for a pulse duration of 1.5 msec.
During the entire discharge period a reversed field configuration can be maintained.

Experimental arrangement:

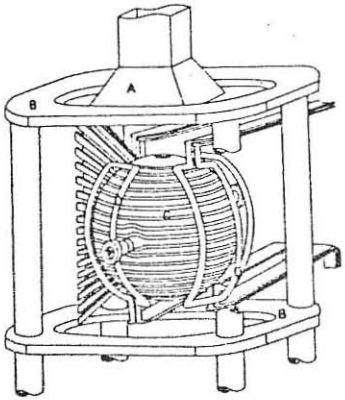

A: Antenna for pre-ionasation
B: Coils for static magn. field
C: Spherical coil-assembly for theta-pinch heating
D: D-Type coils for rotating magnetic field

Fig. 1: Schematic Diagram of the Spheromak device

Using Hydrogen as working gas it is difficult to produce a plasma by electrical dischasrges at low pressures. In order to achieve the favorable initial conditions for an effective interaction of the rotating magnetic field with the Plasma, an electron cyclotron resonance (ECR) preionasation (Fig. 1, A) and a theta-pinch kind of preheating (Fig. 1, C) of the plasma were included to our Spheromak device. A quasi-static magnetic bias field (Fig. 1, B) is used to fulfill the ECR condition and as initial field for the reversed field configuration. The rotating field is applied by two coil pairs (Fig. 1, D).

The ECR preionasation:
For the generation of the plasma a magnetron with a pulse power of 4 kW is used, radiating at a frequency of 2.45 GHz. As the magnetic bias field has a mirror configuration the ECR condition is fulfilled first in the polar region of the vessel and moves with increasing bias field through the center to the wall in the equatorial plane.
Measurements with electrostatic probes indicate that for the ignition of the discharge ECR is necessary but the plasma can even be sustained during periods where the ECR condition is no longer fulfilled.
The density of the ECR-Plasma is of the order of 10^{11} cm^{-3} and the electron temperature is about 10 eV. The pressure limit for ignition is $5*10^{-4}$ mbar.

The theta-pinch preheating:
Initial plasma heating is achieved by discharging a 4.3 kJ capacitor bank over 17 coils surrounding the spherical discharge vessel in horizontal planes (Fig. 1, C). The ion temperature is determined by measuring the Doppler broadening of impurity lines and of H_α (Fig. 2).

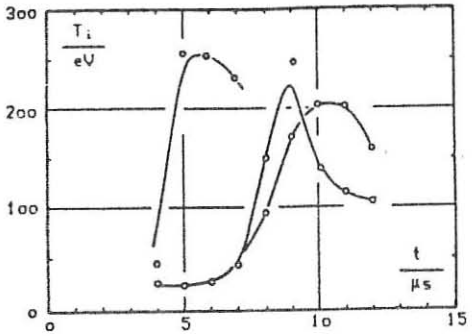

Fig. 2: Ion temperatures evaluated of the Doppler broadening of different ionasiation stages of Nitrogen impurities

All observed ionisation states of the impurity lines show a temperature of the same order of magnitude between 200 and 300 eV. NII and NIII reach the temperature maximum later than NIV due to their longer energy equipartition time with Hydrogen. The ion temperature evaluated from H^* is lower by a factor of 4, since the Ha radiation of the hot plasma core is covered by the more intensive radiation of plasma in the wall region of the vessel. The electron temperature has been estimated by the appearance of ionisation stages to be of the order of 60 eV.

The rotating r.f. field:

The rotating magnetic field is produced by r.f. currents passing through two pairs of coils (Fig. 1, D) with a phase shift of 90 degrees in space and time. The power is supplied by a two-channel transmitter of 5 MW at a frequency of 1 MHz for a pulse duration of 1.5 msec.

At these experiments up to 1MW can be coupled into the plasma maintaining a stable reversed field configuration for about 1.2 msec (Fig. 3). Measurements of the radial distribution of the magnetic field show plasma currents in the order of some kA proportional to the magnetic bias field (Fig. 4).

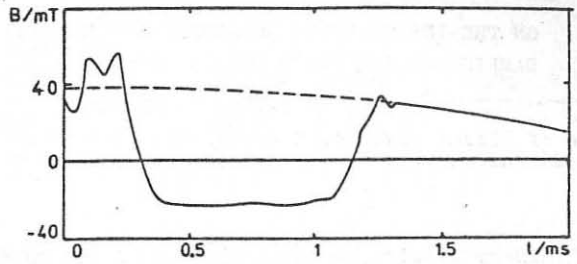

Fig. 3: Poloidal magnetic field as a function of time near the center of the sphere

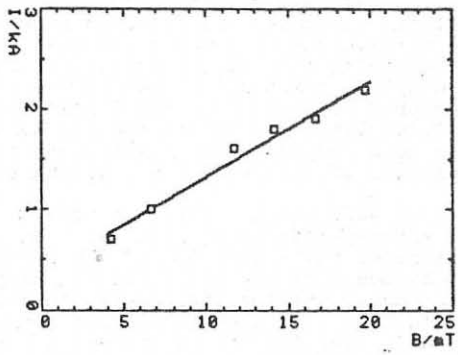

Fig. 4.: Plasma current as a function of the bias magnetic field

Experiments are carried out to study the generation of rotating magnetic fields in a plasma by the Blevin-Thonemann end effect /4/.

References:

/1/ I.R. Jones, The Flinders University of South Australia, FUPH-R-151

/2/ N.N. Hugrass, I.R. Jones, K.F. McKenna, M.G.R. Phillips, R.G. Storer and H. Tuczek, Phys. Rev. Letter, 1976, 44, (1980)

/3/ H. Tuczek, Proc. of the 3rd Int Conf. on Heating in Toroidal Plasma, Grenoble (1982) G17

/4/ W.A. Blevin and P.C. Thonemann, Nucl. Fusion, Suppl., 55, 1, (1979)

ON THE INFLUENCE OF α-PARTICLE CYCLOTRON DAMPING ON THE LOWER HYBRID CURRENT DRIVE

L. Krlín, P. Pavlo, Z. Tlučhoř

Institute of Plasma Physics, Czechoslovak Academy of Sciences
Pod vodárenskou věží 4, 182 11 Prague 8, Czechoslovakia

Abstract

Some preliminary results on the influence of the cyclotron harmonic damping of lower hybrid waves by thermonuclearly produced alpha-particles are presented. Recently, the usefulness of the lower hybrid current drive (LHCD) in reactor regime was doubted in connection with this effect. The quasilinear change of the slope of the alpha-particle distribution function is taken into account. Analytical estimates are obtained showing that at a sufficiently high wave energy density the power absorbed by alpha-particles saturates (in the approximation used). For the parameters of a hybrid reactor, the saturated power was found much lower than that computed from the linear theory. It seems, therefore, that, at least for hybrid reactor conditions, the alpha-particles need not represent a serious obstacle to LHCD. Some further aspects of this effect are discussed.

In recent paper of WONG and ONO [1], the effect of thermonuclearly generated alpha-particles on LHCD has been investigated. The authors estimated the absorption of LHW by the alpha-particles component by means of the ion cyclotron damping in the linear regime. For usual reactor parameters, they found very strong absorption (the effective absorption length L_α was of the order of 5 cm). Even for the parameters of the hybrid reactor [2] (when their procedure yields $L_\alpha \sim 0.5$m), the absorption is strong enough to make the usefulness of LHCD scheme questionable.

In this paper we try to extrapolate the mentioned calculations into the quasilinear regime. Here, the original alpha-particle distribution function (determined by alpha-particles collisions with electrons and ions), which has been used in the mentioned paper, obviously changes its slopes and, consequently, also the absorption rate. It can be expected that this effect wil reduce the strong absorption, obtained in the linear approximations. As follows from our preliminary estimations, the absorption of LHW by the alpha-particle component really sufficiently decreases.

The estimation of WONG and ONO is based on the evaluation of the space Landau decrement γ_x

$$(1)\quad \gamma_x = \frac{k_\perp \left[\mathrm{Re}\ (k_{zz}) - (\mathrm{Re}\ n_\perp)^2\right]}{2\ \mathrm{Re}\ (k_{xx})\ (\mathrm{Re}\ n_\perp)^2} \left\langle \mathrm{Im}\ (k_{xx}) \right\rangle ,$$

$$k_{xx} = \frac{1}{n\alpha_T}\,\frac{2\pi}{\omega}\,\frac{\omega_{p\alpha}^2}{\omega_{c\alpha}}\sum_n \int dv_\parallel \cdot \int dv_\perp \cdot 2v_\perp n^2\,\frac{\omega_{c\alpha}^3}{k_\perp^2}\cdot$$

$$\cdot\,\frac{1}{k_\parallel v_\parallel + n\omega_{c\alpha} - \omega}\; J_n^2\left(\frac{k_\perp v_\perp}{\omega_{c\alpha}}\right)\left[\frac{\partial f_\alpha}{\partial v_\perp^2}\left(1-\frac{k_\parallel v_\parallel}{\omega}\right)+\frac{k_\parallel v_\parallel}{\omega}\,\frac{\partial f_\alpha}{\partial v_\parallel^2}\right]$$

$$\mathrm{Re}\;k_{xx} = 1 + \frac{\omega_{pe}^2}{\omega_{ce}^2} - \frac{\omega_{pi}^2}{\omega^2};\quad \mathrm{Re}\;k_{zz} = 1 - \frac{\omega_{pe}^2}{\omega^2}\,.$$

For parameters of the hybrid reactor [2], the basic influence on the absorption is expected to come from the derivative $\partial f/\partial v_\perp^2$ (since $k_\parallel v_\parallel/\omega < 0.1$). We therefore investigated mainly the quasilinear change of $\partial f/\partial v_\perp^2$, also due to the fact that the quasilinear diffusion in $v_\perp$ is predominant.

The quasilinear diffusion equation with the collisional term, source term and the quasilinear diffusion in perpendicular velocities has the form [3, 4]

$$\left\{\frac{1}{v_\perp}\,\frac{\partial}{\partial v_\perp}\left[v_\perp\,\tau_s\;D_\perp\,\frac{\partial f}{\partial v_\perp}\right]\right\}_{\chi,\,v} + \frac{1}{v^2}\,\frac{\partial}{\partial v}\left[(v^3+v_c^3)\,f\right] +$$

$$+\,k\,\frac{v_c^3}{v^3}\,\frac{\partial}{\partial\chi}\left[(1-\chi^2)\,\frac{\partial f}{\partial\chi}\right] + \tau_s S_o\cdot\delta(v-v_\alpha) = 0 \qquad (2)$$

Here $\{\}_{\chi,v}$ means the corresponding expression of $v_\perp$, $v_\parallel$ in coordinates $v = \sqrt{(v_\perp^2 + v_\parallel^2)}$, $\chi = v_\parallel/v$, τ_s is the slowing-down time, v_α is the velocity of born particles; the velocity v_c and the coefficient k are given as in [4].
According to [3], the quasilinear diffusion coefficient $D_\perp$ is given

$$D_\perp = \sum \frac{\pi e_\alpha^2}{m_\alpha^2}\,E_{k_\perp}^2\;J_n^2(\lambda)\,\frac{n^2}{\lambda^2}\,\frac{1}{/v_\parallel - v_g/};\quad \lambda = \frac{k_\perp v_\perp}{\omega_{c\alpha}} \qquad (3)$$

v_g being the group velocity.
The basic problem arises from the complicated form of $D_\perp$. To obtain at least some qualitative results, we approximate the expression $v_\perp \cdot D_\perp$ by some average constant value $\Sigma\, v_\perp D_{\perp n} = \bar{\mathcal{D}}$. After normalizing of all velocities to v_α, the equation (2) can be then rewriten into the form

$$\left\{\frac{\partial^2 f}{\partial x_\perp^2}\right\}_{\chi,x} + \frac{\sqrt{1-\chi^2}}{x\,\mathcal{D}}\,\frac{\partial}{\partial x}\left[(x^3+a^3)\,f\right] +$$

$$+\,\frac{ka^3}{\mathcal{D}}\,\frac{\sqrt{1-\chi^2}}{x^2}\,\frac{\partial}{\partial\chi}\left[(1-\chi^2)\,\frac{\partial f}{\partial\chi}\right] + \frac{\tau_s S_o}{\mathcal{D}}\,\frac{x\sqrt{1-\chi^2}}{v_\alpha}\,\delta(x-1) = 0 \qquad (4)$$

where $x_\perp = v_\perp/v$, $x = v/v_\alpha$, $a = v_c/v_\alpha$ and $\mathcal{D} = \bar{\mathcal{D}}/v_\alpha^2$. Let us further normalize f to $f_\alpha(v_\alpha)$, where f_α is the unperturbed distribution function of alpha-particles

(5) $f_\alpha = \frac{A}{x^3+a^3}$; $A = \tau_s S_o$

and where S_o is alpha-particle source term.

Since all velocities are of the order of v_α, $x_\perp$ and x are close to 1. Supposing that the dimensionless derivatives are of roughly the same order, and under the condition

(6) $\mathcal{D} \gg 1$

we get for the zero order solution f_o from (4) a simple relation (7) $\frac{\partial^2 f_o}{\partial v_\perp^2} = 0$. This condition imples the solution $\frac{\partial f_o}{\partial x} = \frac{\partial f_o}{\partial x}(\chi x = v_\parallel)$, i.e. independent of $x_\perp$. This value can be determined from boundary conditions. Supposing that in the quasilinear region (extending from $x_{\perp min}$, $\Delta n^2(x_{\perp min})$ is considered negligible), the predominant flux of particles in velocity space is in $x_\perp$, $(\partial f/\partial x_\perp)/x_{\perp min}$ can be determined by equating the fluxes of particles over the boundary $x_{\perp min}$ between the collisional and quasilinear regions. In this case,

(8) $$\left.\frac{\partial f}{\partial x_\perp}\right|_{x_{\perp min}} = \frac{x_{\perp min}\, f_\alpha(x_{\perp min},\ x_\parallel = \frac{v_\parallel}{v_\alpha})}{\mathcal{D}},$$

where $f\alpha$ is the undisturbed distribution function for $x_{\perp min}$, $v_\parallel/v_\alpha$. In the approximation used for $\mathcal{D}$, the condition (6) reads

(9) $$0.05\,\Delta n \frac{\pi e_\alpha^2}{m_\alpha^2} E_{k_\perp}^2 J_{n_o}^2(n_o)\, n_o \frac{\tau_s}{/v - v_g/} \frac{\omega_{c\alpha}}{k_\perp v_\perp} \frac{1}{v_\alpha^2} \gg 1,$$

where Δn is the number of harmonics, appearing in the interval $v_\parallel(0, v_\alpha)$, n_o is the average order of this harmonics, τ_s is the slowing-down time. Expressing the condition in terms of wave energy density $W_{k\parallel}$, we obtain for the parameters of the hybrid reactor [2] $\bar{n}_e = 6.7\times10^{19} m^{-3}$, $\bar{T}_{e,i} = 11$ keV, $B_T = 6$ T, $\omega = 1.5\times10^{10} sec^{-1}$, $k_\parallel = 84 m^{-1}$ the condition

(10) $W_k \gg 10^{-2}$ J m^{-2}.

The value on RHS of eq. (10) corresponds roughly to 100 MW of the input rf power in case of the hybrid reactor [2].

The flattening of the derivative $\partial f/\partial v_\perp$ leads to the saturation of the absorbed power, analogously to the estimation of FISCH [5] and KLIMA [6]. Neglecting the component of the absorption coming from $\partial f/\partial v_\parallel$, the absorbed power is given by

$$P_{tot} = -2\int_{k_\perp} \frac{k_\perp \left[\mathrm{Re}\,(k_{zz}) - (\mathrm{Re}\,(n_\perp))^2\right]}{2\,\mathrm{Re}\,(k_{xx})\,(\mathrm{Re}\,n_\perp)^2} \cdot \mathrm{Im}\left[\frac{1}{n_{\alpha T}} \frac{2\pi}{\omega} \frac{\omega_{pe}^2}{\omega_{c\alpha}}\right.$$

(11) $$\sum_n \int dv_\parallel \int dv_\perp J_n^2\left(\frac{k_\perp v_\perp}{\omega_{c\alpha}}\right) \frac{1}{\mathcal{D}(v_{\perp min},\ v_\parallel,\ E_k^2)} f\,(v_{\perp min},\ v_\parallel) \cdot$$

$$\left. \frac{1}{k_\parallel v_\parallel + n\,\omega_{c\alpha} - \omega} \right] v_{gr} W_{k_\perp} dk_\perp .$$

Supposing a rectangular form of $E_{k\perp}^2$ (and therefore also $W_{k\perp}$), it is seen that P_{tot} does not depend on the wave energy density.

Rough comparison of this saturated absorbed power with the power determined in the linear approximation for $W_{k_\parallel} = 10^{-2}$ Jm^{-2} yields, for our parameters ($\Delta k_\parallel = 0.2\, k_{\parallel 0}$)

$$P_{sat} \sim 10^{-2}\, P_{lin}.$$

The contribution to the absorbed power due to the neglected term $\partial f/\partial v_\parallel$ may modify the relation. However, since in our case this contribution represents approximately 1 % of P_{lin}, it can be concluded that for parameters of the hybrid reactor, the power absorbed by alpha-particles estimated from the quasilinear theory may represent only a small fraction of the linear estimate.

There are further effects associated with the strong absorption by alpha-particles and with the quasilinear perturbation of the alpha-particle distribution function. Since the absorption in alpha-particle component strongly increases with the alpha-particle density (exponentially dependent on the ion temperature), the increase in the ion temperature will lead to the decrease in the driven current. This may worsen the ion confinement. Through this effect, an intrinsic negative feed-back might be established to stabilize the thermal instability.

The quasilinear perturbation of the alpha-particle distribution brings a possibility of a current drive by alpha-particles, analogously to the ECR scheme. Further, the asymmetry possibly generates a new wave spectrum which can have an influence on the total driven current.

Our results bear, of course, the character of rough estimates. More precise results will be obtained from 2-D computer simulations now under progress.

The authors are grateful to Drs. R. Klíma, V. A. Petržílka and J. Preinhaelter for valuable discussions.

References

[1] Wong K.L. and Ono M.: Preprint PPPL-2058 of the Plasma Physics Laboratory of Princeton University, Princeton, November 1983.

[2] Krlín., Pavlo P. and Tluchoř Z.: Czech. J. Phys. B 35 (1985), 133.

[3] Akhiezer A.I.: Electrodynamics of Plasmas, Nauka, Moscow 1974 (in Russian).

[4] Lisak M., Anderson D., Hamnén H. and Wilhelmson H.: Nucl. Fusion 22 (1982), 515.

[5] Fisch N.J.: Phys. Rev. Lett. 41 (1978), 873.

[6] Klíma R. and Longinov A.V.: Fiz. Plazmy 5 (1979), 496.

Comment on paper GO Fr 1130 S

"A Class of Special Toroidal MHD Equilibria, including Minimum-B" by C.M. Bishop and J.B. Taylor

D. Palumbo
EURATOM, Brussels, Belgium

As I have worked on this problem since many years (/1./ D. Palumbo, Il Nuovo Cimento, X, B(1968) 507; /2./ D. Palumbo, in "Instability and Confinement in Toroidal Plasmas" Varenna Course 1971, page 91), I'm glad that Bishop and Taylor's paper gives me the opportunity of making several comments and add some details.

1. The generalisation of the isodynamic solution considered by Bishop and Taylor by adding to the square of the toroidal field the square of a vacuum toroidal field - k/R^2 in their notations - was already considered in /1/, and was the main reason for publishing paper /2/. These extended solutions are no longer isodynamic but still allow an arbitrary choice of the pressure profile. There are some differences in the notations: Bishop and Taylor's R^2, f (ψ), $\beta(\psi)$, and k correspond, respectively, to X, $T(\psi)$, $\eta(\psi)$, and C^2 in my ref. /2./. I agree that apart from pure relabelling these solutions are the only possible ones which conserve the magnetic surfaces.

2. In ref. /1/ I noted that the purely isodynamic equilibrium is always unstable. In ref. /2/ I considered in more detail the stability problem. On the basis of the fact that the toroidal field of the purely isodynamic equilibrium is too low ($q \ll 1$), I determined the k-values required for stability (C^2 in my notations) by imposing that the Mercier criterion be fulfilled throughout the whole plasma volume, for different pressure profiles. The average for Mercier (only) stable equilibria are calculated, using

$$\langle \beta \rangle = \frac{8\pi}{B^2_{MAX}} \left(\frac{1}{v_1} \int_0^{v_1} p^2 dv \right)^{1/2} ;$$

the toroidal q factor is given as a function of ψ and c^2.

3. The search for equilibria with congruent drift- and magnetic- surfaces, now called omnigeneous equilibria, was the starting point for Ref. /1/. There I have proved that isodynamicity is, strictly speaking, a sufficient condition for this property, the necessary condition being that the magnetic lines are geodesics of the magnetic surfaces (geodesic configuration). However, it should be noted that the distinction between geodesic and isodynamic configurations is rather academic, the only possible exception of any practical interest being the Stellarator /2/, which in principle could have geodesic but not necessarily isodynamic solutions.

4. I also had the curiosity of looking whether non-axisymmetric isodynamic equilibria do exist. In ref. /2/ I searched by cumbersome differential geometry for the existence of solutions with weaker symmetry (plane of symmetry instead of axis of symmetry), but with negative result. More recently (Acc. Sc. Let. Art. Palermo, 1984, in press) by the same method, I have shown the non-existence of the isodynamic Stellarator and, finally, in collaboration with M. Balzano the non-existence of non-axisymmetric toroidal isodynamic equilibria with continuous scalar pressure (ibid in press). This last result can also be deduced from more general considerations (see M. Bineau, Proc. 6th European Conference on controlled Fusion and Plasma Physics, Moskow 1973, Vol. I, 221).

Finally, let me add a few remarks on possible areas for future work.

The unique property of the generalized ($c^2 \neq 0$) solutions - the possibility of accommodating a variety of pressure profiles for a fixed geometry - can be exploited in various problems:

- Study of the specific influence of the P profiles on the stability.

- Heating, during which the P profiles will possibly change (a few weeks ago at Erice I discussed a somewhat naive example).
- Dependence of P and J profiles from the temperature profile. For instance, in the purely isodynamic case ($C^2 = 0$) the dependence is so drastic, in inductive discharges, that with realistic temperature profiles no interesting equilibria can exist.

Another possible application is in the search for new exact solutions of the Grad-Shafranov equation. In fact, if we consider the family of all possible configurations having a given pressure profile, this family certainly contains the isodynamic solution. Along these lines, and making use of a coordinate system with $\sqrt{g} = 1$, in collaboration with M. Balzano, we are looking for families of exact, and possibly new, solutions.